An Implantable Device for Localized Drug Delivery and Sensing

by

Karen D. Daniel

B.S. Chemistry
University of South Carolina, 1998

M.S. Chemical Engineering
University of South Carolina, 2003

Submitted to the Department of Chemical Engineering in
Partial Fulfillment of the Requirements for the Degree of

Doctor of Philosophy in Chemical Engineering
at the
Massachusetts Institute of Technology

February 2009

Signature of Author.....

Karen D. Daniel
Department of Chemical Engineering
September 16, 2008

Certified by .....

Robert S. Langer
Institute Professor
Thesis Supervisor

Accepted by .....

William M. Deen
Professor of Chemical Engineering
Chairman, Committee for Graduate Students

An Implantable Device for Localized Drug Delivery and Sensing

by

Karen D. Daniel

Submitted to the Department of Chemical Engineering
on September 16, 2008 in partial fulfillment of the requirements for the degree of
Doctor of Philosophy in Chemical Engineering

ABSTRACT

There are many potential clinical applications for localized drug delivery and sensing systems, such as cancer, vaccinations, pain management, and hormone therapy. Localized drug delivery systems reduce the amount of drug required for a therapeutic effect and the severity of side effects. Delivery of multiple chemicals has been demonstrated previously from a polymeric microreservoir device. This dime-sized device contains small reservoirs loaded with drug and separated from the outside environment by a degradable polymer membrane. This device was modified to allow minimally invasive implantation with a large-bore needle and has demonstrated *in vitro* pulsatile release of a model compound after a mock implantation step. A biodegradable sealing method was developed for the polymeric microreservoir device, which makes the device completely resorbable and eliminates the surgical removal step needed with a non-resorbable device.

Localized sensing systems will allow early detection of diseases and provide a tool for developing personalized treatment programs. The polymer microchip platform has been combined with magnetic relaxation switch (MRSw) nanoparticle sensors to create an *in vivo* sensing device. MRSw are magnetic nanoparticles (iron oxide core, crosslinked dextran shell) that can detect a variety of analytes. MRSw are kept in the device by a molecular weight cut-off (MWCO) membrane which allows analytes free access to the nanoparticle sensors. The MRSw aggregate in the presence of the analyte they were designed to detect and this aggregation causes a decrease in the transverse relaxation time (T_2), which can be detected with magnetic resonance imaging (MRI) or nuclear magnetic resonance relaxometry. *In vitro* sensing experiments were used to optimize the device design and characterize its performance. *In vivo* device-based sensing of hCG, a soluble biomarker that is elevated in testicular and ovarian cancer, has been demonstrated. Cell lines secreting hCG were used to produce ectopic tumors in nude mice. The sensing device was implanted and magnetic resonance imaging (MRI) quantified a T_2 decrease in mice with tumors compared to control mice (no tumors). This device may be the first continuous monitoring device for cancer that can be implanted at the tumor site and demonstrates feasibility of MRSw measurements *in vivo*.

Thesis Supervisor: Institute Professor Robert S. Langer
Thesis Committee: Professor Michael J. Cima (MIT)
Professor Paula T. Hammond (MIT)

Acknowledgements

Science is a collaborative effort and my work was influenced by many others in the form of guidance, technical advice, intellectual stimulation, and emotional support. MIT is full of people who not only love science, but love helping other people achieve their goals, and I have thoroughly enjoyed being here for the past five years. Time has flown by.

I'd like to thank my thesis supervisor, Professor Robert Langer for his guidance and support throughout my research project. His leadership style fosters an environment in the Langer lab that is conducive to hard work, creativity, collaboration, and intellectual growth. I'd also like to thank Professor Michael Cima, one of my thesis committee members, who has in effect served as a co-advisor for my research. The path to my thesis defense was less circuitous because of his input and feedback. Weekly meetings with the Cima group have always been interesting, helpful, and even entertaining. I'd like to thank Professor Paula Hammond, one of my thesis committee members, for always being ready with a list of possible solutions when I encountered difficulties in my research.

My work with developing an implantable sensor device depended on the advice and collaboration of many people. At CMIR: Ralph Weissleder, Lee Josephson, Matthew Spotnitz and Alex Guimaraes in particular. They supplied me with nanoparticles, welcomed me into their lab to use their machines, arranged MRI imaging sessions for my mice, and even assisted with MRI data analysis. Al Charest and Stephen Woolfenden were instrumental in training me for animal experiments. They implanted devices and tied many sutures while I was learning.

Past and present members of the Langer and Cima labs have always been willing to help. In particular, I'd like to thank Grace Kim and Christophoros Vassiliou, labmates who started the new cancer sensor project with me. Also Seth, Frank, Jeff, Yoon, Sharon, Mikhail, and Audrey from the Langer lab and Yawen, Rebecca, Melinda, Hong Linh, Heejin, Dan, Yoda and Noel from the Cima lab. The newest Cima group members: Yibo, Kay, Byron and Alex have added a new energy to the group meetings. Technical and administrative support at both labs was also greatly appreciated: Barbara, Lenny, Connie, Ilda, Tiffany and Bethany.

Several UROP students made a significant impact on my research and helped me learn how to become a better mentor: Ashley Thomas, Jina Kim, Steven Froelich, Farzad Jalali-Yazdi and Marilyn Galindo. Zad and Marilyn, in particular, were both very helpful. Marilyn became an expert at polymer device fabrication and then finished her UROP by putting in many hours at the animal facility, assisting with mouse surgeries. Zad became an expert at sensor device fabrication and diffusion studies. They were dedicated, efficient, and easy to work with. I only regret that they didn't start working with me as freshmen! I enjoyed spending time with them in lab and wish them the best as they move on to life after MIT.

My friends and family have helped me maintain balance during this sometimes all-consuming process. I know that many people have supported me in prayer, and for that I am grateful. My parents taught me to love learning and hard work, both of which have been important. I would not have ended up at MIT without their support and encouragement, both while growing up and since then. They have been excellent role models. I hope that I can be just

as positive an influence on my daughters. My in-laws helped out with childcare during the first two years, which allowed me to focus on my first year classes, qualifying exams and getting started on research. They also made the transition to a new city and school much easier on my daughter. My siblings and their families are a continual source of joy. It is impossible to talk with any of them for more than a few minutes without laughing about something. My husband Charles and daughter Katie were dragged along with me to MIT five years ago, and they have never complained. In fact, they have been great supporters. Charles is the one who talked me into changing my major to chemistry as an undergrad and I am so thankful! It was a much better fit. Later he prodded me along to a masters in chemical engineering and finally to MIT for my PhD. He has always encouraged me to try harder and take risks and I have benefited because of his influence. Life is much more interesting with him around. Katie has spent many hours reading in the conference room while I was in lab taking time points. She is great fun to talk with and is always ready with helpful suggestions. My daughter Clara is a funny little baby and has provided hours of comic relief over the last six months, which was certainly appreciated. You can never have too much comic relief while writing a thesis.

Table of Contents

List of Figures

List of Tables

Chapter 1 Introduction and Background

There are many potential clinical applications for localized drug delivery and sensing systems, such as vaccinations, cancer therapy, pain management, and hormone therapy. Localized drug delivery systems reduce both the amount of drug required for a therapeutic effect and the severity of side effects associated with treatment. Localized sensing systems will allow early detection of diseases and provide a tool for developing personalized treatment programs. Cancer, for examples, is diagnosed by histologic examination of tissue samples often taken by biopsy[1-4]. These invasive procedures offer an opportunity to leave behind a device to locally monitor tumor biomarker, chemotherapeutic agent, and tumor metabolite concentrations. The ability to repeatedly sample the local environment, in addition to sampling easily accessible fluids, could improve both early detection of metastasis[5,6] and personalized therapy[7,8].

1.1 Microchip for Localized Drug Delivery

One example of a drug that would benefit from localized delivery is carmustine (BCNU), a small, hydrophobic chemotherapeutic agent that is used in the treatment of malignant brain tumors. Although BCNU is commonly administered intravenously, the poor permeability of the blood-brain barrier requires large systemic doses in order to achieve therapeutic drug levels in the brain. The large systemic BCNU concentrations can induce harmful side effects in the liver, kidneys and spleen. Localized delivery systems have been developed to reduce the amount of BCNU required and to reduce the severity of these side effects[9,10]. The Gliadel® Wafer, a biodegradable polymeric delivery system for the continuous release of BCNU, was approved by the FDA in 1996 for recurrent glioblastoma multiforme (GBM) brain tumors, and in 2003 as initial therapy for GBM brain tumors. The wafer consists of a compressed polyanhydride (PA)

matrix that is impregnated with BCNU. It is implanted at the tumor site during surgery for tumor resection and delivers BCNU directly to the brain tumor site[9]. In addition to BCNU, local delivery of interleukin-2 (IL-2) has recently shown improved survival in animal brain tumor models by eliciting an antitumor immune response[11]. *In vivo* studies using an animal glioma model have shown that combining BCNU with IL-2 has a synergistic therapeutic effect, and is able to significantly improve survival[12-14]. In the most efficacious therapy, IL-2 microspheres were first implanted at the intracranial tumor site, followed five days later by implantation of BCNU-containing polymer implants[14]. For this complex therapy, a single device that could deliver both IL-2 and BCNU with precise control over the temporal release profile of each drug would be desired. In comparison, existing therapies would require multiple surgeries for implantation and would likely not be capable of the same level of control over the release profiles.

Local delivery of multiple chemicals has been demonstrated from a silicon microchip[15] (active device, Figure 1-1a and b) and a resorbable polymeric microchip[16] (passive device, Figure 1-1c and d). The microchips contain small reservoirs that are loaded with drug and separated from the outside environment by a membrane. In the active device, the membrane is a thin layer of gold. When drug needs to be released from a reservoir, a voltage is applied which causes electrochemical dissolution of the gold anode membrane[15,17]. The passive microchip contains degradable polymer membranes. The composition, molecular weight, and thickness of the membrane determine when the drug depot will be released from the reservoir[16]. These microchips are unique because they contain no moving parts and are capable of delivering drugs in the solid, liquid, or gel state. Also, the microchip is a significant improvement over commercially available polymeric delivery systems because it is not limited to a continuous

release profile. There are many cases where pulsatile, not continuous, delivery of a drug is preferred. Another benefit of the microchip is that the drug depot is protected from the outside environment before release.

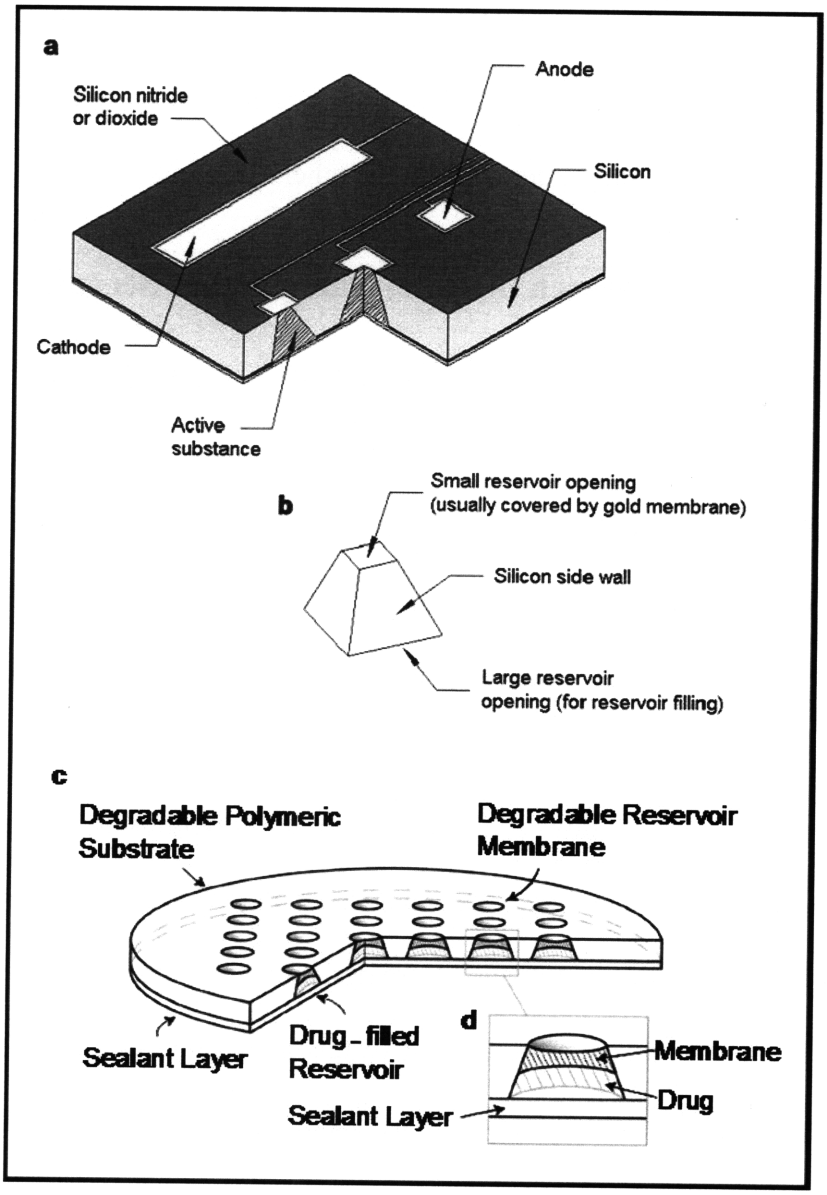

Figure 1-1. Schematic of two types of drug delivery microchip devices. a) Active, silicon device, b) Close-up of single reservoir in active device[15]. c) Passive, polymeric device, d) Close-up of single reservoir in passive device[16].

Both the active and the passive microchip have demonstrated *in vitro* pulsatile release of multiple compounds, such as sodium fluorescein, dextran, heparin, and human growth

hormone[15,16]. In addition, both devices have shown controlled, pulsatile release of certain chemicals *in vivo* (using a rat model). The passive microchip has demonstrated controlled *in vivo* release of mannitol[18] and the active microchip has demonstrated controlled *in vivo* release of sodium fluorescein, mannitol and BCNU[19]. However, the microchips are not limited to just pulsatile release of chemicals. The release profile from a microchip is essentially unlimited, since each reservoir can be opened independently from the other reservoirs.

1.2 Magnetic Resonance Switch (MRSw) Nanoparticle Sensors

MRSw are magnetic nanoparticles (iron oxide core, crosslinked dextran shell (CLIO)) that can detect a variety of analytes[20]. MRSw have previously been functionalized to detect peptides, oligonucleotides, nucleic acids, receptor ligands, proteins, small molecules and antibodies [21-26]. The lower limit of detection and working concentration range is determined by the nanoparticle design. In some cases the lower limit of detection is in the low femtomole range[24]. These MRSw have been used extensively for *in vitro* agglutination assays where the MRSw and analyte solutions are mixed together. Continuous monitoring of glucose with MRSw contained within a dialysis membrane has also been demonstrated *in* vitro[25]. The MRSw aggregate in the presence of the analyte they were designed to detect and this aggregation causes a decrease in the transverse relaxation time (T_2). Magnetic resonance imaging (MRI) or nuclear magnetic resonance (NMR) relaxometry can be used to quantify the T_2 of the MRSw and determine if aggregation has occurred[24,27,28].

Figure 1-2 is a schematic of MRSw used to detect hCG-b, a soluble biomarker (~23 kDa) that is elevated in testicular and ovarian cancer[29-32]. Serum concentrations up to 16 μg/ml were reported in one condition, persistent trophoblastic disease, whereas they are usually less than 0.005 μg/ml in normal men and women[33]. These MRSw have been previously shown to detect

0.5 to 5 μg/mL hCG-β[26]. hCG is a monovalent analyte, so two populations of MRSw were prepared (C_{95} and C_{97}), each conjugated with a different monoclonal antibody for hCG-b. HCG or hCG-b, when present, creates a bridge between C_{95} and C_{97}, similar to an ELISA sandwhich. There is some variability in the average number of antibodies conjugated to the MRSw (valency) each time a batch of nanoparticles are functionalized[26]. Aggregation occurs when both types of MRSw are present with either the hCG-b subunit or the hCG dimer. The MRSw are initially dispersed (high T_2), whereas addition of the analyte (hCG-b or hCG) causes the MRSw to aggregate in clusters. The aggregated MRSw are more efficient at dephasing the spins of surrounding water protons, which is seen as a decrease in the T_2[26].

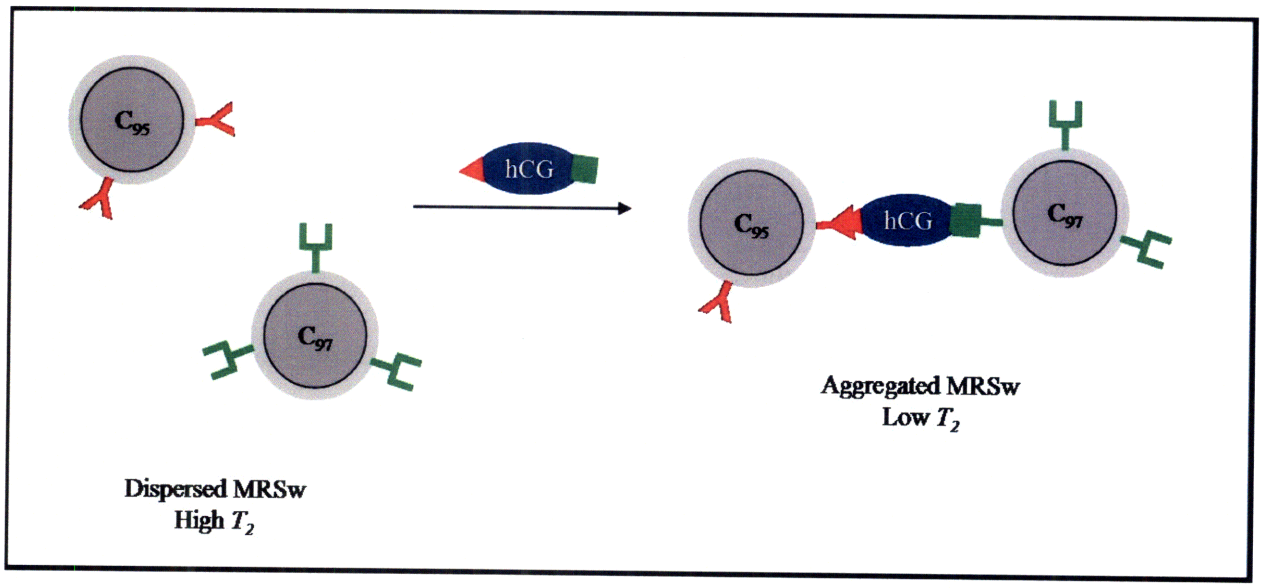

Figure 1-2. Schematic of MRSw aggregation with hCG-b. When hCG is present it causes aggregation of the two MRSw populations. The aggregated MRSw are more efficient at dephasing the spins of the surrounding water protons, which is seen as a decrease in T_2, the transverse relaxation time.

The optimum range of operation, in terms of analyte and MRSw concentration, depends on the specific analyte and MRSw being used[26,28,34]. The signal from the aggregated particles is masked by the signal from the many un-aggregated particles when there is too little analyte present, and there is no detectable decrease in T_2. Bridges are formed that network together

multiple MRSw resulting in aggregates that can be detected by a decrease in T_2 when the relative concentrations of analyte and MRSw are in the correct range. Every receptor on the surface of the MRSw is filled with an analyte molecule when too much analyte is present. Aggregates are not able to form because there are no open binding sites to create bridges between particles. This is a common phenomena in agglutination assays, and is called the prozone or hook effect[26,28,34-36]. Insolubility and precipitation of aggregates will also occur if the network of aggregated MRSw grows too large[26,28]. Insolubility and precipitation of aggregates is more common with high valency MRSw (i.e. 4 or more Ab per particle) when detecting hCG, but can also occur with lower valency MRSw that are combined with high hCG solutions[26]. The response of MRSw to hCG is studied for each batch to determine the relative MRSw and hCG concentrations that lead to stable aggregates.

1.3 Implantable Device for Localized Sensing

The main objective of my thesis is to combine the polymer microchip drug delivery platform with MRSw nanoparticle sensors to create an *in vivo* sensing device. This sensing device could be used in a variety of applications, but this thesis will focus on applications in the detection and treatment of cancer. Figure 1-3 is a generic schematic of a proposed sensing device. MRSw are kept in the reservoirs by a molecular weight cut-off (MWCO) membrane. The MWCO membrane allows analytes free access to the nanoparticle sensors but does not allow the MRSw to diffuse out of the wells. Erodible timing films can also be added to control when each well is exposed to the sensing environment. Packaging the MRSw in our device addresses two key challenges related to using the MRSw *in vivo*: possible immune response to the protein modified nanoparticles, and T_2 fluctuations due to changes in MRSw concentration. The semi-permeable membrane exposes the MRSw to analytes in the local environment but prevents the

MRSw from invoking a possible immune response. The rigid device substrate provides a constant-volume reservoir so the concentration of MRSw remains constant. This allows any T_2 changes to be attributed solely to aggregation of the nanoparticles[28].

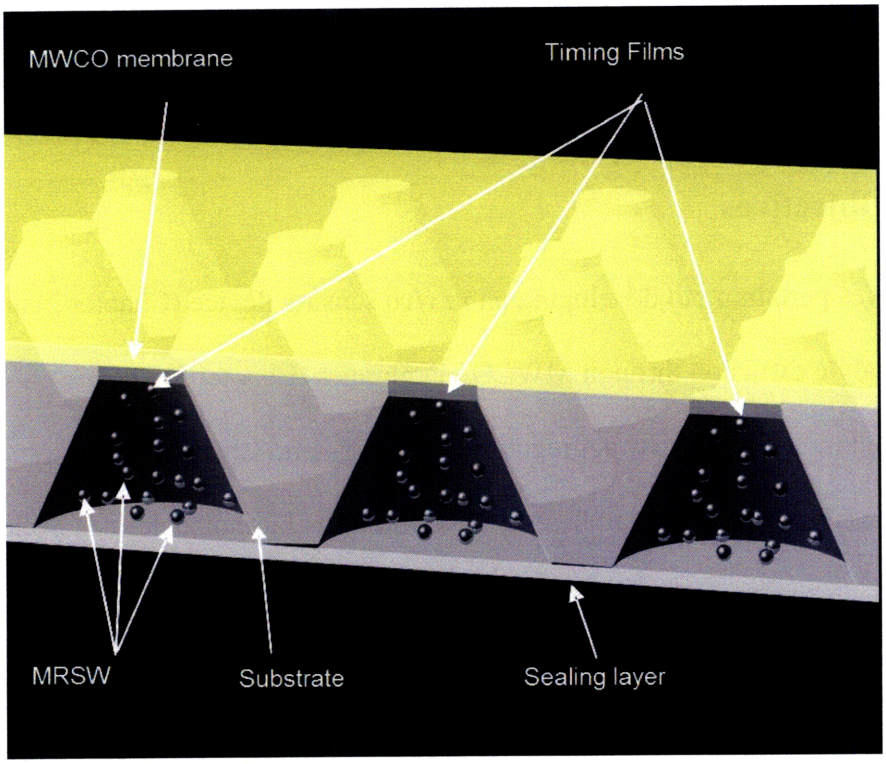

Figure 1-3. Schematic of proposed sensing device. MRSw are contained in reservoirs in the device substrate. Molecular weight cut-off (MWCO) membranes keep the MRSw in the reservoirs but allow analytes to diffuse into the reservoirs and interact with the MRSw. Each reservoir could be filled with MRSw designed to detect a different analyte. Resorbable timing films could be added to each reservoir to initially isolate the MRSw from the *in vivo* environment.

Technologies for early detection of cancer through cancer-associated biomarkers will have far-reaching impact on cancer research and clinical care[37,38]. The ability to monitor soluble cancer markers locally in real-time could improve sensitivity and allow for detection of cancer cells before they are recognizable by standard MRI and could also provide information on the delivery of current or experimental drugs to tumors. Current clinical methods of measuring cancer markers or drug concentrations are limited to sampling easily accessible fluids (such as blood) or surgical procedures[38-40]. Surgical procedures allow sampling of the local tumor

environment, where concentrations of cancer biomarkers are significantly higher than serum levels[41,42]. These invasive sampling techniques, however, are not feasible for continuous monitoring and widespread clinical use. This thesis describes a sensing device that could be made small enough to allow local minimally invasive sensing and real-time analysis of cancer-related molecules.

1.4 Thesis Objectives

Thesis objectives pertaining to developing an *in vivo* sensing device (Chapter 2) are:

1. Quantify analyte diffusion through MWCO membranes (Chapter 3).

2. Characterize kinetics of MRSw aggregation (Chapter 4 and Chapter 5).

3. Perform *ex vivo* diffusion studies to determine if biomolecule adsorption to MWCO membranes affects analyte diffusion (Chapter 3).

4. Perform *in vivo* sensing experiments (Chapter 6).

My final thesis objective is to modifying the previously developed polymer microchip for drug delivery applications:

5. Engineer a resorbable sealing mechanism and design the passive microchip to allow implantation through a trocar or large-bore needle (Chapter 7).

Chapter 2 Sensor Device Fabrication

2.1 Summary

The most reliable design for the sensing device is a cup-shaped device made from HDPE. Double-sided pressure-sensitive adhesive is used to seal a polycarbonate membrane to the device substrate. MRSw are added to the reservoir through a filling port on the back of the device which is then sealed with pressure sensitive adhesive. This device design has proven to be very reliable for the *in vitro* and *in vivo* studies carried out to date. The device reservoir, 5 mm in diameter and 2.5 mm deep, allows the T_2 to be quantified using either MRI or single-sided MR.

2.2 Introduction

There are several key elements in the sensor device fabrication and design. The substrate material must be magnetically inert, biocompatible, and able to create a leak proof seal with the MWCO membrane. The device must be filled with the MRSw solution and sealed in a manner that minimizes air bubbles within the reservoir and prevents the MRSw from leaking out of the back of the device. This sealing method cannot employ high temperatures since the MRSw are thermally sensitive. Devices used in *in vivo* sensing experiments will experience mechanical stresses while implanted and the device substrate and membrane must be able to withstand these stresses without failure of the membrane-substrate or substrate-sealing layer bonds. A cup-shaped device has proven to be the most reliable format for *in vitro* and *in vivo* sensing applications. The device substrate is made from high density polyethylene (HDPE) and a pressure-sensitive adhesive is used to seal the polycarbonate membrane to the substrate. *In vitro*

leak tests for several weeks at 37°C have shown that the MRSw are well contained within the reservoirs.

2.3 Materials and Methods

2.3.1 In vitro devices for MRI detection

Polydimethylsiloxane (PDMS) was chosen as the substrate material for the first generation in vitro sensing devices because it is magnetically inert, biocompatible and easily fabricated into arrays of wells. PDMS (Sylgard® 184, Dow Corning, Midland, MI) was prepared according to manufacturer directions in a custom-machined aluminum mold. The mold was placed under a vacuum for at least one hour to remove air bubbles and then cured in a 60°C oven overnight. The devices are 3 mm thick with 2 mm square reservoirs and can be cut into single-reservoir or multi-reservoir devices.

Membrane bonding to PDMS was tested by filling a reservoir with a concentrated non-functionalized MRSw solution (8.43 mg Fe/mL) then applying a thin layer of silicone adhesive (Loctite®, Henkel Loctite Corp, Rocky Hill, CT) between the substrate and MWCO membrane. Polycarbonate (SPI Supplies, West Chester, PA), polyethersulfone (Millipore, Billerica, MA), aluminum oxide (SPI Supplies, West Chester, PA) and nitrocellulose (Millipore, Billerica, MA) were tested. The adhesive was cured at room temperature for at least 24 hours and then the devices were placed in water at 37°C for up to one week. Optical microscopy was used to visually inspect for gross failure of the substrate-MWCO membrane bond.

The ability of polycarbonate membranes (10 nm pores, $6x10^8$ pores/cm^2, SPI Supplies, West Chester, PA) to bond to PDMS was also tested quantitatively. The PDMS substrate was turned on its side and cut to turn the square reservoirs into through holes. The polycarbonate

membrane was adhered to the substrate with a thin layer of silicone adhesive. The adhesive was cured at room temperature for 12 - 24 hours and then the reservoir was filled with a solution of functionalized MRSw (12 μL, 2 - 16 μg Fe/mL). The back of the reservoir was sealed with a pressure sensitive adhesive (Ideal 9144, American Biltrite, Lowell, MA) and the devices were placed in a solution of phosphate buffered saline pH 7.4 with 1 mg/mL bovine serum albumin and 1% penicillin-streptomycin (PBS-BSA-PS) at 37°C. The T_2 of the MRSw in the reservoir was quantified by MRI 3 or 5 hours after being placed in the PBS-BSA-PS bath and again 24 hours later. An increase in T_2 at the second time point would indicate leakage of the MRSw, since T_2 increases as MRSw concentration decreases[43].

2.3.2 In vitro devices for single-sided MR detection

The substrate material and reservoir size were modified to allow for detection with the single-sided MR, which has lower resolution than MRI. Low density polyethylene (LDPE) and high density polyethylene (HDPE), which are more solid polymers than PDMS, were used for the device substrate. These polymers have a lower $T_{2,eff}$ than PDMS, so even if the device substrate is within the sensitive volume of the single-sided MR, it will not interfere with quantifying the $T_{2,eff}$ of the MRSw solution inside the reservoir. An additional benefit with these polymers is increased mechanical strength of the substrate.

Low density polyethylene (LDPE) was cut with cork punches into a washer-shaped device with an inner diameter of 10 mm, outer diameter of 14 mm, and thickness of 2 mm. A thin layer of silicone adhesive or double-sided pressure sensitive adhesive was used to adhere polycarbonate membranes to the washer devices. The devices were filled with functionalized MRSw (160 μL, 8 μg Fe/mL), sealed on the back with a pressure sensitive adhesive, and placed in a solution of PBS-BSA-PS at room temperature. Single-sided MR was used to quantify the

$T_{2,eff}$ of the MRSw in each device immediately after fabrication and again after 12 - 24 hours to confirm that the devices were not leaking.

Washer-shaped devices were also drilled from a sheet of high density polyethylene (HDPE), with an inner diameter of 6 mm, outer diameter of 10 mm, and thickness of 3 mm. Pressure sensitive adhesive was used to adhere the polycarbonate membrane to the HDPE substrate. The devices were filled and sealed in the same manner as the LDPE washer devices.

2.3.3 In vitro and in vivo devices for MRI or single-sided MR detection

Devices were modified to a cup-shaped HDPE substrate to improve reliability during *in vitro* and *in vivo* sensing experiments. Cylinders of HDPE (10 mm diameter) were cut from a 3 mm thick sheet to make the device substrate. The centers of the cylinders were drilled out to create a cup-shaped device with a reservoir that is 5 mm in diameter and 2.5 mm deep. This reservoir size is larger than needed for MRI detection but allows the same device to be measured by MRI and single-sided MR. A 1.5 mm diameter hole was drilled through the bottom of the cup as a filling port. Double-sided pressure sensitive adhesive was used to attach the polycarbonate membrane to the top of the device. The reservoir was filled with 50 μL of MRSw solution through the filling port and it was then sealed with pressure sensitive adhesive. The MRSw solutions were diluted to 8 μg Fe/mL using PBS-BSA-PS. The devices were immediately placed in PBS-BSA-PS and kept at room temperature. Single-sided MR was used to quantify the $T_{2,eff}$ of the MRSw in each device immediately after fabrication and again after 12 - 24 hours to confirm that the devices were not leaking.

2.4 Results and Discussion

2.4.1 Devices for MRI detection

Aluminum oxide, nitrocellulose and polyethersulfone membranes exhibited gross failure of the PDMS/membrane bond after less than one day in solution. These MWCO membranes could be used in future devices with better substrate-adhesion properties, but were not used with the PDMS substrate. Aluminum oxide membranes are also very brittle, so it was difficult to trim them to the appropriate dimensions without creating cracks across the membrane. Visual inspection of the polycarbonate membranes suggested that they were able to bond to the PDMS substrate. Figure 2-1 shows the PDMS devices used for quantitative leak tests and *in vitro* sensing with MRI detection. A concentrated MRSw solution was used for the photo to make the reservoirs more visible. MRSw solutions at the concentrations used for leak tests and *in vitro* sensing (around 8 μg Fe/mL) are colorless.

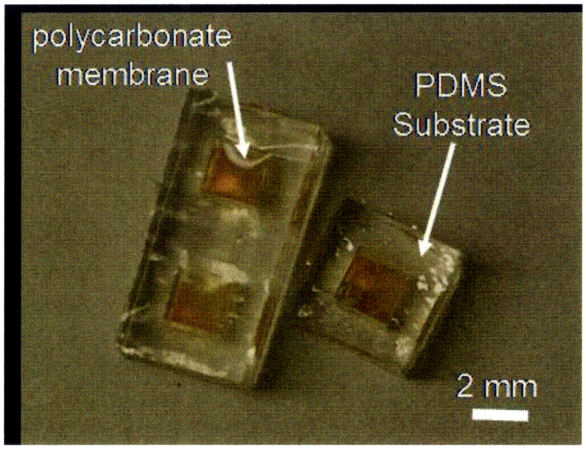

Figure 2-1. PDMS devices for *in vitro* sensing with MRI detection. The devices can easily be fabricated as single or multi-well devices. A concentrated MRSw solution was put in the reservoirs to make them more visible. Each reservoir holds 12 μL of MRSw solution[44].

Figure 2-2 shows quantitative leak test results for PDMS devices with polycarbonate membranes (10 nm pores). All devices showed no significant increase in T_2 one day after being

placed in a bath of PBS, indicating that the MRSw were well contained within the reservoirs. The devices filled with MRSw at a concentration of 2 μg Fe/mL showed more variation in T_2 than other MRSw concentrations, perhaps indicating that this iron concentration is near the detection limit for the MRI protocol used to collect the T_2 data. *In vivo* sensing experiments were done with MRSw concentrations around 8 μg Fe/mL.

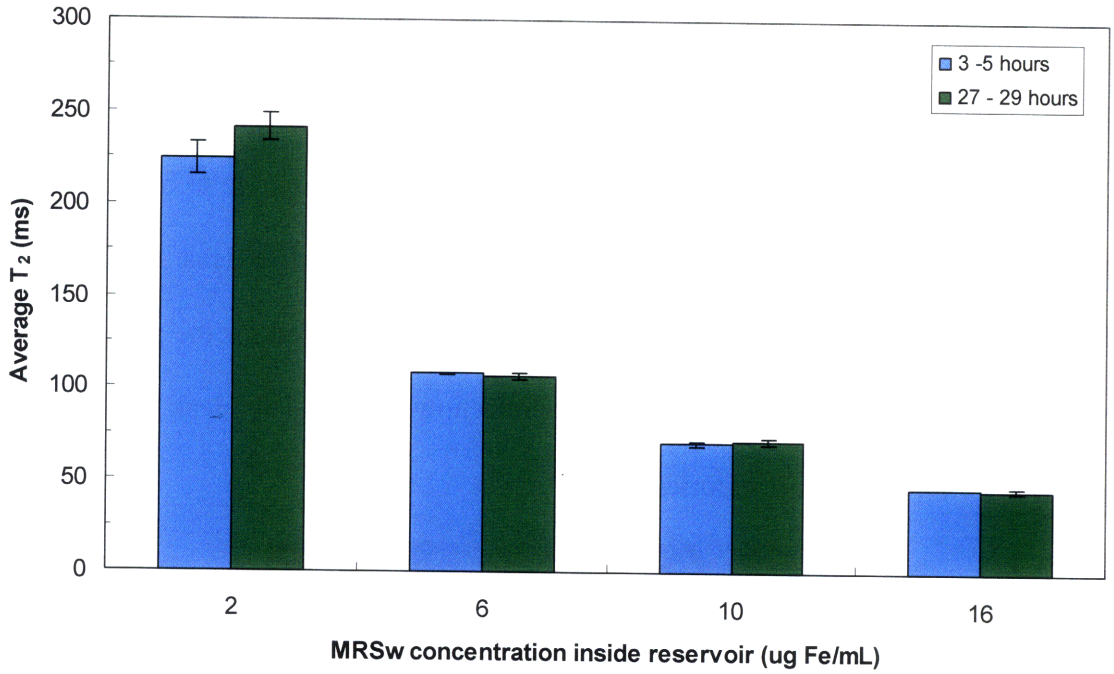

Figure 2-2. Leak test results for PDMS devices with MRI for T_2 detection. Polycarbonate membranes (10 nm pores) were sealed to the device substrate with a silicone adhesive. Devices were stored in PBS at 37°C between the two time points. The first imaging time point was 3-5 hours after the devices were placed in PBS (blue columns) and the second was 27-29 hours after the devices were placed in PBS (green columns). Leaking of MRSw would cause a significant increase in T_2 at the second time point. Error bars represent standard deviation (n≥2 for each group).

2.4.2 Devices for MRI or single-sided MR detection

2.4.2.1 Washer devices

Figure 2-3 shows the washer devices used for *in vitro* sensing with single-sided MR detection. The device on the left uses a silicone adhesive to adhere the polycarbonate membrane

to the LDPE substrate. The device on the right uses a double-sided pressure sensitive adhesive to adhere the polycarbonate membrane to the HDPE substrate.

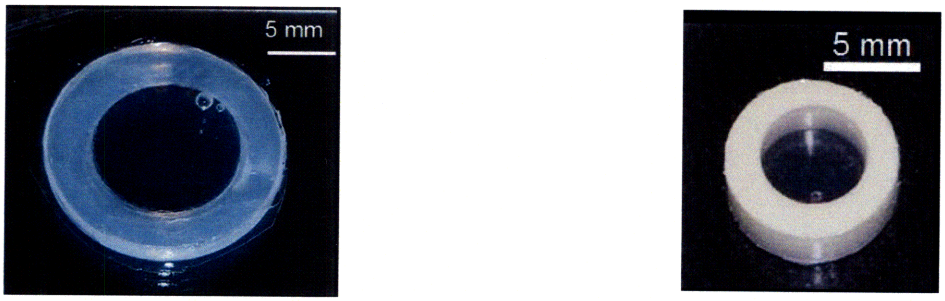

Figure 2-3. Washer devices used for *in vitro* leak tests and sensing experiments. The device on the left is an LDPE substrate and uses a silicone adhesive to seal the polycarbonate membrane to the device substrate. The device on the right is an HDPE substrate with double-sided pressure sensitive adhesive used to adhere the polycarbonate membrane to the device substrate.

Figure 2-4 compares leak test results for LDPE washers with two different methods for adhering the polycarbonate membrane (10 nm pores) to the substrate: silicone adhesive and double-sided pressure sensitive adhesive. Two devices were tested with each method. All four devices were sealed on the back with single-sided pressure sensitive adhesive. Figure 2-4 shows that one of the devices made with pressure sensitive adhesive immediately began leaking when placed in a bath of PBS-BSA-PS, as indicated by the rapid increase in $T_{2,eff}$ (light blue triangles). The other three devices were able to maintain a leak proof seal until day 11, when one of the devices made with silicone adhesive began to show an increase in $T_{2,eff}$ (pink circles). Previous experiments showed that the MRSw are not able to pass through the pores of the polycarbonate membranes (see Sections 3.3.1 and 3.4.1). The leaking of MRSw in this experiment, then, must be from failure of either the substrate/membrane seal at the front of the device or the substrate/pressure sensitive adhesive seal at the back of the device. The most likely failure site is the back of the device, since this seal is done after the reservoir is filled with the MRSw solution and some of the solution often wicks out of the reservoir during sealing.

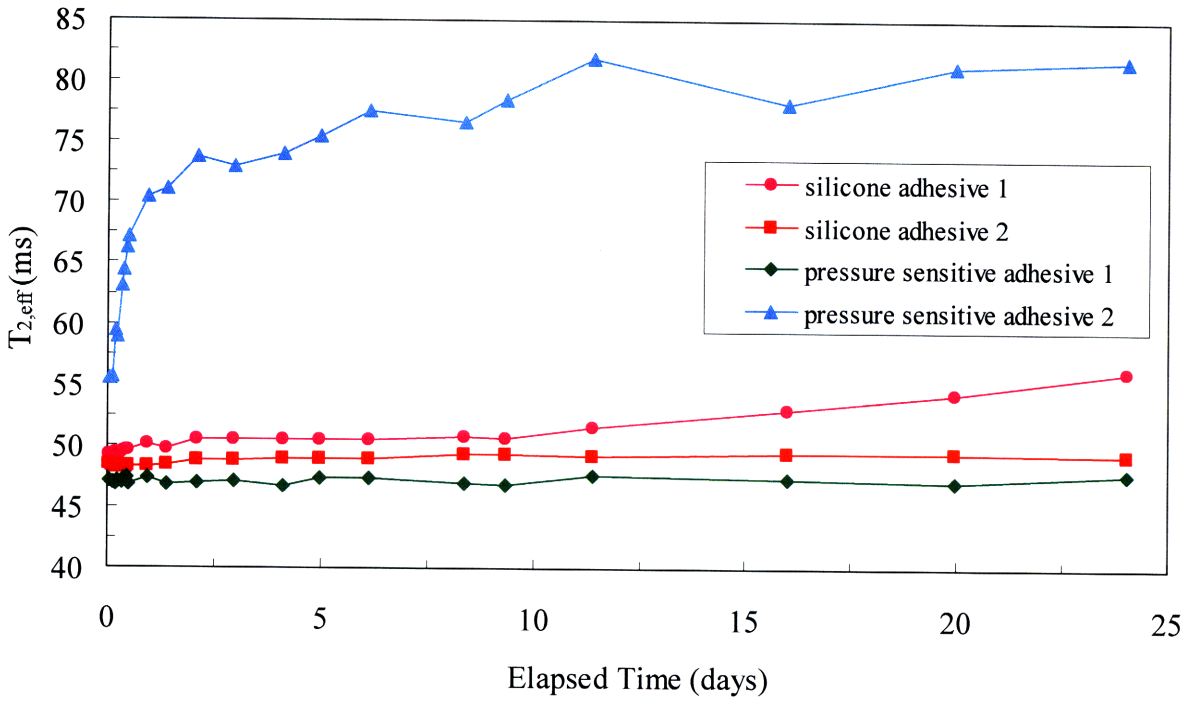

Figure 2-4. Leak test results for LDPE washer-shaped devices in PBS at 37°C. Devices were fabricated with either a silicone adhesive or a double-sided pressure sensitive adhesive to seal the polycarbonate membrane (10 nm pores) onto the device substrate. One device shows immediate leaking of MRSw (blue triangles). A second device initially contains the MRSw within the reservoir, but begins leaking about twelve days later (pink circles).

2.4.2.2 Cup devices

The leak test results shown in Figure 2-4 (1 out of 4 devices immediately leaks MRSw) were common anytime washer-shaped devices were used in a leak test or sensing experiment. Cup-shaped devices were fabricated in an attempt to decrease the number of devices that began leaking MRSw immediately after being placed in PBS. Figure 2-5 is a picture of a cup-shaped device with double-sided pressure sensitive adhesive used to seal a polycarbonate membrane to the HDPE substrate. The membrane is first attached to the top of the reservoir and then the device is turned over and the reservoir filled with MRSw solution through the small hole in the back. Single-sided pressure sensitive adhesive is used to seal the filling hole.

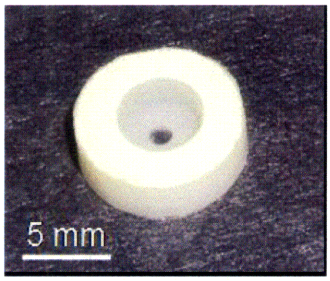

Figure 2-5. Cup device for *in vitro* and *in vivo* sensing experiments with single-sided MR or MRI detection. These devices are made from an HDPE substrate and use double-sided pressure sensitive adhesive to attach the polycarbonate membrane to the substrate. The small hole in the bottom of the cup is a filling port which is sealed with pressure sensitive adhesive after filling the reservoir with the MRSw solution..

Figure 2-6 shows leak test results for four cup-shaped HDPE devices with polycarbonate (10 nm pore) membranes. All four of the devices maintained a constant $T_{2,eff}$ while in PBS at 37°C for over 12 days. Cup-shaped devices were always tested for leaks before being used in an *in vitro* or *in vivo* sensing experiment, but no cup-shaped device ever showed an immediate MRSw leak. This suggests that the immediate leaks seen with washer-shaped devices were probably from failure of the seal at the back of the device. The larger surface area for sealing on the back of the cup devices eliminated this source of device failure.

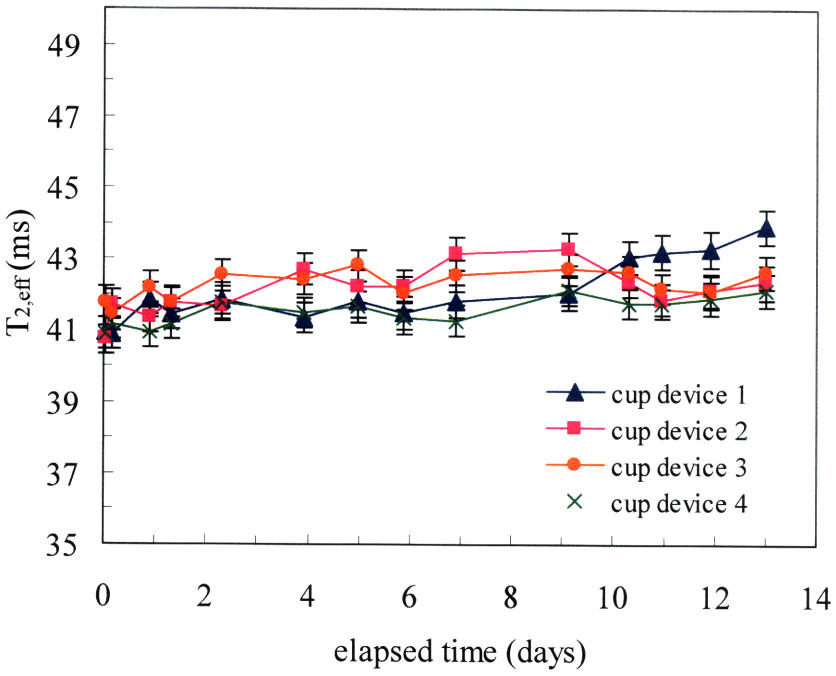

Figure 2-6. Leak test results for four HDPE cup-shaped devices in PBS at 37°C. Devices were made with polycarbonate membranes (10 nm pores) that were sealed to the device substrate with double-sided pressure sensitive adhesive. Single-sided MR was used to quantify the $T_{2,eff}$ in each device. Error bars represent 95% confidence limits in the fit to determine $T_{2,eff}$.

2.5 Conclusion

Several different device designs were made and tested. The most reliable design is a cup-shaped device made from HDPE, with a 5 mm diameter and 2.5 mm deep reservoir. Double-sided pressure-sensitive adhesive is used to seal a polycarbonate membrane to the device substrate. MRSw are added to the reservoir through a filling port on the back of the device which is then sealed with pressure sensitive adhesive. This device design has proven to be very reliable for the *in vitro* and *in vivo* studies carried out to date. The double-sided pressure sensitive adhesive used to seal the MWCO membrane to the device substrate, however, may not be able to create a leak proof seal in longer term sensing experiments. A mechanical means of attaching the MWCO membrane to the device substrate, such as two plastic pieces that are machined to fit

snugly together while holding the membrane in place between them, may improve the long term reliability of the device.

Chapter 3 Characterization of MWCO Membranes

3.1 Summary

Several commercially available membranes are able to retain the MRSw while allowing analyte diffusion. Apparent permeability values for hCG (38 kDa) and dextran (40, 70 and 500 kDa) with polycarbonate membranes (10 nm pores) suggest that for the conditions studied, diffusion is influenced more by the charge and conformation of the analyte rather than the molecular weight. High porosity nano-channel membranes, fabricated in the Cima lab, were also able to retain MRSw functionalized to detect hCG. The apparent permeability for hCG through these nano-channel membranes is about two orders of magnitude higher than for commercially available polycarbonate membranes (10 nm pores). This increased P_{app} is most likely due to the higher porosity (20% for nano-channel membranes vs. 0.05% for polycarbonate membranes) and decreased thickness (50 nm for nano-channel membranes vs. 60 μm for polycarbonate membranes) of the nano-channel membranes.

3.2 Introduction

The MWCO membrane used in the sensing device should allow diffusion of the analyte while restricting diffusion of MRSw, bond to the substrate material (see section 2.3.1) and be biocompatible. Commercially available MWCO membranes were tested first for their ability to restrict diffusion of MRSw. Analyte diffusion through two commercially available membranes, polycarbonate and aluminum oxide that were able to restrict MRSw diffusion was then quantified. High porosity membranes fabricated by Noel Elman, a post doc in the Cima lab, were also characterized. These membranes were fabricated using a novel mass producible process that

combines laser interferometry lithography (LIL) to define nano-channels (pores), and micro-machining techniques to produce free-standing amorphous silicon membranes (Figure 3-1).

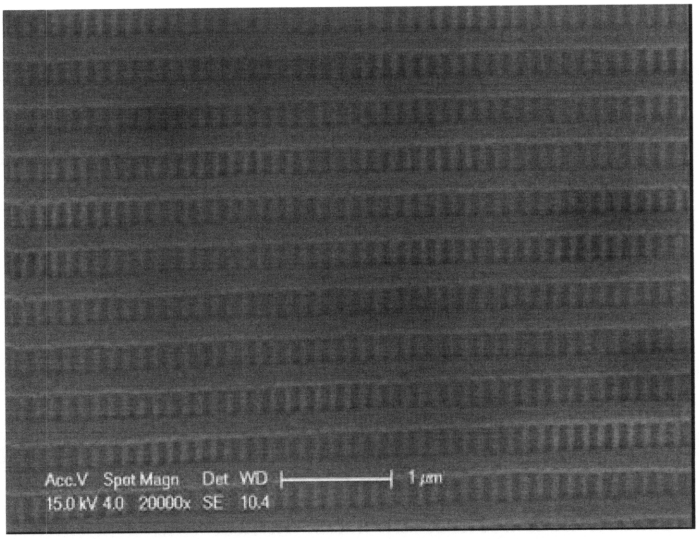

Figure 3-1. High resolution SEM of a high porosity nano-channel membrane fabricated from a combination of laser interferometry lithography and micro-machining tools. A 7x7 array of membranes, each 70x70 µm square, was fabricated with struts between them for increased mechanical support. This image is a a close-up of one of the 70x70 µm square membranes. Image provided courtesy of Noel Elman, PhD.

The chosen membrane material should also be biocompatible, since the MWCO membranes will be used in *in vivo* sensing experiments. Polycarbonate is a common material in medical devices and is considered biocompatible[45,46] but adsorption of biomolecules to nanoporous membranes due to implantation or incubation in serum containing media could impair the device function over time[47]. Adsorption of biological molecules onto the pore walls would reduce the pore size and hinder or completely prevent analyte diffusion through the membrane. Polycarbonate membranes were tested to determine the effects of biomolecule adsorption on analyte diffusion.

3.3 Materials and Methods

3.3.1 Ability to restrict MRSw

Several commercially available MWCO membranes were screened for ability to retain MRSw: Aluminum oxide Anopore™ (20 nm pores) and polycarbonate SPI-Pore™ (10, 30 and 50 nm pores) (SPI-Supplies, West Chester, PA), and polyethersulfone (100, 300 and 500 kDa MWCO), (Millipore Corp, Bedford, MA). These membranes were tested with non-functionalized MRSw which have an effective diameter around 40 nm by dynamic light scattering. MRSw that have been functionalized on the surface with antibodies are usually slightly larger (80-90 nm). The membranes were placed in a syringe-tip filter holder and a solution of CLIO-NH_2 (16 μg Fe/mL) was filtered through each membrane by applying steady, gentle pressure to the syringe plunger. The amount of iron in the filtrate was quantified by proton relaxation time measurements at 0.47 T and 40°C (Bruker NMR Minispec, Billerica, MA).

This strict test for the ability to retain MRSw was used to identify membranes that would be acceptable for use in any sensing experiment. Membranes that can retain the smallest, non-functionalized MRSw when the solution is forced through the membrane will also be able to retain larger functionalized MRSw when the only force for diffusion across the membrane is passive diffusion. A second, less strict, test for the ability to retain MRSw was performed with commercially available polycarbonate membranes (10, 30 and 50 nm pores) and with the high porosity nano-channel membranes that were fabricated in the Cima lab. These membranes were tested to see if they could prevent passive diffusion of functionalized MRSw.

Cup-shaped devices were made with polycarbonate membranes, filled with the functionalized MRSw (80 nm diameter), and placed in PBS/BSA/PS for nearly two weeks. The MRSw were functionalized with antibodies to detect human chorionic gonadotrophin (hCG), a

protein associated with testicular and ovarian cancer. The devices were kept at 37°C and the T_2 of the MRSw in the devices was periodically quantified by single-sided MR. An increase in T_2, caused by a decrease in the MRSw concentration, would indicate that the membrane was not able to retain the MRSw inside the device. The sensitivity of the single-sided MR corresponds to a detection limit of approximately 3% of the MRSw solution initially loaded in the devices.

The high porosity nano-channel membranes were placed in side-by-side glass diffusion cells (PermeGear Inc, Bethlehem, PA) and a concentrated solution (40 μg Fe/mL) of functionalized MRSw (80 nm diameter) was added to the donor side of the diffusion cells. The MRSw were functionalized with hCG protein. The diffusion cells were kept at 37°C for one week and then the solution on the receiver side was removed and the iron concentration in the solution was quantified by proton relaxation time measurements on the single-sided MR (Profile NMR MOUSE, ACT Center for Technology, Aachen, Germany). Dilutions of the concentrated MRSw solution were used to generate a linear calibration curve relating $1/T_1$ to MRSw concentration. The limit of detection using this NMR technique was 0.6 ug Fe/mL, which corresponds to approximately 1.6% of the MRSw concentration that was initially loaded in the diffusion cell.

3.3.2 Analyte diffusion

Side-by-side glass diffusion cells (PermeGear Inc, Bethlehem, PA) or 24-well plate diffusion inserts (Nalge Nunc, Rochester, NY) were used to characterize analyte diffusion through the MWCO membranes. Diffusion experiments were carried out at 37°C in phosphate buffered saline with 1 mg/mL bovine serum albumin (PBS-BSA) to minimize surface adsorption of the analyte. Diffusion of ^{14}C-dextran (Sigma, 40, 70 or 500 kDa), a model analyte, and ^{125}I-hCG (Perkin Elmer, 38 kDa) was studied. The separate components of the diffusion experiment

(membranes, diffusion cells, donor and receiver solutions) were incubated at 37°C for at least 30 minutes before starting the diffusion experiment.

The 24-well plate diffusion inserts, shown in Figure 3-2, feature a 10-mm diameter opening for diffusion and are preassembled with an Anopore™ membrane (0.02 μm pore size, 10^{11} pores/cm^2). The receiver solution (600 uL of PBS-BSA) was added to each well of a 24-well plate, then the diffusion inserts were placed in each well and the donor solution (500 uL of analyte/PBS/BSA solution) was immediately added to each insert. One diffusion insert was removed from the plate at each timepoint, the receiver solution was mixed, and 500 uL removed. Receiver solutions were placed in a scintillation vial with 5 mL of scintillation fluid (ScintiSafe Plus 50%, Fischer Chemicals, Fairlawn, NJ) and the amount of radioactivity was quantified by scintillation (Packard Tri-Carb 2200CA, PerkinElmer, Waltham, MA). Raw data (disintegrations per minute, DPM) were converted to nanocuries (nCi) by using the conversion factor 2,200 dpm = 1 nCi.

Figure 3-2. 24-well plate format for quantifying analyte diffusion through aluminum oxide membranes. A close-up of the diffusion insert is shown in the bottom left corner. The insert held the radiolabeled analyte solution and the solution in the well of the 24-well plate (receiver solution) was removed at each time point to quantify the amount of radioactivity that had diffuse across the membrane. Each time point in a diffusion experiment came from a different membrane.

The side-by-side diffusion cells, shown in Figure 3-3, have a 15 mm or 5 mm diameter opening for diffusion and can be assembled with any MWCO membrane. The side-by-side diffusion cell format was started by simultaneously adding the donor and receiver solutions (approximately 4 mL each). Each compartment was continuously stirred throughout the experiment. The receiver compartment was sampled at each time point by removing 100 uL of solution and replacing it with fresh PBS/BSA. Receiver samples were placed in a scintillation vial with 5 mL of scintillation fluid and the amount of radioactivity was quantified by scintillation.

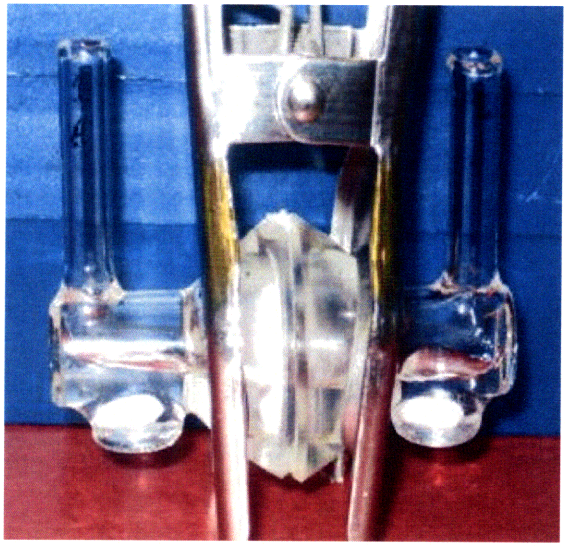

Figure 3-3. Side-by-side diffusion cell used to quantify analyte diffusion. The membrane is clamped between the two glass chambers. A radiolabeled solution is added to one chamber and at each time point a small volume of liquid is removed from the other chamber to quantify the amount of radioactive material that has diffused across the membrane. In this experimental set-up, all the time points are taken using the same membrane.

Diffusion of analyte into the receiver compartment can be described by Fick's first law:

$$\frac{dn_{rec}}{dt} = P_{app} A_c \left(C_d(t) - C_{rec}(t)\right) \tag{3-1}$$

where n_{rec} is the amount of analyte in the receiver compartment, t is time, P_{app} is the apparent permeability of the analyte (with dimensions of length/time), A_c is the cross-sectional area for

diffusion, and $C_d(t)$ and $C_{rec}(t)$ are the analyte concentrations in the donor and receiver compartments at time t, respectively. The diffusion experiment was designed such that initially $C_{rec} << C_d$ and $C_d \approx$ constant. Equation 3-1 simplifies with these conditions to:

$$\frac{dn_{rec}}{dt} = P_{app} A_c C_{d,i} \tag{3-2}$$

where $C_{d,i}$ is the initial concentration of analyte in the donor compartment. Integrating equation 3-2 with the initial condition $n_{rec}(0) = 0$ results in:

$$n_{rec} = P_{app} A_c C_{d,i} t \, . \tag{3-3}$$

The apparent permeability can be calculated from the slope of a n_{rec} vs time plot during the initial diffusion (i.e $C_{rec} < 0.05 C_{d,i}$).

3.3.3 Adsorption of biomolecules

Ex vivo transport studies were performed to determine if adsorption of biomolecules would significantly affect analyte diffusion into the device. Devices for *ex vivo* diffusion studies had a ring-shaped polyethylene substrate (10 mm inner diameter). The devices were filled with a PBS, 0.1% BSA, 1% penicillin-streptomycin solution and sealed on the back with a pressure sensitive adhesive. The devices were soaked overnight in the same PBS/BSA/PS solution. Mice were anesthetized with an intraperitoneal injection of ketamine (100 mg/kg) and xylazine (10 mg/kg). Preemptive analgesics (buprenorphine, 0.1 mg/kg) were administered subcutaneously before the first incision. The mice received a dorsal midline incision, and blunt dissection was used to tunnel subcutaneously to the flank and create a pocket for the device. All devices were placed in the pocket with the membrane facing the muscular layer and the incision was closed with silk sutures. Mice were monitored daily for signs of distress and infection until the incision healed, and were then monitored weekly. The devices were left in the mice for either one week

or one month and then explanted. The pressure sensitive adhesive on the back of the device was removed after explantation and the device was placed in a side-by-side diffusion cell (PermeGear) to quantify diffusion of ^{14}C-dextran (40 kDa, Sigma-Aldrich) through the membrane (see section 3.3.2). All work involving mice was performed according to the policies of the Massachusetts Institute of Technology Committee on Animal Care. Mice were housed in autoclaved cages and had access to autoclaved food and water *ad libitum*.

3.4 Results

3.4.1 Ability to restrict MRSw

Several of the MWCO membranes tested are able to restrict diffusion of the non-functionalized MRSw (Table 3-1). Polycarbonate membranes (10 nm pores), aluminum oxide membranes (20 nm pores), and polyethersulfone membranes (100 and 300 kDa MWCO) can prevent the small non-functionalized MRSw from passing through even when the MRSw solution is forced across the membrane. These membranes would be suitable for use in many different *in vitro* and *in vivo* sensing applications.

Table 3-1. MRSw Retention Results

Material	Membrane Cut-Off Value	Retain Non-Functionalized MRSw?
Polycarbonate	10 nm pores	Yes
	30 nm pores	No
	50 nm pores	No
Aluminum Oxide	20 nm pores	Yes
Polyethersulfone	100 kDa*	Yes
	300 kDa*	Yes
	500 kDa*	No

* An approximate conversion factor, assuming a globular protein conformation, is 100 kDa ~ 10 nm.

Two high porosity nano-channel membranes that were fabricated in the Cima lab were able to retain functionalized MRSw (80 nm diameter) during a one week leak test. Figure 3-4 shows the $1/T_1$ values (measured using the single-sided MR) plotted against iron concentration, with a relaxivity (R1) of $4.2x10^{-4}$ μg Fe/(mL*ms). After one week, the receiver solutions were removed and the iron concentration for one of the membranes was found to be below the detection limit (0.6 μg Fe/mL), meaning that more than 98.6% of the MRSw were retained by the membrane. The concentration of the receiver solution for the other membrane was 0.7 μg Fe/mL indicating that only 1.8% of the MRSw loaded in the donor cell was able to diffuse across the membrane during one week. The high porosity nano-channel membranes are more brittle than the commercially available polycarbonate membranes, and several nano-channel membranes fractured during either analyte diffusion tests or MRSw leak tests. The design of the nano-channel membranes can be changed to improve the mechanical stability. This would allow the membranes to be used in device-based *in vitro* and *in vivo* sensing experiments.

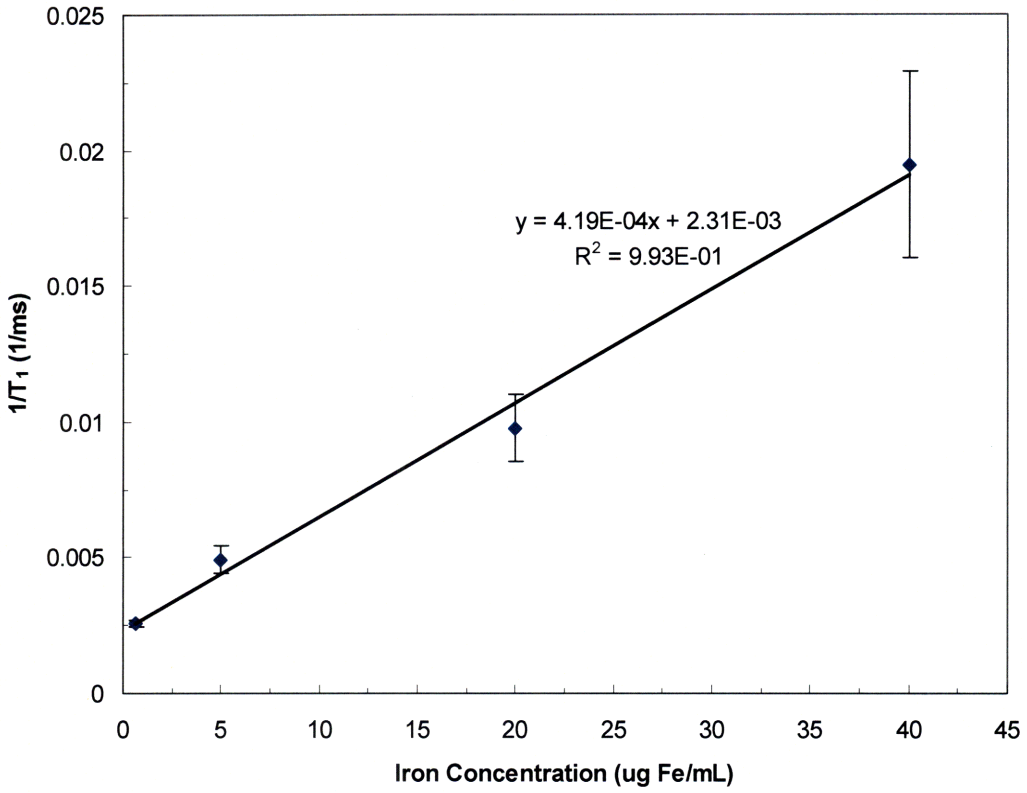

Figure 3-4. Relaxivity curve for calculating iron concentration in MRSw leak test with high porosity nano-channel membranes. Error bars are calculated from the 95% confidence interval in the fit to determine T_1.

Figure 3-5 shows MRSw leak test results for devices made with polycarbonate membranes. Devices made with polycarbonate membranes with 50 nm pores showed a significant increase in $T_{2,eff}$ after only two days, indicating that MRSw were able to diffuse out of the reservoir by passing through the MWCO membrane. The $T_{2,eff}$ for the devices made with polycarbonate membranes with 10 or 30 nm pores, however, were approximately constant for nearly two weeks. This indicates that the MRSw were well contained within these devices, according to the detection limit of the single-sided MR (able to detect a leak of 3% or more of the MRSw solution in the device). This result was expected for the 10 nm pore membranes, since they were able to retain non-functionalized MRSw when the solution was forced across the membrane. The 30 nm pore membranes, however, allowed a significant portion of the non-

functionalized MRSw to cross the membrane when the solution was forced across the membrane. These leak test results suggest that the 30 nm pore membranes would be an appropriate choice for functionalized MRSw in short term (up to two week) sensing experiments. The benefit in using 30 nm pore membranes in sensing experiments is that the percent porosity of the 30 nm pore membranes (0.4%) is nearly ten times higher than for the 10 nm pore membranes (0.05%), and therefore analyte diffusion should be faster in devices made with the 30 nm pore membranes.

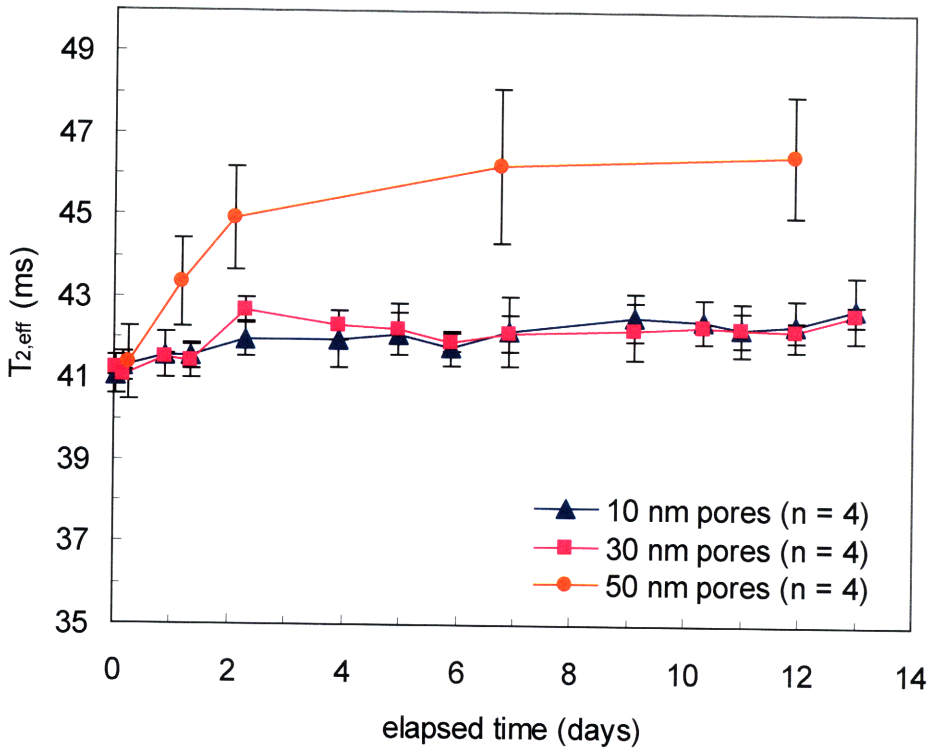

Figure 3-5. MRSw leak test for polycarbonate membranes with larger pores sizes and higher porosity. Cup-shaped devices were in this leak test with pressure-sensitive adhesive for sealing the membrane to the device substrate. The highest porosity membranes (50 nm pores, orange circles) showed immediate leaking of MRSw. Error bars represent standard deviation (n = 4 in each group).

3.4.2 Analyte diffusion

We have demonstrated that high molecular weight analytes (38 kDa protein and up to 500 kDa dextran) are able to diffuse through polycarbonate membranes with 10 nm pores. Figure 3-6 is an example of data collected from side-by-side diffusion experiments with polycarbonate (10

nm pore) membranes. The slope of the trendline is directly equal to the apparent permeability, with units of μm/min.

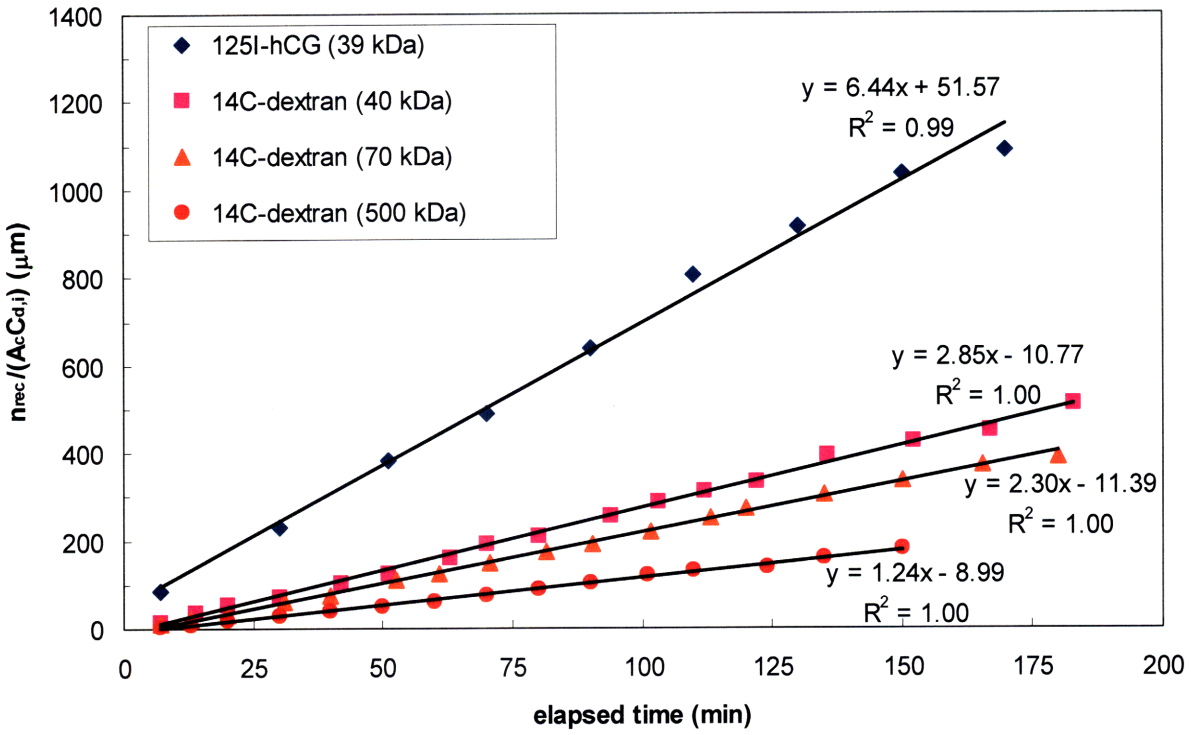

Figure 3-6. Typical data for analyte diffusion through a polycarbonate (10 nm pore) membrane at 37°C. Data was collected using a side-by-side glass diffusion cell.

Table 3-2 shows the apparent permeability of several different compounds through the polycarbonate, aluminum oxide, and high porosity nano-channel membranes. For the polycarbonate and aluminum oxide membranes, P_{app} of 40 and 70 kDa ^{14}C-dextran are similar, but P_{app} of ^{125}I-hCG (~ 38 kDa) is significantly higher than 40 kDa dextran. This observation suggests that for the range considered here, molecular weight is not the controlling factor in diffusion. Previous studies have shown that analyte charge and conformation and membrane characteristics (size, pore density, thickness, and charge) can also play a role in determining

P_{app}[48-50]. The polycarbonate membranes were also tested with 500 kDa dextran, which has a P_{app} approximately half that of 40 and 70 kDa dextran, indicating that molecular weight is beginning to have an effect on diffusion at this size. The hydrodynamic radius of 40 and 70 kDa dextran is similar (4.8 and 6.5 nm respectively) while 500 kDa dextran has a larger hydrodynamic radius (16 nm)[51]. The hydrodynamic radii were calculated from viscosity data and represent the size of a solid spherical particle that would be required to cause the same change in viscosity as observed with the dextran molecules. The P_{app} is higher in the Anopore™ and nano-channel membranes than the SPI-Pore™ membranes, which is most likely due to different porosities (31% for Anopore™, 20% for nano-channel, and 0.05% for SPI-Pore™). Although the aluminum oxide membranes have a slightly higher percent porosity than the high porosity nano-channel membranes, the P_{app} of ^{125}I-hCG with the nano-channel membrane is more than twice as high as with the aluminum oxide membrane. This is most likely due to the different thickness of the two membranes: the pores in the aluminum oxide membrane are approximately 60 μm thick while the nano-channels in the high porosity nano-channel membrane are only about 50 nm thick. The shorter diffusion path in the high porosity nano-channel membranes results in a larger P_{app}.

Table 3-2. Analyte Diffusion Results

			P_{app} (μm/min)			
Membrane	Percent Porosity (%)	Pore Size (nm)	^{14}C-Dextran			^{125}I-hCG (~38 kDa)
			40 kDa	70 kDa	500 kDa	
Aluminum oxide	31	20	15.8±0.5	19.6±0.4	*	50±2
Polycarbonate	0.05	10	2.81±0.07	2.5±0.1	1.24±0.02	6.4±0.3
High porosity nano-channel	20	60	*	*	*	170±70

* indicates that this analyte/membrane combination was not tested

The membrane permeability calculated from these diffusion experiments can be used to predict analyte concentration inside a device at different time points. The *in vitro* sensing experiments can be designed such that $V_d >> V_{rec}$, so the assumption that $C_d \approx$ constant is still a valid approximation. Equation 3-1 under this assumption simplifies to:

$$\frac{dC_{rec}}{dt} = \frac{P_{app}A_c}{V_{rec}}\left(C_{d,i} - C_{rec}(t)\right). \tag{3-4}$$

Integrating equation 3-4 with the initial condition $C_{rec}(0) = 0$ results in:

$$C_{rec} = C_{d,i}\left(1 - e^{\left(\frac{-P_{app}A_c}{V_{rec}}t\right)}\right). \tag{3-5}$$

From the P_{app} for ^{125}I-hCG (6.4 μm/min for 10 nm pore polycarbonate membranes) and using typical *in vitro* device dimensions (A_c = 0.02 cm^2 and V_{rec} = 0.05 mL) the concentration inside the reservoir should be approximately 95% of the donor bath concentration after approximately 20 hours. MR imaging in animal or clinical studies will be conducted on a daily or weekly basis, so equilibrium diffusion time of approximately one day is an appropriate time frame for an *in vivo* cancer sensor. The time to reach equilibrium for the same size device could be decreased to approximately 7 hours if high porosity nano-channel membranes (P_{app} = 170 μm/min) were used in the devices.

3.4.3 Adsorption of biomolecules

Ex vivo diffusion studies have shown that there is no noticeable decrease in analyte transport after the membranes have been implanted for one week or one month. The apparent permeability (P_{app}) for the analyte (dextran, 40 kDa) through the conditioned membranes (one week: 3.0 +/- 0.5 μm/min, n=3, one month: 2.9 +/- 0.2 μm/min, n = 3) was approximately the

same as the P_{app} for fresh membranes (2.81+/- 0.07 μm/min, n=3)[44] (p = 0.7 for one week, p = 0.4 for one month). Three of the one month devices showed a dramatic increase in the analyte diffusion rate, indicating the presence of a defect in the membrane. These devices were excluded from the P_{app} analysis, resulting in n = 3 for the P_{app} calculations. These results indicate that adsorption of biomolecules onto the membrane pores does not have a significant effect on analyte transport into the device for the implantation duration reported here. The higher variability in the P_{app} of the conditioned membranes may be caused by manipulation of the membranes during the device fabrication and implantation process.

3.5 Conclusion

Several commercially available membranes were identified that are able to both retain MRSw and allow analyte diffusion. Analyte diffusion times are reasonable for an *in vivo* cancer sensor device. The effect of biomolecule adsorption on polycarbonate membranes was tested in an animal model. The diffusion of dextran (40 kDa) does not change significantly after the membranes have been implanted for up to one month. High porosity nano-channel membranes, made in the Cima group, were also tested. These membranes were able to retain MRSw functionalized to detect hCG. The apparent permeability of hCG through the nano-channel membranes is about two orders of magnitude higher than for commercially available polycarbonate membranes (10 nm pores). Future studies should examine the effects of longer implantation times and fibrous capsule formation on membrane biofouling and analyte transport. Recent work with a silicon device gives promising evidence that a fibrous capsule may not significantly hinder protein transport up to 6 months in beagle dogs[52]. Previous research has shown that permeability of polycarbonate membranes *in vivo* can be enhanced by plasma surface

treatment[45]. We will explore this technique if *in vivo* transport kinetics vary significantly from *in vitro* results after longer implantation times.

Chapter 4 Characterization of MRSw Aggregation

4.1 Summary

Several batches of MRSw functionalized to detect hCG were tested to determine the stability of the MRSw, stability of the aggregates, and kinetics of aggregation. Some batches of high valency MRSw were not suitable for device-based sensing, due to insolubility and precipitation of aggregates. The batch of MRSw referred to as Cmix-3000 was found to form stable aggregates in an appropriate time frame for device-based sensing. Cmix-3000 is a 50:50 mixture of C95-6 (3.5 Ab/CLIO) and C97-7 (3.7 Ab/CLIO). Many of the *in vitro* and *in vivo* sensing experiments described in this thesis were performed with Cmix-3000.

4.2 Introduction

MRSw have previously demonstrated sensitive and specific aggregation in *in vitro* agglutination assays[21-26]. These aggregation experiments, however, were carried out under laboratory conditions that are difficult to reproduce in a device setting: the MRSw are stored at 4°C before use, they are thoroughly mixed with the analyte solution, and the T_2 of the MRSw/analyte solution is quantified within ten minutes. A device-based sensing experiment requires the MRSw to be kept inside the device at 37°C, the analyte must first diffuse across the semi-permeable membrane and then throughout the MRSw solution, and the T_2 measurement has to be delayed to allow sufficient time for diffusion and aggregation. Previous work has shown that MRSw behavior can vary significantly from batch to batch[26] and that insolubility and precipitation of aggregates is a common problem[26,28] with higher valency MRSw. MRSw that formed stable aggregates with hCG concentrations up to 6 μg hCG/mL were preferred for the *in*

vitro and *in vivo* sensing experiments. The stability of the MRSw and the aggregates for specific batches of MRSw functionalized to detect hCG was studied. The kinetics of aggregation when the analyte is thoroughly mixed with the MRSw was also studied. The results of these experiments were used to design *in vitro* and *in vivo* device-based sensing experiments.

4.3 Materials and Methods

4.3.1 Stability of MRSw

The ability of MRSw to aggregate depends on the stability of the antibodies attached to the surface of the nanoparticle. The MRSw response to hCG was tested immediately after each batch was functionalized. The two populations of MRSw (C95 and C97) were mixed in equal ratios and diluted with PBS-BSA-PS to an MRSw concentration of 16 μg Fe/mL. Dilutions of hCG (Sigma-Aldrich, St. Louis, MO), from 0.33 to 13.6 μg hCG/mL, were prepared in PBS-BSA-PS. Equal volumes of the MRSw and hCG solutions were mixed together in an 8-well strip and the $T_{2,eff}$ for each solution was quantified using the single-sided MR. The final MRSw concentration was 8 μg Fe/mL and the final hCG concentrations ranged from 0.165 to 6.8 μg hCG/mL. A control solution (8 μg Fe/mL, 0 μg hCG/mL) was also prepared and measured. Stock solutions of the MRSw populations were stored at 4°C. This test of the response of the MRSw to hCG was repeated periodically to ensure that the MRSw were still able to aggregate in the presence of hCG.

The ability of the MRSw to aggregate after being stored at 37°C for one month was also studied. Long term *in vivo* sensing experiments will depend on the MRSw being able to retain their activity when stored in the device at 37°C. The behavior of the MRSw in response to hCG was tested as described above, and then some MRSw solution (50:50 mixture of the two

populations at 16 μg Fe/mL) was placed in an eppendorf tube and incubated at 37°C for one month. The same test of the MRSw ability to aggregate in the presence of hCG was repeated at the end of the one month incubation period.

4.3.2 Stability of aggregates and kinetics of aggregation

Successful *in vivo* sensing depends on the aggregates being able to form and then remain stable enough to cause a decrease in T_2 after being incubated at 37°C for up to four days. The kinetics of aggregation and stability of aggregates was tested using the same hCG/MRSw solutions described above (Section 4.3.1). The hCG/MRSw solutions were stored in a capped 8-well strip at 37°C and the $T_{2,eff}$ of the solutions was measured periodically using single-sided MR. The solutions were allowed to cool to room temperature before each reading.

4.4 Results

4.4.1 Stability of MRSw

The combination of MRSw batches that proved to be the most stable when stored at 4°C were the sixth batch of C_{95} particles (3.5 Ab/CLIO) and the seventh batch of C_{97} particles (3.7 Ab/CLIO). These batches were prepared at the end of September 2007 and this specific combination of MRSw populations is referred to as Cmix-3000. Figure 4-1 (orange bars) shows the response of Cmix-3000 to hCG solutions of 0, 0.167, 0.34, 0.68 and 1.67 μg hCG/mL just days after they had been functionalized. The green bars in Figure 4-1 show the response of the Cmix-3000 MRSw after the stock solutions had been stored at 4°C for seven months. One thing to note from Figure 4-1 is that the $T_{2,eff}$ value for each solution increased slightly after seven months in storage. This is most likely due to precipitation of some particles in the stock solutions, resulting in an actual iron concentration that is slightly lower than expected (a decrease

in iron concentration corresponds to an increase in $T_{2,eff}$). The second thing to note from Figure 4-1 is that after 7 months of storage at 4°C the MRSw are still able to aggregate and the decrease in $T_{2,eff}$ when the MRSw are mixed with hCG is just as pronounced as it was immediately after the MRSw were functionalized. Another batch of MRSw that were tested (C95-4 and C97-4) had a decrease in $T_{2,eff}$ that was much smaller in magnitude when comparing MRSw that had been stored at 4°C for just over four months to recently functionalized MRSw.

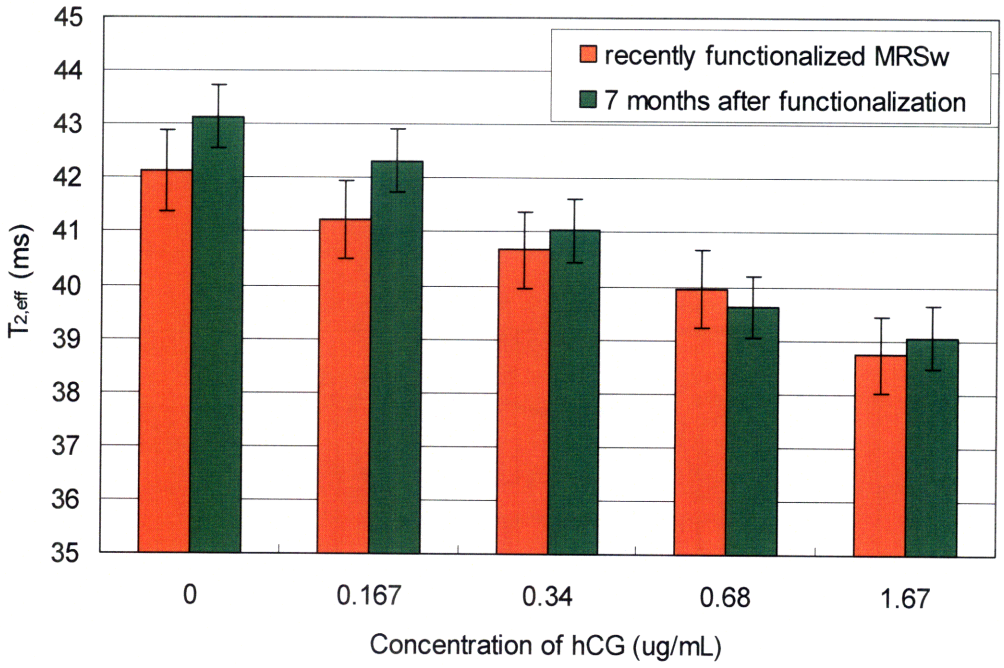

Figure 4-1. Ability of MRSw (Cmix-3000) to aggregate in the presence of hCG. MRSw and hCG solutions were mixed together and placed in an 8-well strip. $T_{2,eff}$ values shown are from approximately 10 minutes after the two solutions were mixed. Orange bars represent the behavior of Cmix-3000 a few days after it was functionalized to detect hCG. Green bars represent Cmix-3000 after stock solutions are stored at 4°C for 7 months. Error bars represent 95% confidence intervals in the fit to determine $T_{2,eff}$.

The ability of Cmix-3000 to aggregate in the presence of hCG after being stored at 37°C for one month was also studied. Cmix-3000 was stored at 16 μg Fe/mL. Figure 4-2 shows the behavior of Cmix-3000 MRSw a few days after they were functionalized to detect hCG (orange bars) and again after the stock solutions had been stored at 37°C for one month (green bars). The

$T_{2,eff}$ of all solutions increased after one month at 37°C, again most likely caused by some MRSw precipitating out of solution. The magnitude of the shift up in $T_{2,eff}$ is larger than was observed when the MRSw were stored at 4°C for one month. A more significant change is that the magnitude of the $T_{2,eff}$ decrease with addition of hCG is dramatically reduced after incubation at 37°C for one month. Concentrations that showed a significant decrease in $T_{2,eff}$ initially are now very similar to the $T_{2,eff}$ of the control solution.

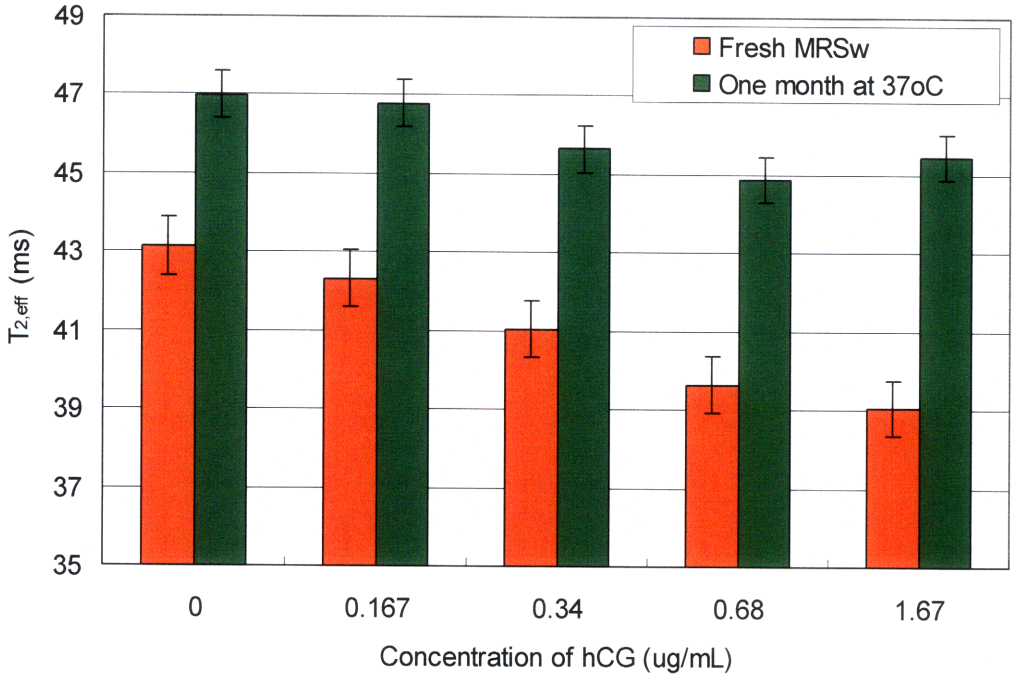

Figure 4-2. Ability of MRSw (Cmix-3000) to aggregate in the presence of hCG. MRSw and hCG solutions were mixed together and placed in an 8-well strip. $T_{2,eff}$ values shown are from approximately 10 minutes after the two solutions were mixed. Orange bars represent the behavior of Cmix-3000 after it had been stored at 4°C for seven months. Green bars represent the behavior of Cmix-3000 after the stock solutions were stored at 37°C for one month. Error bars represent 95% confidence intervals in the fit to determine $T_{2,eff}$.

4.4.2 Stability of aggregates

Stable aggregates are required for successful *in vivo* sensing. Figure 4-3 shows the behavior of low valency MRSw over nearly ten days. The MRSw solution is a 50:50 mixture of C95-4 (2.0 Ab/CLIO) and C97-4 (2.3 Ab/CLIO) at a final concentration of 8 μg Fe/mL. When

the MRSw are mixed with hCG at a final concentration of 0.68 μg hCG/mL (ratio of one hCG molecule per MRSw particle) (filled pink circles) stable aggregates are formed, as seen by a decrease in $T_{2,eff}$ that is stable over the course of the experiment. The control solution (MRSw with no hCG present, open pink circles) also remains constant over the course of the experiment. These MRSw were used in initial *in vitro* sensing experiments.

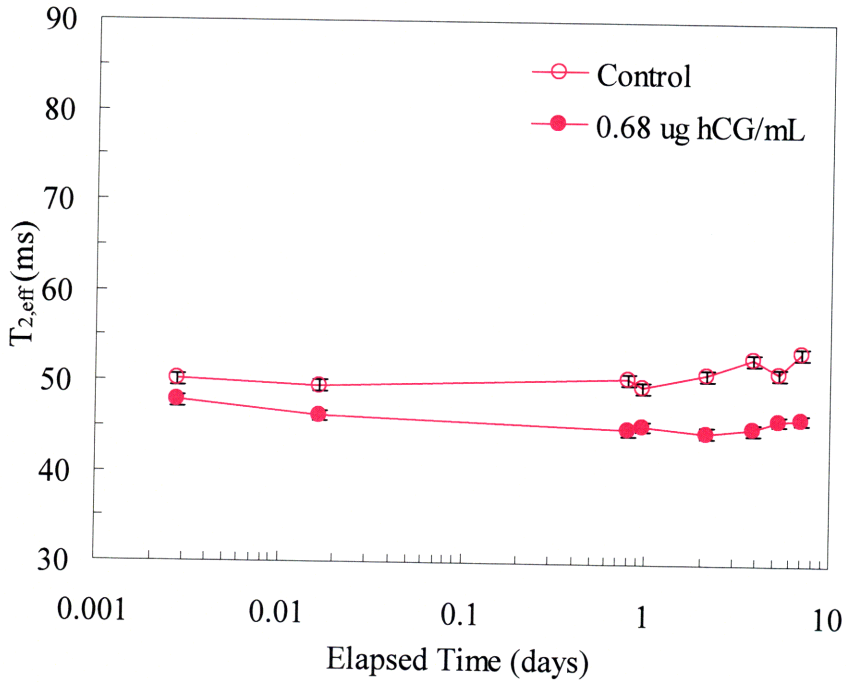

Figure 4-3. Aggregate stability with low valency MRSw. A 50:50 mixture of C95-4 (2.0 Ab/CLIO) and C97-4 (2.3 Ab/CLIO) was mixed with an equal volume of PBS or hCG and $T_{2,eff}$ was periodically measured using single-sided MR. Final MRSw concentration was 8 μg Fe/mL for the control and sample solutions. Final hCG concentrations for the control and sample solutions were 0 and 0.68 μg hCG/mL, respectively. Solutions were kept at 37°C between time points. Error bars represent 95% confidence interval in the fit to determine $T_{2,eff}$.

Figure 4-4 shows the behavior of high valency MRSw over nearly ten days. This MRSw solution is a 50:50 mixture of C95-2 (4.1 Ab/CLIO) and C97-2 (4.5 Ab/CLIO) at a final concentration of 8 μg Fe/mL. There is an immediate decrease in $T_{2,eff}$, caused by aggregation of the MRSw, when the MRSw are mixed with hCG at a concentration of 0.68 μg hCG/mL (ratio of one hCG molecule per MRSw particle, filled green squares). The $T_{2,eff}$ is not stable, however, and

just 30 minutes after mixing the two solutions together the $T_{2,eff}$ of the hCG solution is higher than the control solution (open squares). The $T_{2,eff}$ of the control solution (no hCG) remains stable over the course of the experiment. Particle size data for these high valency MRSw confirm that the aggregates quickly grow to about one micron in size[26]. Precipitates can be seen on the bottom of the cuvette if the solutions are left standing overnight. These MRSw were not used in device-based sensing experiments since instability and precipitation of aggregates was observed even at the relatively low hCG concentration of 0.68 μg hCG/mL.

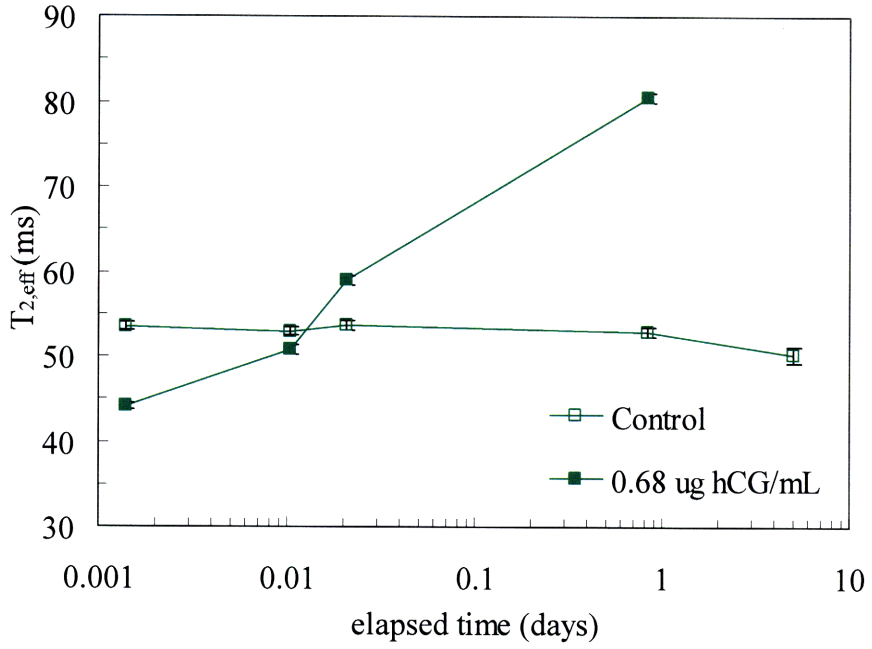

Figure 4-4. Aggregate instability with high valency MRSw. A 50:50 mixture of C95-2 (4.1 Ab/CLIO) and C97-2 (4.5 Ab/CLIO) was mixed with an equal volume of PBS or hCG and $T_{2,eff}$ was periodically measured using single-sided MR. Final MRSw concentration was 8 μg Fe/mL for the control and sample solutions. Final hCG concentrations for the control and sample solutions were 0 and 0.68 μg hCG/mL, respectively. Solutions were kept at 37°C between time points. Error bars represent 95% confidence interval in the fit to determine $T_{2,eff}$.

Kinetics of aggregation when MRSw and hCG are thoroughly mixed together was studied for Cmix-3000. Figure 4-5 shows that the lower hCG concentration solutions (blue diamonds and pink squares) cause a small but steady decrease in $T_{2,eff}$ over three days at 37°C.

The control solution (no hCG present, open purple circles) also exhibits a stable $T_{2,eff}$. The higher hCG concentrations, however, (orange triangles and brown circles) show an immediate drop in $T_{2,eff}$ and then a continued decrease in $T_{2,eff}$ for nearly 24 hours at the highest hCG concentration (6.8 μg hCG/mL). This data suggests that smaller aggregates form rather quickly at low and high hCG concentrations, but at high hCG concentrations the aggregates continue to grow for up to 24 hours after mixing. These MRSw were used for both *in vitro* and *in vivo* sensing experiments because they form stable aggregates at the range of hCG concentrations studied. Even these MRSw, however, would be expected to show instability of aggregates at either higher hCG concentrations or longer times.

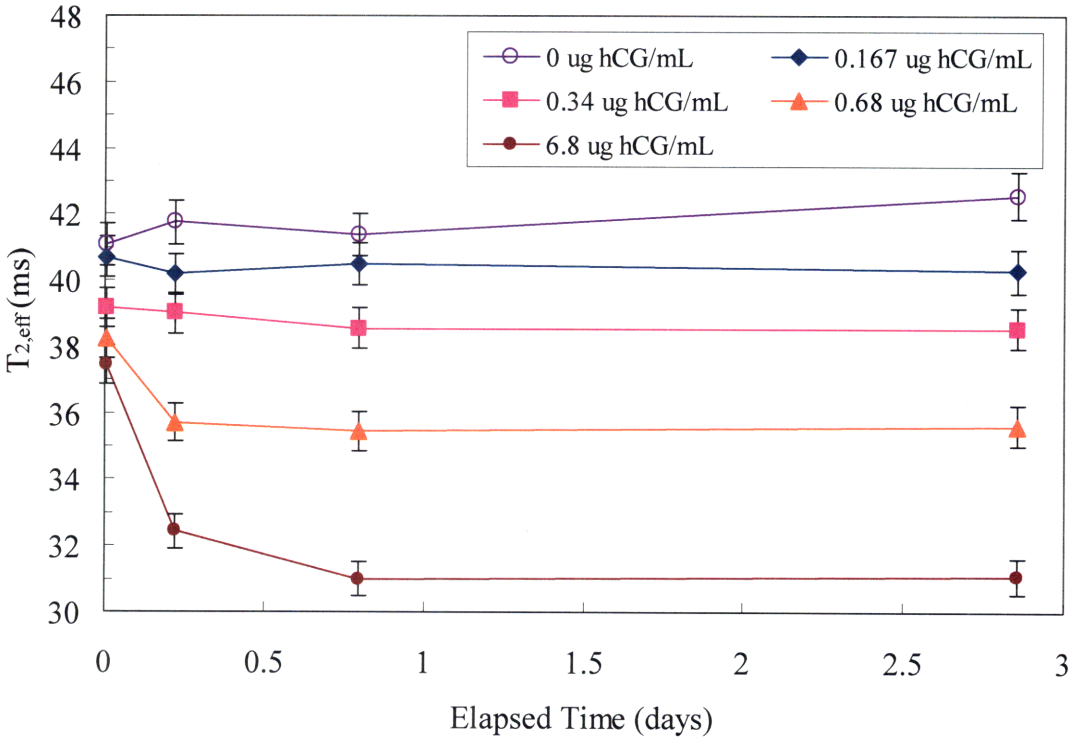

Figure 4-5. Kinetics of aggregation when analyte and MRSw are thoroughly mixed together. The MRSw batch used in these experiments is Cmix-3000. Solutions were stored in an 8-well strip at 37°C between time points. Error bars represent 95% confidence limits in the fit to determine $T_{2,eff}$.

Figure 4-3, Figure 4-4 and Figure 4-5 show that the time required for larger aggregates to form depends both on MRSw valency and hCG concentration. This delayed aggregation could have a significant impact on device-based sensing. The concentration of hCG inside the device will be roughly equal to the hCG concentration outside the device after one day in the analyte bath solution (see Section 3.4.2) for the *in vitro* and *in vivo* sensing devices considered in this thesis. The delay in aggregation should not significantly affect the behavior of the device since both events (diffusion and aggregation) are occurring on the same time scale for the MRSw and hCG concentration ranges shown in Figure 4-5. The smaller aggregates will form quickly and the larger aggregates will have time to form as the hCG continues diffusing into the reservoir. Higher hCG concentrations, however, could take longer than 24 hours to reach a stable $T_{2,eff}$. This would result in the $T_{2,eff}$ continuing to decrease past the time when the hCG concentration inside the reservoir is calculated to be at equilibrium.

4.5 Conclusion

The batch of MRSw referred to as Cmix-3000 was found to retain activity after being stored at 4°C for seven months. Much of the activity of Cmix-3000 was lost, however, after incubation at 37°C for one month. The MRSw were still able to aggregate, but the operating range of hCG concentrations was significantly smaller and the decrease in $T_{2,eff}$ was less pronounced. Stability of aggregates was found to be a function of both MRSw valency and hCG concentration, as expected. Cmix-3000 was found to form stable aggregates for a range of hCG concentrations relevant to *in vivo* experiments and this batch of MRSw was used for many device-based sensing experiments. The kinetics of aggregation for Cmix-3000 may take longer than diffusion of hCG into the device for higher hCG concentrations. This would result in a prolonged decrease in $T_{2,eff}$ in device-based sensing experiments.

The ability to perform long term *in vitro* and *in vivo* sensing experiments depends on MRSw that retain activity when stored at 37°C and produce stable aggregates. Previous work has demonstrated that stabilization of MRSw aggregates can be achieved by trapping them in a matrix that prevents the aggregates from precipitating out of solution[53]. Stability of the MRSw at 37°C may be able to be improved by adding PEG as a linker when attaching the antibodies to the surface of the MRSw[54] or by adding hydrophobic mutations or disulfide bonds to the antibody[55].

Chapter 5 *In Vitro* Device-Based Sensing

5.1 Summary

These *in vitro* sensing experiments are the first step in developing an implantable device for sensing soluble cancer related analytes. These devices have the potential for real time and noninvasive repeat monitoring of local conditions *in vivo* and the format lends itself to a multiplexed device to allow sensing of multiple analytes. We have demonstrated that the analyte (hCG) is able to diffuse across the semi-permeable membrane and cause aggregation of the MRSw. These MRSw aggregates are stable enough in the sensing device to show a T_2 decrease after being incubated in analyte solutions at 37°C for up to three weeks. The stability of the aggregates depends on the concentration of analyte being detected and the type of membrane used in the device. Higher porosity membranes lead to less stable aggregates, suggesting that the increase in T_2 at longer times is caused by either the prozone effect or the aggregates growing so large that they precipitate out of solution.

5.2 Introduction

There are several unique advantages to the sensing device described here. First, MR imaging can be used to read the device even if it is implanted deep within the body. Second, the fixed reservoir volume maintains a constant iron concentration. Changes in T_2 can be directly attributed to changes in aggregate size, which allows for quantitative analysis of analyte concentrations. The optimum MRSw concentration for a sensing experiment depends on both the concentration of analyte being detected and the sensitivity of the NMR technique used to

quantify T_2[26]. These *in vitro* sensing experiments are an important first step in developing an implantable sensor for detecting soluble cancer biomarkers *in vivo*.

5.3 Materials and Methods

5.3.1 MRI detection

PDMS devices were fabricated as described in section 2.3.1 and filled with a 50:50 mixture of the two MRSw populations functionalized to detect hCG (C_{95} and C_{97}) with a final MRSw concentration of 2, 6, 10 or 16 μg Fe/mL. Solutions of known hCG-b concentrations (Scripps Laboratories, 28 kDa) were made in PBS-BSA. The devices were placed in the hCG-b solutions (0.5, 1.5, 3.0 or 5.0 μg hCG-b/mL) at 37°C. These analyte concentrations were previously shown to be in the appropriate range for detection with the MRSw functionalized to detect hCG[26]. Control devices were placed in PBS-BSA. There were at least two devices in each group.

The first sensing experiment with MRI detection was conducted using a 24-well plate to hold the devices and analyte bath solutions. The devices were removed at each imaging time point, blotted on a tissue to remove any drops of analyte solution, and placed together on a piece of plastic for MR imaging. Subsequent sensing experiments were conducted using a custom-machined tool that allowed the devices to remain in their respective analyte bath solutions during MR imaging.

Equilibrium hCG-b concentrations were approximately equal to the initial bath concentration because the bath volume (700 uL) was much larger than the reservoir volumes (12 uL each). Two separate MR imaging sessions (Bruker, 4.7T), approximately 24 hours apart, were used to monitor the change in T_2 of the MRSw solutions in the PDMS devices. Total MR

imaging time was approximately 1 hour at each time point. The imaging protocol was a T_2-weighted multi-slice, multi-echo scan (TR 6000 ms, variable TE 15 – 1500 ms, 4x4 cm field of view, 128x128 imaging matrix, spectral width of 50,000 Hz, 3 slices, 0.7 mm slice thickness, number of excitations = 2). MRI data was analyzed using Matlab (Matlab 7.1, The MathWorks, Natick, MA) to produce a T_2 map. Table 5-1 summarizes the experimental plan for these *in vitro* sensing experiments.

Table 5-1. Experimental Plan for *In Vitro* Sensing with MRI Detection.

MRSw Concentration (μg Fe/mL)	Analyte Bath Concentrations (μg hCG-b/mL)	Elapsed Time Before Imaging (hrs)
2	0, 0.5, 1.5, 3	3, 27
6		
10	0, 3, 5	1, 5, 25, 29
	10	1, 25
16	0, 3, 5	1, 5, 25, 29
	10	1, 25

5.3.2 Single-sided MR detection

MRI is the gold standard for T_2 measurements *in vivo*, but it is time and cost-intensive. Single-sided MR easily allows for multiple time points and devices and is preferred for *in vitro* device-based sensing experiments. A device can be read on the single-sided MR, for both T_1 and T_2, in about one minute. Single-sided MR analysis allows the kinetics of aggregation to be studied in device-based sensing experiments.

5.3.2.1 Optimizing device design

Washer shaped devices were fabricated as described in Section 2.3.2 using two methods to attach the MWCO membrane to the substrate: a silicone adhesive and a double-sided pressure sensitive adhesive. The devices were filled with MRSw functionalized to detect hCG and placed in a bath of PBS-BSA-PS at room temperature. Single-sided MR was used to quantify the $T_{2,eff}$

immediately after fabrication and again almost one day later. Devices were then placed in analyte baths of 0.7 μg hCG/mL and kept at 37°C. The devices were removed from the analyte baths periodically to quantify $T_{2,eff}$ of the MRSw in the reservoirs.

5.3.2.2 Lower analyte concentrations

Cup devices were fabricated as described in Section 2.3.2. The reservoirs were filled with MRSw designed to aggregate in the presence of hCG (8 μg Fe/mL). Single-sided MR was used to quantify the $T_{2,eff}$ of the MRSw in each device immediately after fabrication and again after 12 - 24 hours to confirm that the devices were not leaking (an increase in $T_{2,eff}$ is correlated to a decrease in iron concentration). Sample devices were placed in analyte baths (0.1, 0.2, 0.3 and 0.4 μg hCG/mL) and incubated at 37°C (n = 4, 2, 4 and 4 respectively). Control devices (n = 4) were placed in PBS-BSA-PS. Devices were periodically removed from the analyte bath and $T_{2,eff}$ measurements were taken on the single-sided MR after the devices cooled to room temperature.

5.3.2.3 Higher porosity membranes

Cup devices were fabricated as described in Sections 2.3.2 with 10 nm or 30 nm pore polycarbonate membranes. The 30 nm pore membranes have a percent porosity that is approximately ten times higher than the 10 nm pore membranes. Devices with the 30 nm pore membranes are expected to show a faster decrease in $T_{2,eff}$ compared to 10 nm pore membrane devices. The reservoirs were filled with MRSw designed to aggregate in the presence of hCG (8 μg Fe/mL). Single-sided MR was used to quantify the $T_{2,eff}$ of the MRSw in each device immediately after fabrication and again after 12 - 24 hours to confirm that the devices were not leaking. Sample devices (n = 4 for 10 nm pore membranes, n = 5 for 30 nm pore membranes) were placed in analyte baths of 1 μg hCG/mL and control devices (n = 4 for each pore size) were

placed in PBS-BSA-PS solutions. Devices were periodically removed from the analyte bath for $T_{2,eff}$ measurements on the single-sided MR after the devices cooled to room temperature. Time points were taken for two weeks.

5.3.2.4 MRSw incubation in devices at 37°C

Devices described in Section 5.3.2.3 were also used to test the stability of MRSw when stored in devices at 37°C for two weeks. Two of the control devices (for each pore size) were moved into an hCG analyte bath (1 μg hCG/mL) after taking time points as described in section 5.3.2.3 for two weeks. The behavior of these devices was compared to the sample devices that had been in hCG baths for the previous two weeks and the control devices that remained in the PBS-BSA-PS solutions. This experiment was designed to mimic an *in vivo* sensing experiment where the analyte is not present at the time of device implantation (for example, if the device was used to detect metastasis).

5.4 Results and Discussion

5.4.1 MRI detection

These *in vitro* sensing experiments have demonstrated the ability to detect hCG-b within silicone devices. A typical image from the first *in vitro* sensing experiment with MRI detection is shown in Figure 5-1. Each light square in the image is a device reservoir. The average intensity of each reservoir at each TE was calculated using Matlab and used to produce relaxation curves similar to those shown in Figure 5-2.

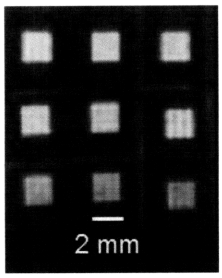

Figure 5-1. Representative MRI image from *in vitro* sensing with PDMS devices. Each light square represents a reservoir filled with MRSw. The average intensity of each reservoir at each echo time was calculated from this type of image. The decay in intensity for each reservoir as a function of echo time was used to calculate the T_2 of the MRSw solution (Equation 5-1).

The T_2 relaxation time can be calculated by fitting the MRI data to an equation of the form:

$$AvgI = Ae^{-\frac{TE}{T_2}} + B. \tag{5-1}$$

Where $AvgI$ is the average intensity, TE is the echo time, A is the amplitude and B is the offset. The curves in Figure 5-2 are for the control devices (6, 10 and 16 μg Fe/mL) and for pure PBS. The T_2 of the control devices increases as the iron concentration decreases, agreeing with previously reported experiments[43].

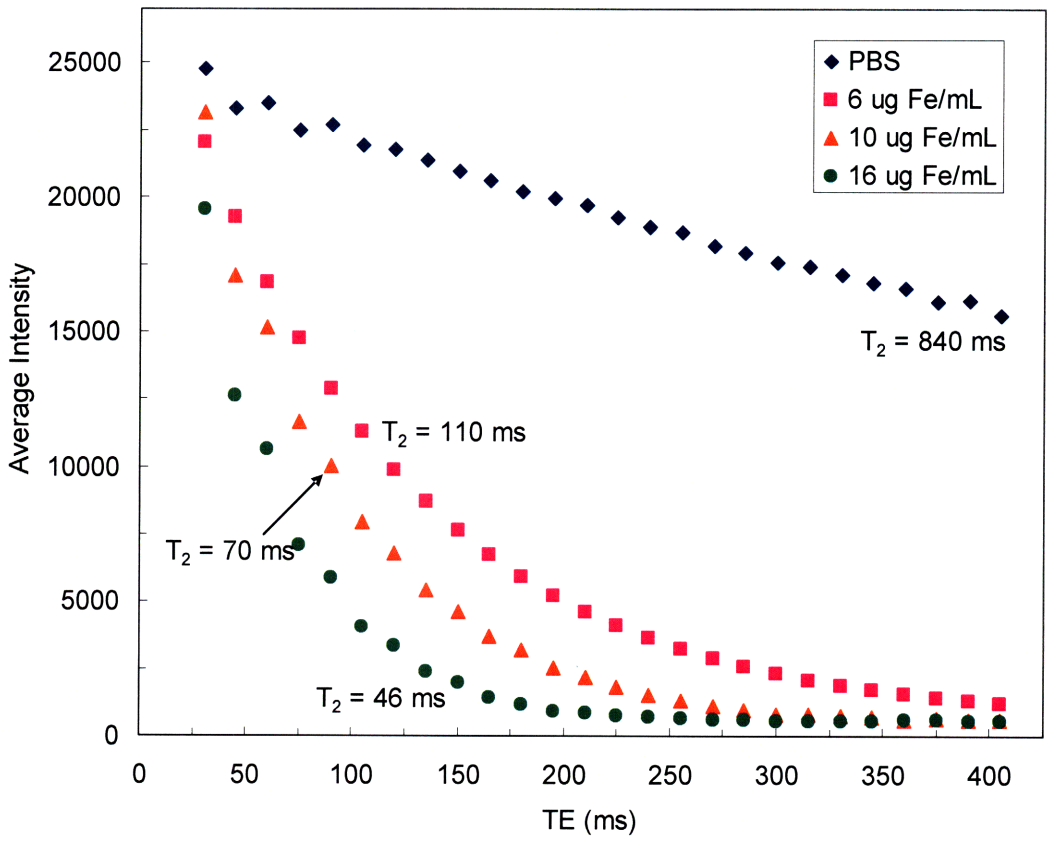

Figure 5-2. MRI decay curves used to calculate T_2 for solutions of MRSw only (no analyte present). An increase in MRSw concentration corresponds to a decrease in T_2.

Several of the devices in the first sensing experiment showed a significant increase in T_2 at the second time point. Figure 5-3 shows the mean T_2 of devices filled with 10 μg Fe/mL at each time point for this first sensing experiment (error bars represent st. dev.). Previous testing of the polycarbonate membranes used in these devices showed that the MRSw are not able to pass through the membrane (Section 3.4.1). The increase in T_2, therefore, is due to either failure of the membrane/substrate seal or leaking of the MRSw from the back of the device, which was sealed with pressure sensitive adhesive after filling the reservoir with MRSw. None of the devices in this experiment showed a decrease in T_2, perhaps because any decreases in T_2 due to aggregation were masked by increases in T_2 due to MRSw leakage.

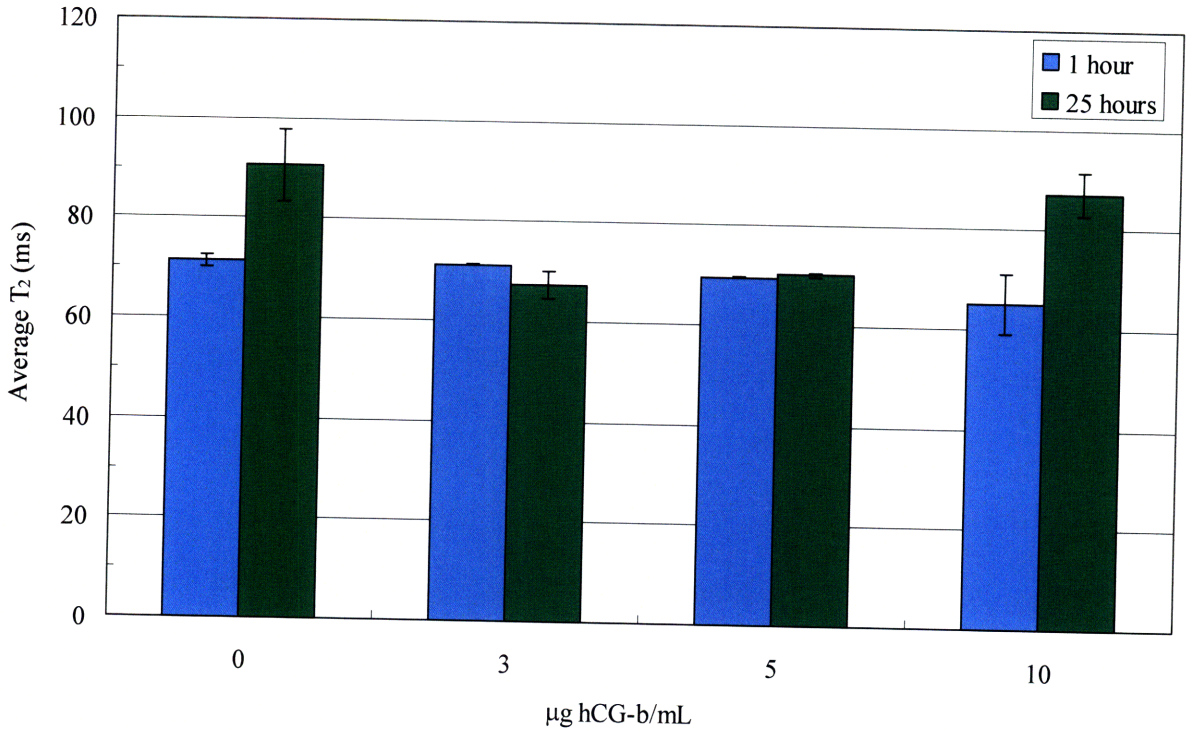

Figure 5-3. Mean T_2 for PDMS devices filled with MRSw at 10 µg Fe/mL and placed in hCG baths of 0, 3, 5 or 10 µg hCG/mL. Several devices showed a significant increase in T_2 at the second time point (green columns), indicating leakage of the MRSw.

The PDMS substrate is very flexible and the seal with the membrane was most likely damaged when the devices were transferred from the analyte baths for imaging. Some reservoirs also developed air bubbles while the devices were being imaged, since they were kept out of the analyte baths for approximately one hour at each imaging time point. These difficulties were solved by designing a tool that allowed the devices to be imaged while remaining in their analyte baths. Figure 5-4 shows a typical MRI image using this tool. Each light square is a device reservoir and the light regions around the devices are the analyte bath solutions. This tool allowed the devices to be left in the analyte bath solutions once filled, which decreased the occurrence of MRSw leaks and allowed detection of the decrease in T_2 due to aggregation.

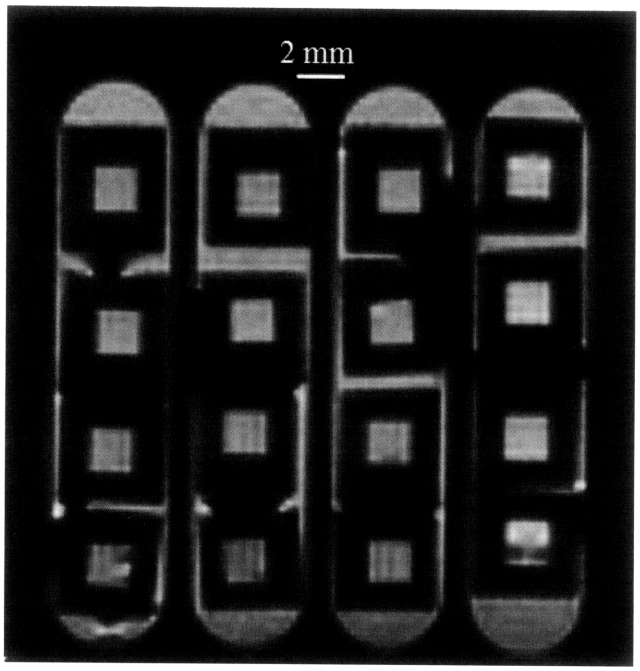

Figure 5-4. Typical MR image from sensing experiments where devices remained in analyte bath during imaging. Each light square represents a reservoir filled with MRSw in the PDMS device. Light regions around the PDMS devices are from the baths of analyte solution.

Figure 5-5 shows T_2 data for the devices filled with 16 μg Fe/mL CLIO solutions. The top figure shows the average T_2 values and the bottom figure shows the average percent change in T_2 compared to the control devices:

$$\% \text{ change in T} = \frac{\left(T_2 - Avg\_T_2^{ctrl}\right)}{Avg\_T_2^{ctrl}} * 100 \tag{5-2}$$

where $Avg\_T_2^{ctrl}$ is the average T_2 of the control devices at the same time point. The error bars represent either the standard deviation for the group or the error associated with the calculated T_2 values (95% confidence limit). Errors were calculated using both methods and the higher value is reported. The T_2 of the control devices remained constant over the course of the experiment, suggesting that the nanoparticles were well contained in the device.

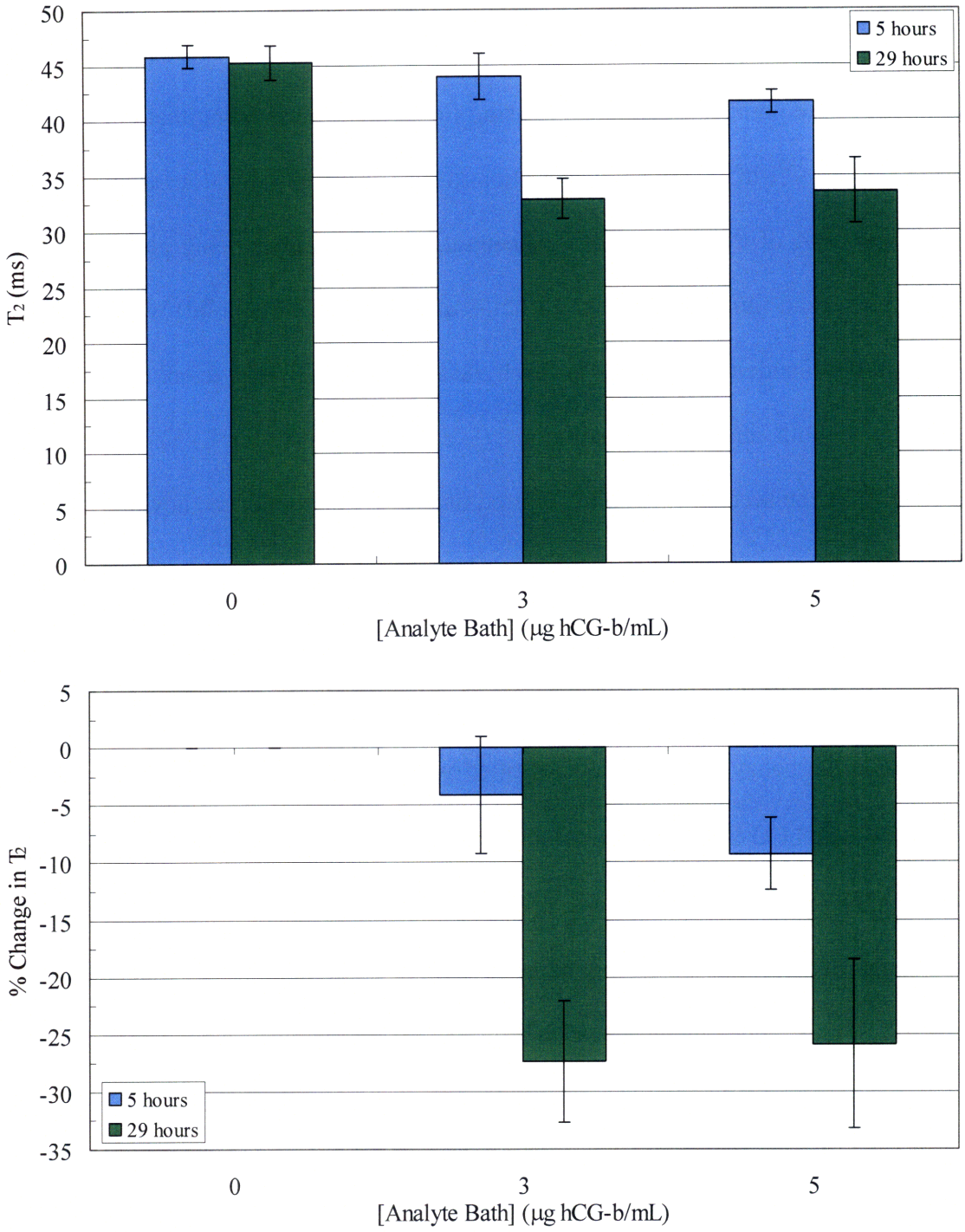

Figure 5-5. ***In vitro*** **sensing results with PDMS devices filled with MRSw at 16 µg Fe/mL. Devices were placed in analyte baths of 0, 3 or 5 µg hCG/mL. Error bars represent either standard deviation (n=2 for each group) or 95% confidence limit in the fit to determine T_2 (the larger error is reported).**

Figure 5-5 shows that at the first imaging time point (5 hours) only the devices placed in 5 μg hCG-b/mL solutions showed a significant drop in T_2. The hCG-b concentration inside the device at each time point can be predicted using Equation 3-5, assuming that Papp for hCG-b is the same as for ^{125}I-hCG. The concentration inside the reservoir, for example, should be approximately 50% of the analyte bath concentration 5 hours after being placed in the analyte solution. The second time point (about 24 hours after the first time point) is sufficient time for the concentration inside the reservoir to reach 98% of the initial analyte solution concentration. The devices in both analyte bath solutions (3 and 5 mg hCG-b/mL) showed a significant decrease in T_2 by the second time point, approximately 29 hours after the devices were placed in the analyte baths.

Devices with MRSw concentrations of 10 μg Fe/mL were also tested in analyte solutions (3 and 5 μg hCG-b/mL). Percent change in T_2 for these devices is summarized in Table 5-2 and compared with the behavior of the devices filled with 16 μg Fe/mL MRSw. The 16 μg Fe/mL devices in the 3 μg hCG-b/mL analyte solution were the only ones that did not show T_2 decreases at the firs time point. All devices showed T_2 shortening at 29 hours. Previous studies have shown that the magnitude of T_2 shortening depends on the ratio of analyte molecules to MRSw molecules[26]. Similar trends were seen with the sensing devices at the 5 hour time point. The 10 μg Fe/mL devices show a larger percent change in T_2 at 5 hours than the 16 μg Fe/mL devices.

Table 5-2. Results for *In Vitro* Sensing of hCG-b with MRI detection.

[CLIO]	% Change in T_2 Compared to Control Devices			
	3 μg hCG-b/mL Analyte Solution		5 μg hCG-b/mL Analyte Solution	
	5 hours	29 hours	5 hours	29 hours
10 μg Fe/mL	-8 ± 4	-27 ± 3	-16 ± 2	-25 ± 3
16 μg Fe/mL	-4 ± 5	-27 ± 5	-9 ± 3	-26 ± 7

Detection of lower concentrations of hCG-b was attempted using devices with lower MRSw concentrations. Devices were filled with either 2 or 6 ug Fe/mL and placed in hCG baths of 0.5, 1.5 and 3 μg hCG-b/mL. Figure 5-6 shows T_2 data for the devices filled with 6 μg Fe/mL MRSw solutions. The top figure shows the average T_2 values and the bottom figure shows the average percent change in T_2 compared to the control devices. The error bars represent either the standard deviation for the group or the error associated with the calculated T_2 values (95% confidence limit). Errors were calculated using both methods and the higher value is reported. The T_2 of the control devices, again, remained constant over the course of the experiment, suggesting that the nanoparticles were well contained in the device. Figure 5-6 shows that at three hours devices in the 3 μg hCG-β/mL analyte bath showed T_2 shortening. Devices in all three analyte baths showed T_2 shortening in a concentration dependent manner at the 27 hour time point.

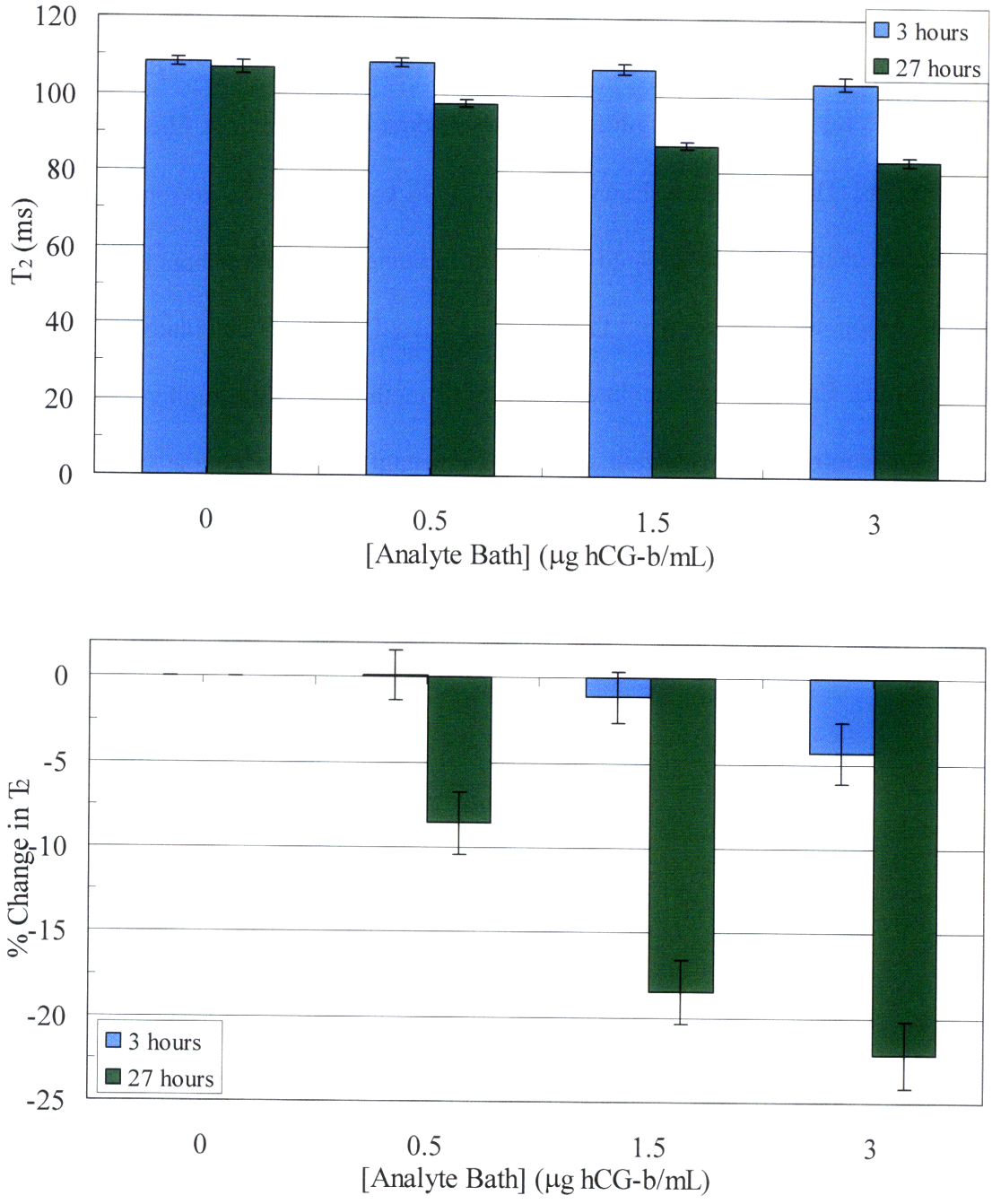

Figure 5-6. ***In vitro*** **sensing results with PDMS devices filled with MRSw at 6 µg Fe/mL. Devices were placed in analyte baths of 0, 0.5, 1.5 or 3 µg hCG/mL. Error bars represent either standard deviation (n=2 for each group) or 95% confidence limit in the fit to determine T_2 (the larger error is reported).**

Table 5-3 summarizes the T_2 results for the 2 and 6 µg Fe/mL devices. Only the devices in the 3 µg hCG-b/mL bath showed a significant decrease in T_2 at the first time point,

but all devices showed a significant decrease in T_2 at the second time point. The ability to detect aggregation in devices placed in analyte baths as low as 0.5 μg hCG-b/mL is significant for *in vivo* sensing experiments. Section 6.4.1 shows that mice with tumors that secrete hCG-b have plasma concentrations around 0.5 μg hCG-b/mL approximately 7-10 days after tumor induction.

Table 5-3. *In Vitro* Sensing Results for Devices with MRSw concentrations of 2 or 6 μg Fe/mL.

	% Change in T_2 Compared to Control Devices					
[CLIO]	0.5 μg hCG-b/mL Analyte Solution		1.5 μg hCG-b/mL Analyte Solution		3 μg hCG-b/mL Analyte Solution	
	3 hours	27 hours	3 hours	27 hours	3 hours	27 hours
2 μg Fe/mL	3 ± 4	-13 ± 2	-4 ± 3	-13 ± 3	-6 ± 1	-10 ± 3
6 μg Fe/mL	0 ± 1	-9 ± 2	-1 ± 2	-18 ± 2	-4 ± 2	-22 ± 2

These experiments demonstrated that the MRSw aggregates are stable enough in the sensing device to show a decrease in T_2 after incubation in analyte solutions at 37°C for approximately 29 hours. Future *in vitro* studies looked at the stability of MRSw aggregates at longer time points. The frequency of time points was also increased to study the kinetics of device operation.

5.4.2 Single-sided MR detection: optimizing device design

The behavior of washer devices with either silicone adhesive or double-sided pressure sensitive adhesive used to attach the membrane to the device substrate was studied in an *in vitro* sensing experiment. Figure 5-7 shows the percent change in $T_{2,eff}$, which was calculated using:

$$\%\ \text{change in } T_{2,\text{eff}} = \frac{\left(T_{2,eff} - Avg^{o}_{T2,eff}\right)}{Avg^{o}_{T2,eff}} * 100 \qquad (5\text{-}3)$$

where $Avg^{o}_{T2,eff}$ is the average $T_{2,eff}$ readings for the device before it was placed in the hCG solution. Devices made with double-sided pressure sensitive adhesive showed a significant

decrease in $T_{2,eff}$ after being in the hCG solutions for just half a day. Devices made using a silicone adhesive, however, did not start to show a significant decrease in $T_{2,eff}$ until two days after being placed in the hCG solutions. It is possible that the silicone adhesive spread onto the polycarbonate membrane covering the reservoir, reducing the cross-sectional area for diffusion of the hCG into the reservoir. Uncured adhesive could also leach into the reservoir and interfere with the MRSw or hCG, causing a delay in the $T_{2,eff}$ decrease. This delay in $T_{2,eff}$ decrease was avoided in future experiments by using double-sided pressure sensitive adhesive to seal the membrane to the device substrate.

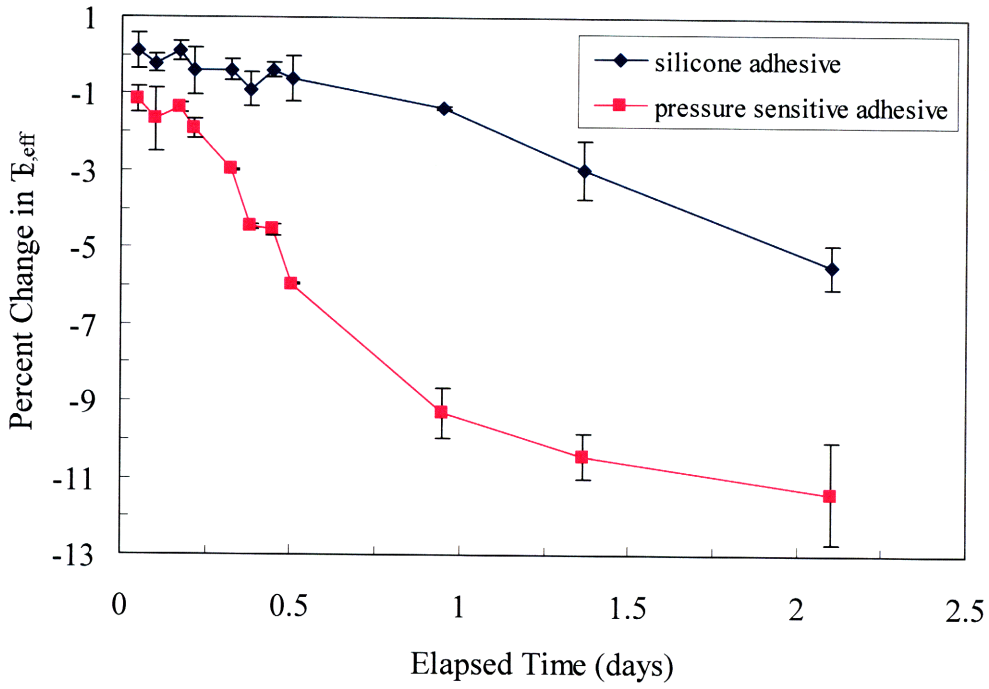

Figure 5-7. Comparison of two methods for adhering membranes to device substrate: silicone adhesive (blue diamonds) or double-sided pressure sensitive adhesive (pink squares). Devices were placed in analyte baths of 0.7 μg hCG/mL. The percent change in $T_{2,eff}$ of the devices, compared to control devices placed in PBS solutions, is reported on the y-axis. Error bars represent standard deviation (n = 2 for each group).

5.4.3 Single-sided MR detection: lower analyte concentrations

Device-based detection of lower analyte concentrations was demonstrated. Figure 5-8 shows the $T_{2,eff}$ for each group of devices as a function of time. The control devices (open diamonds) maintained a constant T2,*eff* over the ten day period indicating that the MRSw did not leak from the reservoirs. The decrease in $T_{2,eff}$ at each time point was larger for higher analyte concentrations for the first four days. The $T_{2,eff}$ of the devices in the highest concentration analyte bath began to increase slowly after this time point, indicating instability of the aggregates or leaking of MRSw. Devices in the lowest analyte concentration (pink squares) showed a significant decrease in $T_{2,eff}$ by day four. The difference between the sample and control devices was even more pronounced by day nine. These results suggest that device-based sensing of low concentrations of analyte is possible if enough time is allowed for the analyte to diffuse into the reservoir and cause aggregation.

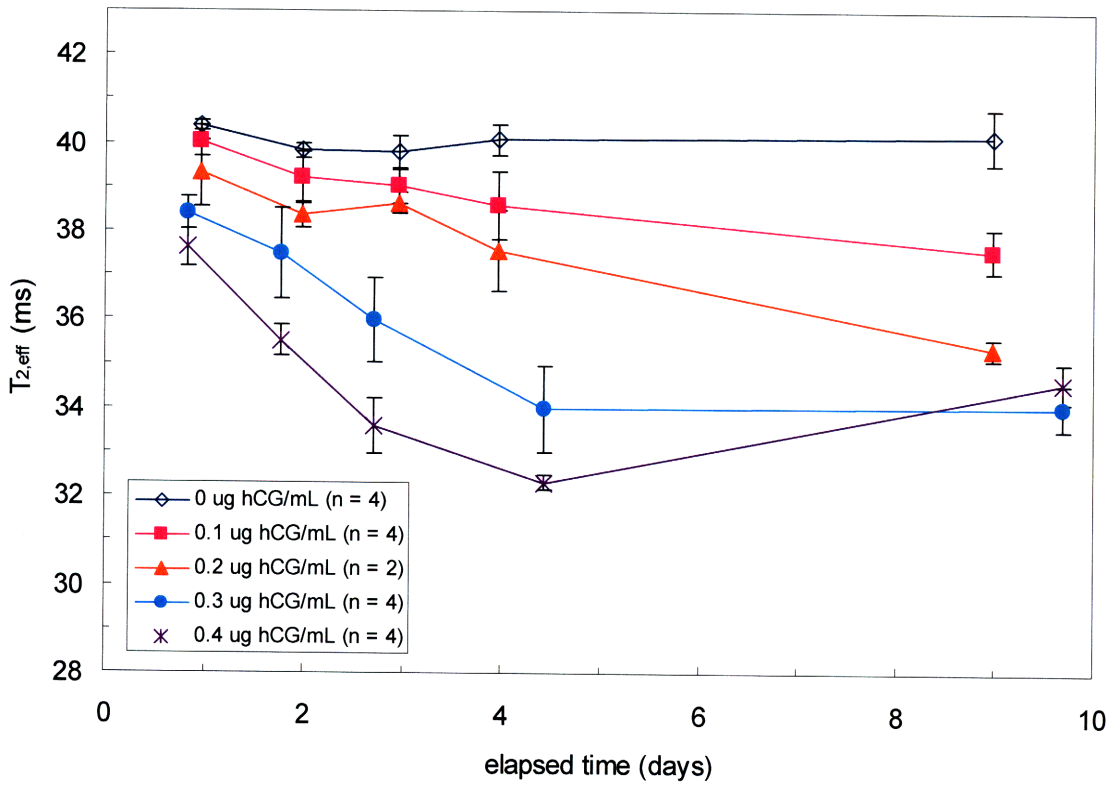

Figure 5-8. *In vitro* device based sensing of low hCG concentrations using cup-shaped devices with polycarbonate (10 nm pore) membranes. $T_{2,eff}$ for control devices, placed in PBS solutions, (open diamonds) remained constant while devices placed in hCG solutions (filled symbols) showed a decrease in $T_{2,eff}$. Error bars represent standard deviation.

Figure 5-9 compares the maximum percent change in $T_{2,eff}$ (compared to control solutions or devices) when the hCG and MRSw are thoroughly mixed together (Figure 4-5) and when the MRSw are contained within a device (Figure 5-8 and Figure 5-10). Figure 5-9 shows that for analyte concentrations between 0.1 to 1 μg hCG/mL, a larger decrease in $T_{2,eff}$ will be observed with device-based sensing. This suggests that the detection limit of the MRSw may be lower when they are used within a device. The high binding affinity of the antibodies favors irreversible MRSw. The signal measured is, thus, an integral of total exposure to the analyte over time and as such could be significantly more sensitive. Further studies at lower hCG concentrations need to be performed to verify this preliminary observation.

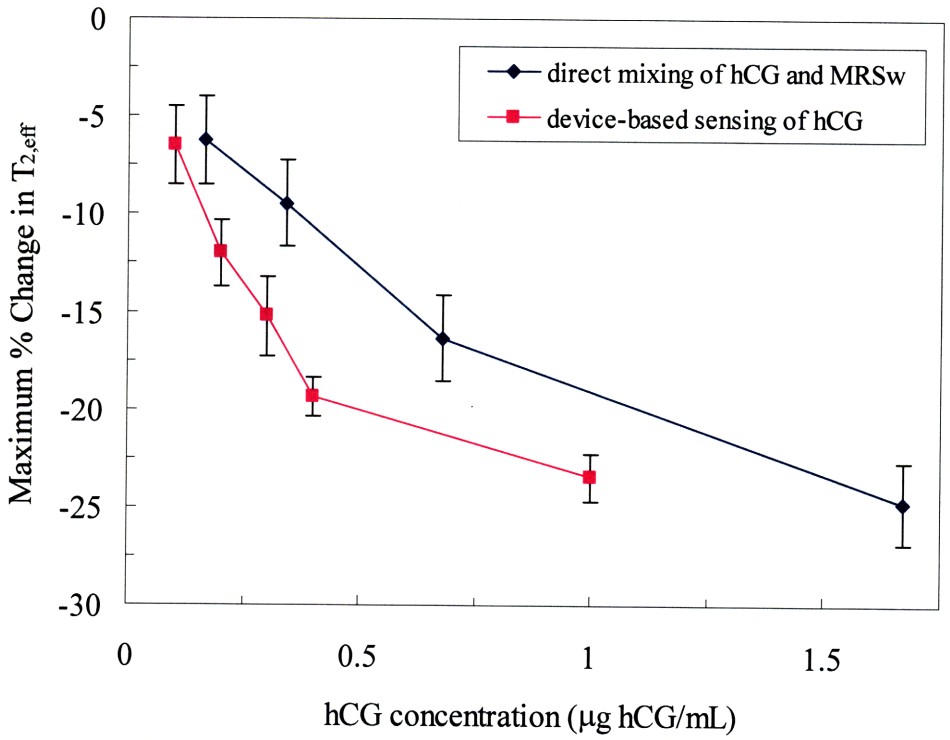

Figure 5-9. Comparison of maximum percent changes in $T_{2,eff}$ for direct mixing of hCG and MRSw and device-based sensing of hCG. Error bars represent 95% confidence interval in the fit to determine $T_{2,eff}$ for the direct mixing of hCG and MRSw data. Error bars represent standard deviation for the device-based sensing data (n = 2 or 4).

5.4.4 Single-sided MR detection: higher porosity membranes

Figure 5-10 shows that the $T_{2,eff}$ of the control devices remained constant over the course of the experiment, suggesting that the nanoparticles were well contained in the devices by both the 10 and the 30 nm pore membranes. Devices placed in hCG solutions, however, showed a significant decrease in $T_{2,eff}$. This suggests that hCG was able to diffuse across the MWCO membrane and cause aggregation of the MRSw. Devices with 10 nm pore membranes showed a decrease in $T_{2,eff}$ for approximately four days after being placed in the hCG solution. Devices with 30 nm pore membranes showed a faster and slightly larger decrease in $T_{2,eff}$ suggesting that the diffusion of hCG into the device is faster with the 30 nm pore membranes. The 30 nm pore

membranes have a percent porosity that is nearly ten times higher than the 10 nm membranes which most likely explains the faster diffusion with the 30 nm pore membranes.

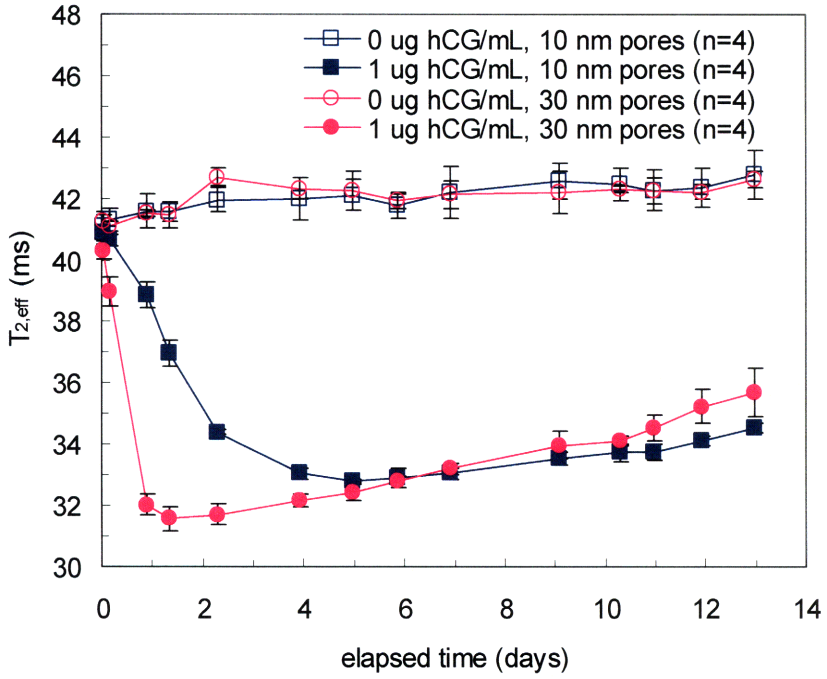

Figure 5-10. ***In vitro*** **device based sensing with single-sided MR detection. Cup-shaped devices were made with either 10 nm (blue squares) or 30 nm (pink circles) pore polycarbonate membranes. Devices placed in hCG solutions (filled symbols) showed a decrease in $T_{2,eff}$ while control devices placed in PBS (open sympols) maintained a constant $T_{2,eff}$. Error bars represent standard deviation.**

Figure 5-10 shows that the devices placed in analyte baths of 1 μg hCG/mL begin to show a gradual increase in $T_{2,eff}$ around day two for the devices with 30 nm pore membranes and day eight or nine for the devices with 10 nm pore membranes. The devices with 30 nm pore membranes initially show a sharper decrease in $T_{2,eff}$ but by day five there is no significant difference in $T_{2,eff}$ for the two types of devices. By day 12 the devices with 30 nm pore membranes have a slightly higher $T_{2,eff}$ than the 10 nm pore membrane devices. It is unlikely that this increase in $T_{2,eff}$ is caused by MRSw leaking out of the reservoir, since none of the eight control devices exhibit this behavior. The increase in $T_{2,eff}$ could be caused by the prozone effect,

instability of the aggregates (i.e. "crashing out"), instability of the antibodies attached to the surface of the MRSw, or leaking of MRSw. The standard deviation for each group of devices placed in hCG solutions is small, suggesting that the increase in $T_{2,eff}$ is not due to leaking of MRSw, since it is unlikely that all the sample devices would leak MRSw at the same rate while all of the control devices were able to contain the MRSw. The kinetics of aggregation for devices with 10 nm pore membranes is slower but seems to be more stable over a two week time period. Devices with 30 nm pore membranes would only be preferred for very short term sensing experiments, on the order or one or two days, due to the instability of the aggregates at longer time points for the combination of analyte and MRSw concentrations used in this experiment.

5.4.5 Single-sided MR detection: MRSw incubation in devices at 37°C

The *in vitro* sensing experiment described in Section 5.4.4 was continued for an additional two weeks. This experiment was designed to mimic an *in vivo* sensing experiment where the analyte is not present at the time of device implantation (for example, if the device was used to detect metastasis). Two control devices of each type of device (10 nm and 30 nm pore membranes) were switched into 1 μg hCG/mL solutions at day 13. Figure 5-11 shows data for the entire experiment. One of the control devices with a 10 nm pore membrane began to leak (increase in $T_{2,eff}$) around day 14, so this data was excluded from Figure 5-11. The dashed lines represent devices that began in control solutions and were switched to hCG solutions at day 13. A decrease in $T_{2,eff}$ was detected in all four of these devices, indicating the that MRSw stored in the devices for nearly two weeks at 37°C were still able to aggregate in the presence of hCG. The lowest $T_{2,eff}$ for these four devices was slightly higher than the lowest $T_{2,eff}$ of devices that were placed directly in hCG solutions. The subsequent increase in $T_{2,eff}$ was also slightly more dramatic for the four devices that were placed in PBS solutions for nearly two weeks. These

results support choosing 10 nm pore membranes for sensing experiments that will last longer than a few days, since for the analyte and MRSw concentrations studied here the $T_{2,eff}$ is slightly more stable in the 10 nm pore membrane devices.

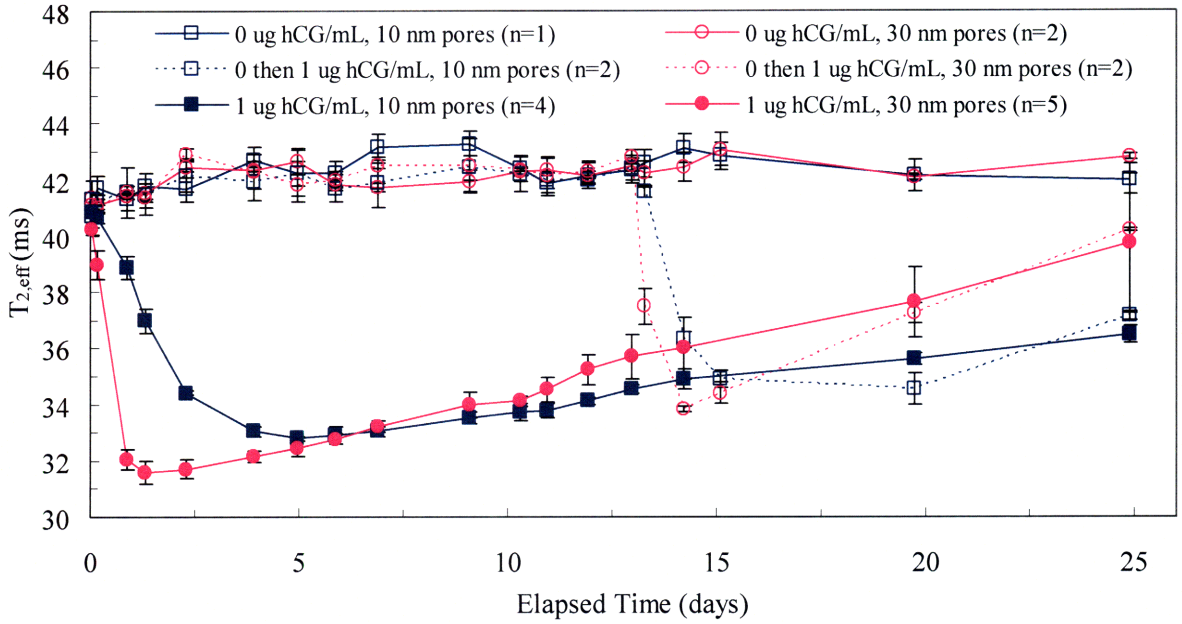

Figure 5-11. Device-based sensing after incubation in PBS for two weeks at 37°C. The experiment shown in Figure 5-10 is continued in this figure. Two of the devices that had previously been incubated in PBS solutions were switched to 1 μg hCG/mL solutions at day 14 (dashed lines). Error bars represent standard deviation.

5.5 Conclusion

Multiple *in vitro* sensing experiments have demonstrated the ability to detect the presence of hCG using MRSw that are contained within a reservoir by a semi-permeable membrane. Aggregation of the MRSw within the device was detected using both MRI and single-sided MR. Device-based sensing was successful in hCG solutions from 0.1 to 5 μg hCG/mL. Devices made with 10 nm pore membranes need approximately four days to reach the maximum decrease in $T_{2,eff}$, for the analyte and MRSw concentrations used in these experiments. Devices with 30 nm pore membranes demonstrate a faster decrease in $T_{2,eff}$, but the aggregates are less stable. Results

from these *in vitro* experiments were used to design the *in vivo* sensing experiments described in Chapter 6. Future studies should be performed to determine what causes the increase in $T_{2,eff}$ observed in the devices placed in hCG solutions. Particle size data could be used to determine if the increase in $T_{2,eff}$ is caused by aggregates growing so large that they precipitate out of solution. This would require the volume of the reservoirs to be doubled, since the current devices do not hold enough MRSw solution for particle sizing.

Chapter 6 *In Vivo* Sensing Experiments

6.1 Summary

An implantable diagnostic device capable of sensing the local *in vivo* environment has been developed. The device uses a semi-permeable membrane to contain nanoparticle magnetic relaxation switches (MRSw). We have used this proof-of-principle device to detect a soluble cancer biomarker in a mouse model. A cell line secreting a model cancer biomarker was used to produce ectopic tumors in nude mice. The device was implanted subcutaneously, and magnetic resonance imaging (MRI) and single-sided magnetic relaxometry (MR) were used to read the device. The transverse relaxation time (T_2) of devices was 38 +/- 1 ms in control mice versus 28 +/- 3 ms in tumor-bearing mice at one day by MRI ($p < 0.001$). This trend was also observed at day four by MRI and upon explantation by single-sided MR. This device may be the first continuous monitoring device for cancer that can be implanted at the tumor site and demonstrates feasibility of MRSw measurements *in vivo*. Future research may use such devices for the development of new therapeutic agents and evaluation of targeted delivery modalities. They may also enable real-time personalized cancer treatment, featuring long-term tracking of treatment and monitoring of local reoccurrence with a single implant.

6.2 Introduction

There are many clinical scenarios in cancer therapy where sampling of the local tissue environment at the tumor site would be beneficial. A patient that has undergone tumor resection would benefit, for example, from sampling of fluids to confirm that all of the neoplastic tissue has been removed. Alternatively, a patient with an inoperable tumor would be able to have

repeated fluid sampling at the tumor site to determine if the administered chemotherapeutic agents were actually reaching the tumor. Sampling the local environment, however, currently requires a surgical procedure such as another biopsy. We have constructed and tested a diagnostic device that could be left behind during a tumor resection and periodically monitored with MRI to provide information about the local environment. Data collected from the sensor device would aide the physician in determining whether another surgical resection or chemotherapy treatment was necessary.

Proof-of-principle *in vivo* sensing experiments were performed using high density polyethylene (HDPE) devices cup-shaped devices (Section 2.3.3). Mice were divided into two main groups: with a tumor (n = 34) and without a tumor (n = 11). Mice with tumors received one device, implanted subcutaneously near the tumor site once the plasma hCG concentrations began increasing. Mice without tumors received two devices, one on each flank. All the devices were filled with the same concentration of MRSw functionalized to detect hCG, non-functionalized MRSw, or MRSw functionalized to detect IL-2, a chemotherapeutic agent. Figure 6-1 summarizes the different groups for device-based *in vivo* sensing.

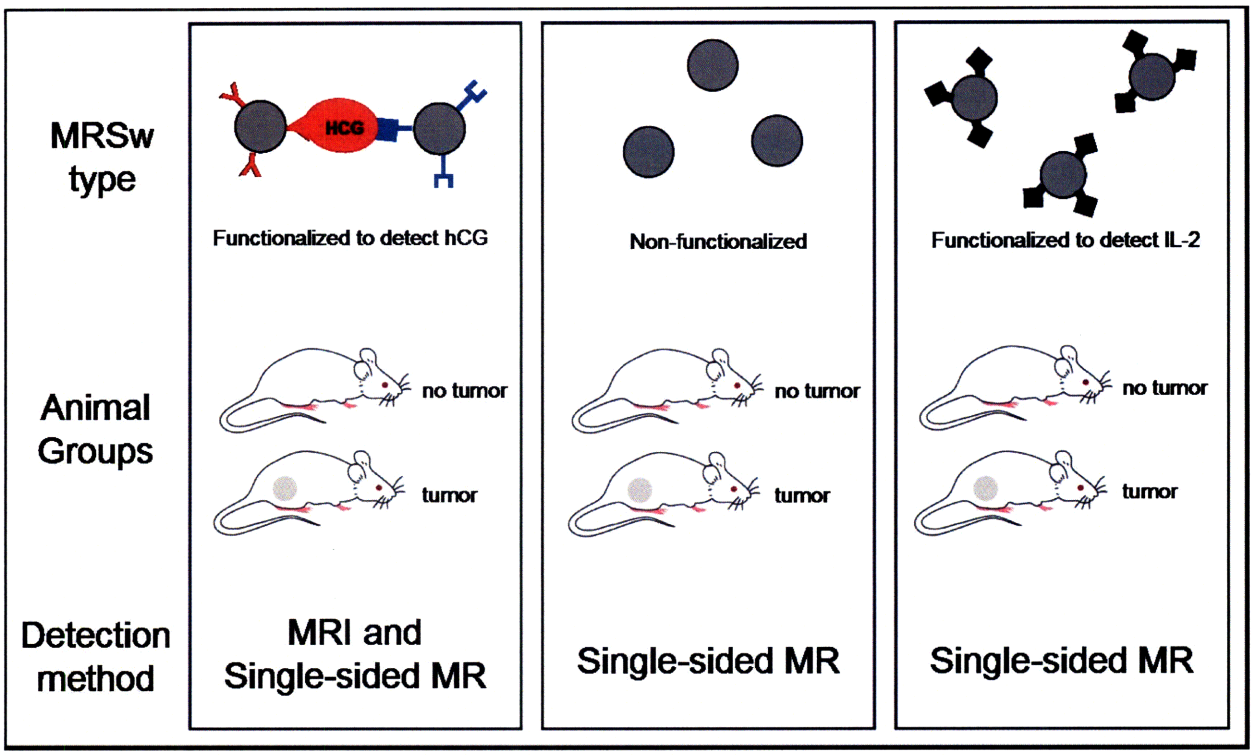

Figure 6-1. Experimental plan for device-based *in vivo* sensing.

6.3 Materials and Methods

6.3.1 Device Fabrication

Cup-shaped devices were used for *in vivo* sensing experiments since they are more robust than the PDMS and washer devices. See Sections 2.3.2 and 2.4.2 for details about device fabrication. Devices were filled with non-functionalized MRSw, MRSw functionalized to detect hCG, or MRSw functionalized to detect IL-2, a chemotherapeutic agent. The non-functionalized MRSw and MRSw functionalized to detect IL-2 were added to ensure that any decrease in T_2 seen with MRSw functionalized to detect hCG was in fact due to hCG induced aggregation.

6.3.2 Tumor Induction

Two commercially available human cell lines that secrete hCG and are tumorigenic in mice were considered: JAR (ATCC) and JEG-3 (ATCC). The cells were propagated and

subcultured according to the manufacturer's instructions until the time of tumor induction. The cells were then harvested and counted with a particle counter (Beckman Z1 Coulter Particle Counter) to determine the cell concentration. The cells were washed three times and re-suspended in sterile PBS to a concentration of 10^7 cells/mL. Equal volumes of cell solution and growth factor reduced Matrigel™ matrix (BD Biosciences) were mixed together. Mice were anesthetized with an intraperitoneal injection of ketamine (100 mg/kg) and xylazine (10 mg/kg). A 16 gauge needle was tunneled subcutaneously from the shoulder to the flank of the mouse, and 200 μL of the cell mixture was slowly injected (total of 10^6 cells per mouse) in the flank of each female NCr nude mouse (Taconic) (n = 34). The skin around the needle tip was compressed and held while the needle was removed and for the next 30-45 s to allow the cell solution to solidify as a depot. Control mice (no tumors, n = 11) underwent the same subcutaneous injection procedure on both flanks, with a solution of equal volumes of sterile PBS and Matrigel™. Retroorbital bleeding was performed periodically after tumor induction. Mice were anesthetized with continuous 1-4% isoflurane/oxygen inhalation, and the blood was collected in serum gel tubes (Sarstedt). The samples were centrifuged at 13,000 rpm for 5 minutes and then frozen for later analysis. Plasma hCG concentrations were determined using an ELISA kit (United Biotech Inc). The assay was performed according to the manufacturer's instructions using dilutions as necessary in the provided assay buffer. All work involving mice was performed according to the policies of the Massachusetts Institute of Technology Committee on Animal Care. Mice were housed in autoclaved cages and had access to autoclaved food and water *ad libitum*.

6.3.3 Device Implantation

Two different *in vivo* sensing experiments were conducted. In one experiment, devices were implanted subcutaneously and the incision was allowed to heal for 9 or 14 days before

injection of Matrigel™/cell solution or Matrigel™/PBS solution (see Section 6.3.2). Devices were explanted 12 or 15 days after tumor induction. This experiment was designed to mimic an application where the analyte being detected is not present at the time of device implantation. The other experiment tested short term *in vivo* sensing: tumor cells were injected and device implantation was performed when a sharp increase in either tumor size or plasma hCG concentration was observed, between 13 to 19 days after tumor cell injection. Control devices were implanted around the same time as sample devices. Devices were explanted two to four days after implantation. Figure 6-2 is a schematic of the schedule for the two sensing device-based sensing experiments.

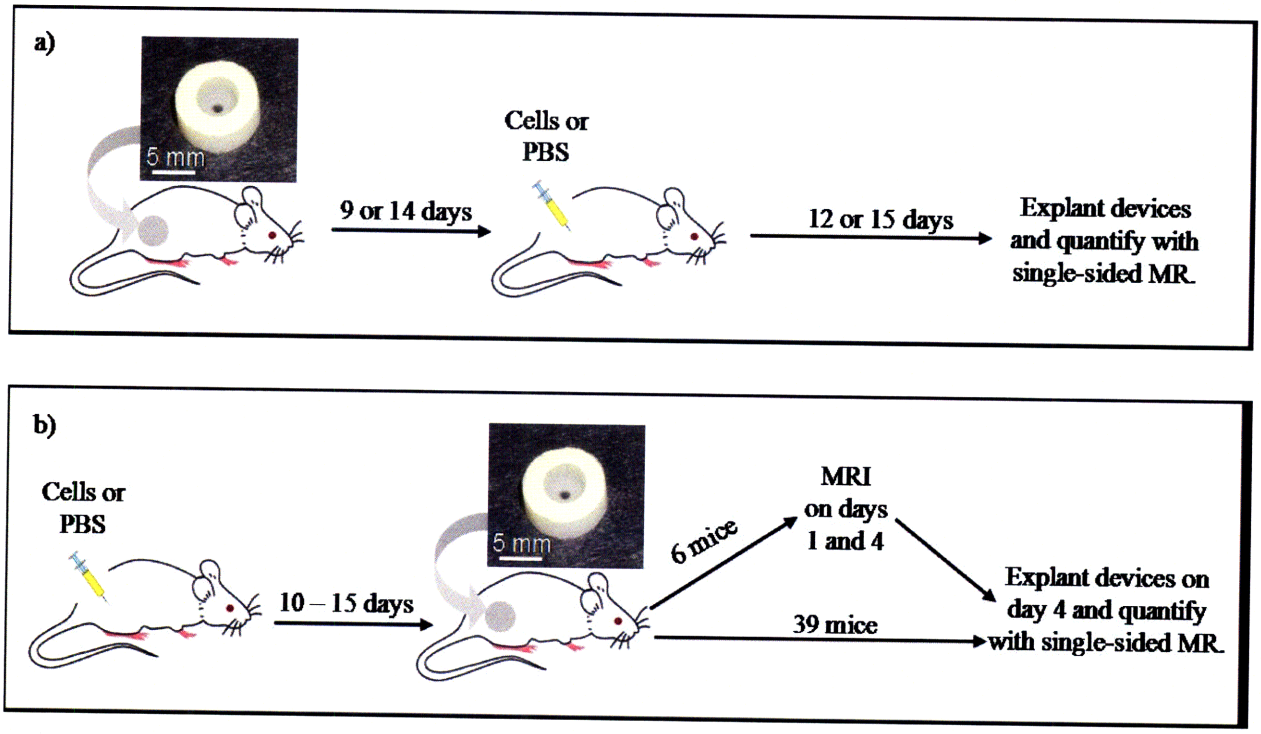

Figure 6-2. Schedule for *in vivo* sensing experiments. a) Device-based sensing where the device is implanted before the analyte is present. Devices were implanted for a total of 21 to 29 days. b) Short term device-based sensing experiment with devices implanted for four days.

For device implantation, mice were anesthetized with an intraperitoneal injection of ketamine (100 mg/kg) and xylazine (10 mg/kg). Preemptive analgesics (buprenorphine, 0.1

mg/kg) were administered subcutaneously before the first incision. Mice with tumors (n = 34) received a dorsal midline incision, and blunt dissection was used to tunnel subcutaneously to the tumor site and create a pocket for the device. Mice without tumors (n = 11) also received a dorsal midline incision and blunt dissection was used to create a pocket on each flank (two devices per mouse). All devices were placed in the pocket with the membrane facing the muscular layer and the incision was closed with silk sutures. Mice were monitored daily for signs of distress, infection, or excessive tumor burden.

6.3.4 NMR Relaxometry Measurements

Two techniques were used to quantify the transverse relaxation time of the MRSw in the device: MRI (reported as T_2) and single-sided MR (reported as $T_{2,eff}$). A benefit of MRI is that it allows for live animal imaging, so the same device can be imaged multiple times. Single-sided MR requires the device to be explanted, so the $T_{2,eff}$ can only be quantified at one time point using this technology. MRI is more time and cost-intensive than single-sided MR, however, so a subset of animals were chosen for MR imaging, while all devices were analyzed with single-sided MR. MR imaging was performed one day and four days after device implantation. Four of the mice had tumors, two did not have tumors. Mice without tumors received a device on each flank, so there were four devices in each group. The imaging time points were chosen based upon the measured P_{app} of hCG through the polycarbonate membrane and the kinetics of aggregation for the MRSw. The analyte concentration in the reservoir was calculated to be more than 95% of the equilibrium concentration at one day[44]. This calculation assumes an infinite source of hCG, meaning that the concentration of hCG outside the reservoir remains constant. The infinite source assumption may not be valid *in vivo* and the time required to reach an equilibrium concentration may increase. The kinetic behavior of MRSw aggregation is another

factor that could increase the time needed to see a decrease in T_2, as it continues to decrease for approximately 24 hours after mixing the analyte and MRSw solutions (Figure 4-5). The imaging session on day four was selected to allow for longer diffusion and aggregation times.

Mice scheduled for MR imaging were transported to the Center for Molecular Imaging Research (CMIR) at Massachusetts General Hospital (MGH) after they awoke from anesthesia from the device implantation surgery (n = 6). They were imaged on day one and day four post device implantation, and subsequently transported to MIT so the devices could be explanted and measured on the single-sided MR. MRI was performed at 7 T on a Bruker imaging system (Pharmascan). Animals were anesthetized during imaging with 1-1.5% inhaled isoflurane, and monitored during imaging with respiratory monitoring. Imaging protocols included a Tri-plane and axial RARE localizer. Multi-slice multiecho (MSME) T_2-weighted imaging was performed utilizing the following parameters: Flip angle = 90°; Matrix size (128 x184); TR = 2330 ms.; TE = 16 equally spaced echoes at 8.8 ms intervals ranging from 8.8 ms to 141 ms; field of view (FOV) = 4 x 4 cm, slice thickness = 1mm. T_1-weighted imaging was performed utilizing the following parameters: Flip angle = 90°; Matrix size (192 x 256); TR = 700 ms; TE = 14 ms; field of view (FOV) = 4 x 4 cm, slice thickness = 1mm. Region of interest analysis was performed and T_2 fit by using a mono-exponential fitting algorithm for the multi-TE data (Osirix). ROI incorporating the center 2-3 slices of the device were analyzed. The fitting of the T_2 was modified by subtracting the mean background noise, and only points above this mean baseline threshold were used for the fit.

In the first sensing experiment, all devices were explanted two to four days post implantation and a $T_{2,eff}$ measurement was immediately made using a single-sided NMR probe (Profile NMR MOUSE, ACT Center for Technology, Aachen, Germany). In the second sensing

experiment, all devices were explanted 12 to 15 days after tumor induction and immediately measured on the single-sided MR. The explanted devices were individually positioned over the sensitive volume. The sensitive volume of the probe was located 2 mm above the center of the probe surface. The probe has a field strength of 0.43 T and a static field gradient of 15 mT/mm. It was maintained at 25°C using a circulating water bath. The similarity in magnitude between T_2 measured by MRI and $T_{2,eff}$ measured by single-sided MR is coincidental. A Minispec spectrometer (Bruker Optics) was used for pulse sequence generation and data acquisition. $T_{2,eff}$ was measured using a 2000-echo CPMG pulse sequence with TE = 0.035 ms and TR = 1 s. The data were averaged over 48 scans. The measurements took approximately one minute per sample. The echo peak intensities were fit to the equation

$$I = I_0 e^{-t/T_2} \tag{6-1}$$

using a custom script running on MATLAB (The Mathworks).

6.4 Results and Discussion

6.4.1 Tumor Induction

The two cell lines (JAR and JEG-3) were used to induce ectopic tumors in mice. Figure 6-3 shows the plasma hCG-b concentrations in eight mice (four for each cell line). The JAR cell line is represented by blue dashed lines and the JEG-3 cell line by solid pink lines. The plasma hCG-b concentrations of the mice with the JAR cells ranged from 0.13 to 0.95 μg hCG-b/mL 18 days after tumor induction. Plasma concentrations of mice with JEG-3 cells, however, were between 0.34 and 0.64 μg hCG-b/mL on day 18. JEG-3 cells were chosen for tumor induction in the *in vivo* sensing experiments because they seemed to produce more consistent plasma hCG-b concentrations.

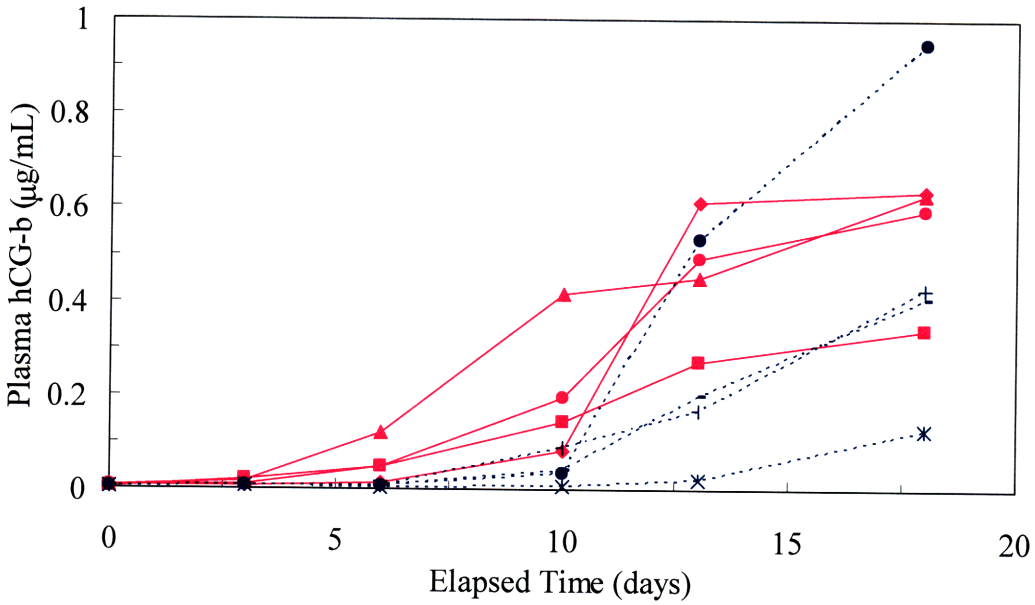

Figure 6-3. Plasma hCG-b concentrations in mice from ectopic tumors induced by two different cell lines: JAR (dashed blue lines) and JEG-3 (solid pink lines). A commercially available ELISA was used to quantify hCG-b levels in plasma samples.

6.4.2 Device-based sensing: Single-sided MR detection

Devices were filled with MRSw functionalized to detect hCG (Cmix-3000, 8 μg Fe/mL) and implanted in 12 mice. Mice scheduled to undergo tumor induction received one device on the flank. Mice scheduled to undergo control injections received a device on each flank. Nine days after device implantation, six mice received injections near the device (two control mice, four sample mice). The remaining six mice received injections 21 days after device implantation (two control mice, four sample mice). Sample mice received an injection of Matrigel™ and JEG-3 cells next to the device. The JEG-3 cells were washed three times prior to injection to ensure removal of any hCG that was present in the media. Control mice received control injections (Matrigel™ and PBS) at each device. Devices were explanted 12 or 15 days later, depending on tumor size and the $T_{2,eff}$ of the devices quantified using single-sided MR. Figure 6-4 shows the $T_{2,eff}$ for each device after being explanted. Figure 6-4a shows the results for devices that were

implanted a total of 21 to 24 days. There is no significant difference (p = 0.06) between the control devices on the left ($T_{2,eff}$ = 41.9 +/- 0.6 ms) and the sample devices on the right ($T_{2,eff}$ = 41.2 +/- 0.5 ms). Figure 6-4b shows the results for devices that were implanted a total of 26 to 29 days. There is no significant difference (p = 0.4) between the four control devices on the left (mean $T_{2,eff}$ = 42 +/- 1 ms) and the four sample devices on the right (mean $T_{2,eff}$ = 42 +/- 1 ms).

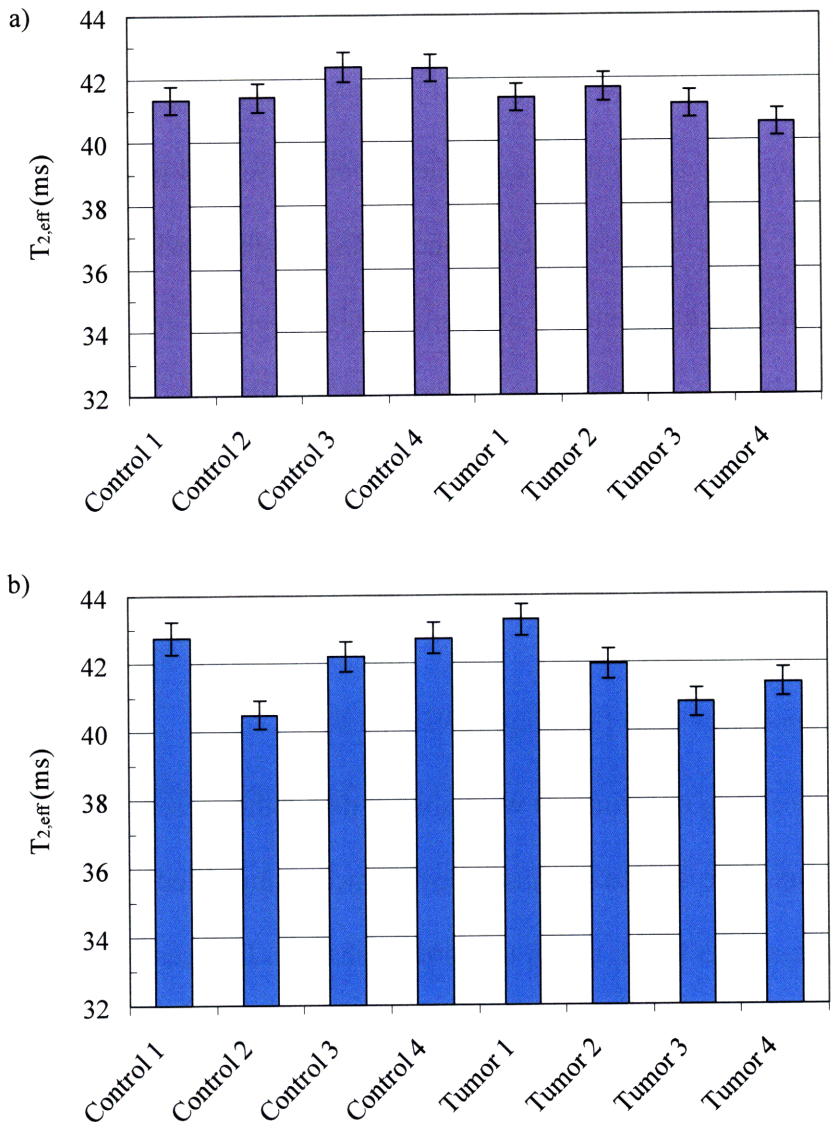

Figure 6-4. Results for device-based *in vivo* sensing where devices are implanted before the analyte is present. Single-sided MR was used to detect MRSw aggregation. a) $T_{2,eff}$ measurements for devices that were implanted for a total of 21 to 24 days (nine days before tumor induction, 12 or 15 days after tumor induction). b) $T_{2,eff}$ measurements for devices that were implanted for a total of 26 to 29 days (14 days before tumor induction, 12 to 15 days after tumor induction).

The lack of a decrease in $T_{2,eff}$ could be caused by several different factors. It is possible that the devices began to leak after being implanted for three to four weeks, and any decrease in $T_{2,eff}$ is masked by an increase in $T_{2,eff}$ due to the MRSw leak. It is also possible that the MRSw in devices implanted next to the tumors did aggregate and cause a decrease in $T_{2,eff}$. The $T_{2,eff}$ then began to increase, either because of the prozone effect or insolubility of large aggregates, and by the time the devices were explanted and read there was no longer a significant difference between the control and sample devices. This problem would easily be solved by using live animal MRI imaging to quantify the $T_{2,eff}$ in the devices at several points during the experiment. Matrix stabilization could also be added to the MRSw in the devices. This would prevent the aggregates from precipitating out of solution, resulting in a stable $T_{2,eff}$[53]. A third possible explanation for the behavior seen in this sensing experiment is that the MRSw were not able to aggregate in the presence of hCG after being implanted in vivo for 9 to 14 days before tumor induction. Section 4.5 discusses some techniques that may be able to improve the stability of the antibodies on the MRSw surface.

6.4.3 Short term device-based sensing: MRI detection

Short term sensing experiments were able to detect the presence of hCG *in vivo*. In these experiments, tumors were started first, and devices were implanted next to the tumor once the tumor size or plasma hCG levels began to increase sharply. Devices were explanted two to four days later. Six mice (two control, four sample) underwent live animal MRI imaging on day one and four after device implantation. Figure 6-5 is an example of the type of MRI images obtained. Superimposed over each device is a pseudo-colorized map that represents the T_2 within the device. The T_2 of the control device did not change from day one (Figure 6-5a) to day four

(Figure 6-5b) indicating that the MRSw were well contained within the reservoir by the polycarbonate membrane. The T_2 of the device implanted near a tumor decreased from day one (Figure 6-5c) to day four (Figure 6-5d) and was lower than the control device on both days. This indicates that hCG was secreted by the tumor, diffused into the devices, and caused aggregation of the MRSw. Calculations based on the P_{app} for hCG with these membranes predicted the concentration inside the reservoir to be more than 95% of the equilibrium concentration by the first MRI time point.

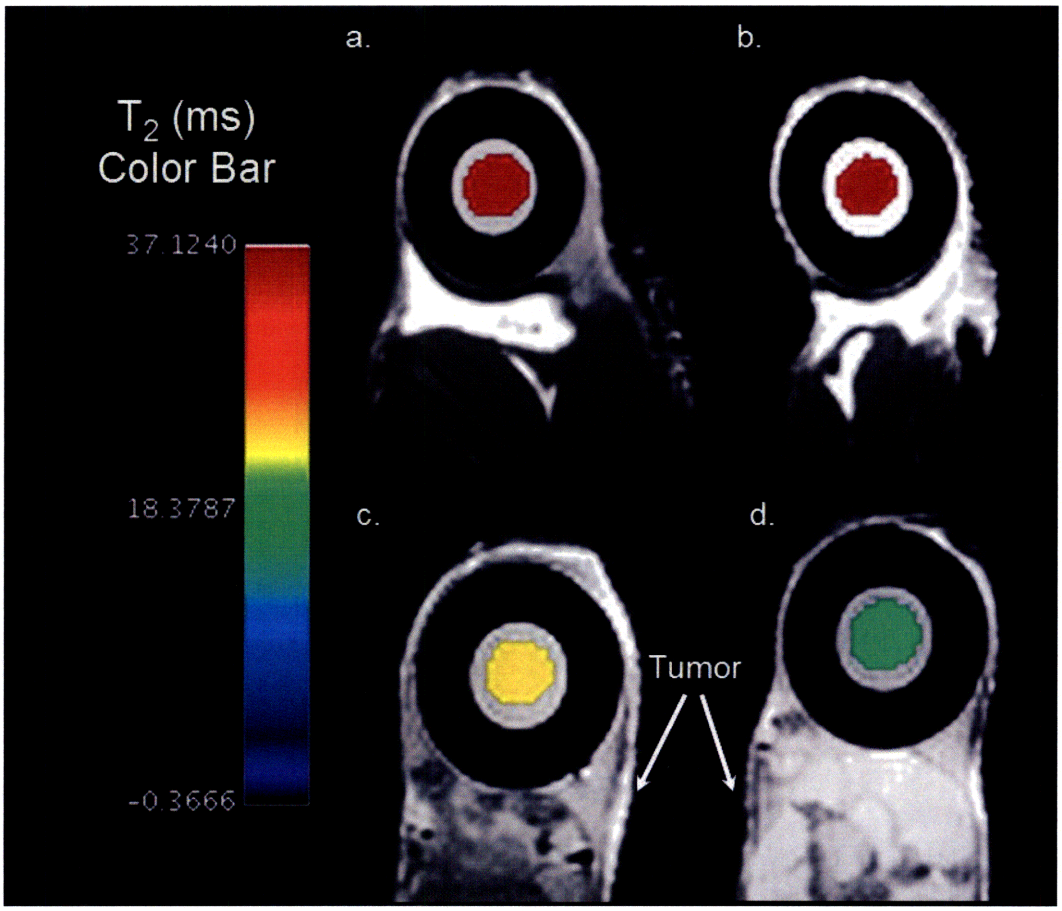

Figure 6-5. T_1-weighted *in vivo* MR images for a control (a and b) and tumor (c and d) device. Superimposed over the device is a pseudo-colorized map of the T_2 within the device (color bar on the left). The control device showed no change in T_2 from day one (a) to day four (b). The T_2 of the sample device decreased from day one (c) to day four (d) and was lower than the control device on both days.

Figure 6-6 shows the T_2 for each device at each MRI time point. The T_2 of the control devices (no tumor present) were approximately constant over the two imaging time points. T_2 of the sample devices were all lower than the control devices on day one and an even larger decrease in T_2 was observed on day four. The mean T_2 of the control devices (n = 4) was 38 +/- 1 ms on day one and 37 +/- 2 ms on day four. The mean T_2 of the sample devices (n = 4) was 26 +/- 4 ms on day one and 20 +/- 2 ms on day four. The decrease in T_2 of the sample devices compared to the control devices is statistically significant (Student's t-test, one tail, equal variances) for both time points (p = 0.001 day one, p = $3x10^{-6}$ day four).

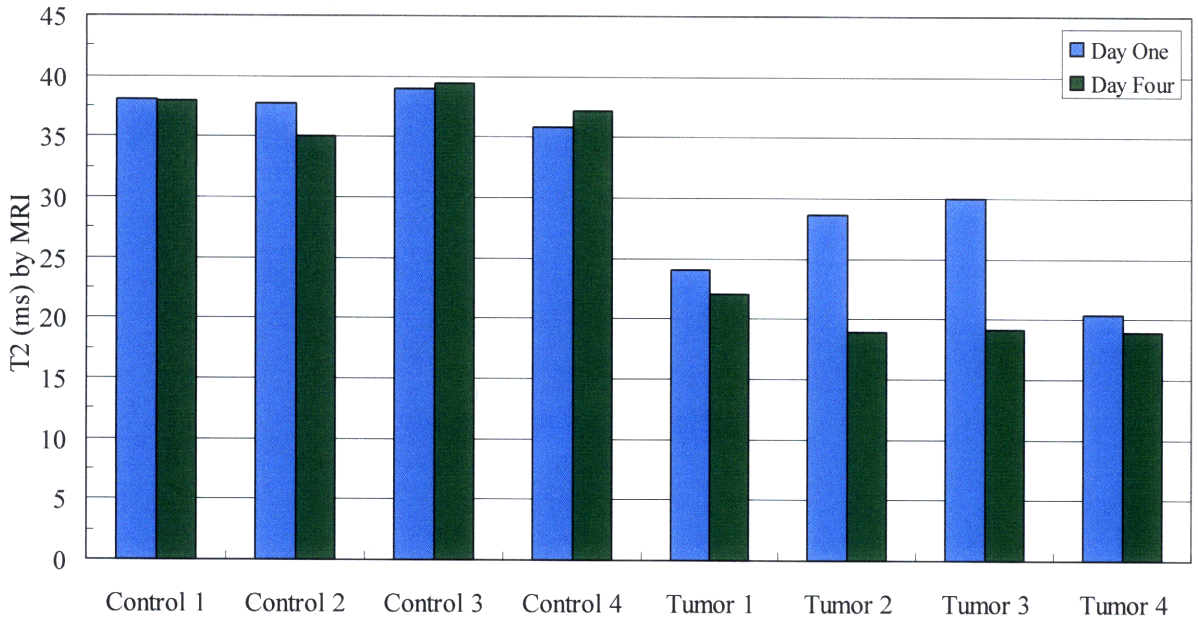

Figure 6-6. T_2 values for each device in the short term device-based sensing experiment that was sent for MR imaging. Imaging took place one day (blue columns) after device implantation and again four days (green columns) after device implantation.

6.4.4 Short term device-based sensing: Single-sided MR detection

Immediately after the second MRI time point, the six mice were transported back to MIT, the devices were explanted, and the $T_{2,eff}$ was quantified by single-sided MR. This allowed the

results from the single-sided MR to be verified by MRI. Figure 6-7 compares the percent change in T_2 or $T_{2,eff}$, compared to the average value of the control devices (Equation 5-2), for the four sample devices. The magnitude of the percent change in T_2 is greater for MRI analysis, as expected. The two measurement techniques reveal the same trend, though. Tumor 1 is the smallest percent change for both measurement techniques, while there is little difference between the other three devices. These results verify that explanting devices to be read on the single-sided MR is a valid method of detecting MRSw aggregation for *in vivo* sensing experiments.

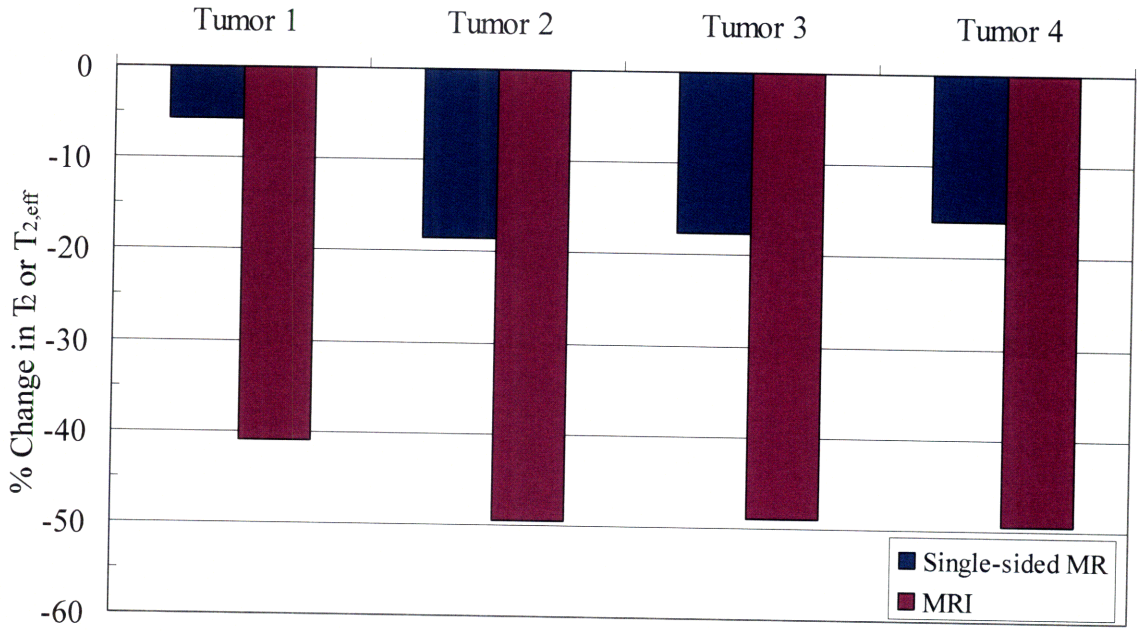

Figure 6-7. Comparison of single-sided MR (blue columns) and MRI (purple columns) results from short term device-based sensing experiment. Values are reported as a percent change in $T_{2,eff}$, compared to control devices that were placed in PBS solutions.

Single-sided MR was used to measure the $T_{2,eff}$ of all the remaining *in vivo* devices at explantation. Furthermore, devices filled with non-functionalized MRSw and devices filled with MRSw functionalized to detect IL-2 (a chemotherapeutic agent) were implanted in mice with and without tumors as additional controls. These controls were to test that the decrease in $T_{2,eff}$

seen in devices filled with MRSw functionalized to detect hCG and implanted near a tumor site was indeed due to the presence of hCG, not some other effect of implantation near the tumor. Figure 6-8 shows the mean $T_{2,eff}$ of each group as quantified by single-sided MR. Only mice with tumors and devices filled with MRSw functionalized to detect hCG showed a statistically significant ($p = 3x10^{-10}$) decrease in $T_{2,eff}$ (33 +/- 2 ms, n = 19) compared to the same MRSw in devices implanted in mice without tumors ($T_{2,eff}$ = 37.6 +/- 0.3 ms, n = 8). There was no statistically significant difference (p = 0.3) in $T_{2,eff}$ between the control devices ($T_{2,eff}$ = 39.0 +/- 0.6 ms, n = 6) and sample devices ($T_{2,eff}$ = 38.9 +/- 0.5 ms, n = 8) when the devices were filled with non-functionalized MRSw. There was also no statistically significant difference (p = 0.08) in $T_{2,eff}$ between the control devices ($T_{2,eff}$ =37.4 +/- 0.5 ms, n = 8) and sample devices ($T_{2,eff}$ = 37.9 +/- 0.7 ms, n = 7) when the devices were filled with MRSw functionalized to detect IL-2. Thus, the decrease in $T_{2,eff}$ is caused by hCG induced aggregation of the nanoparticles functionalized to detect hCG.

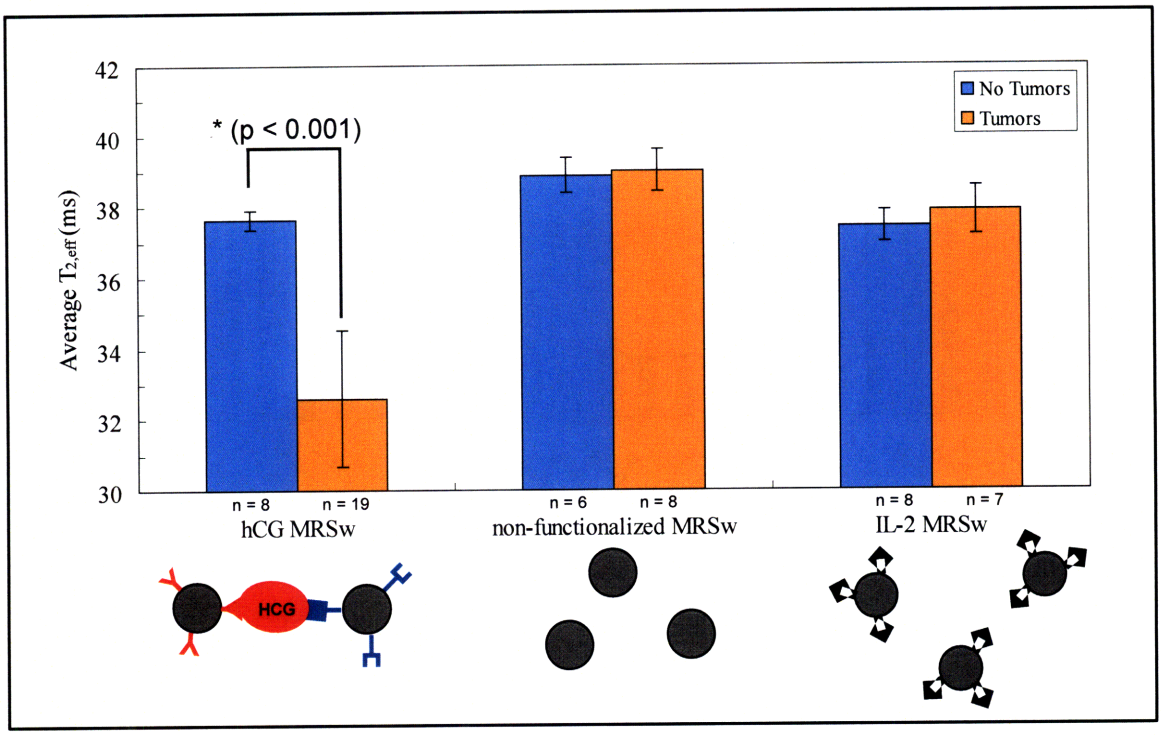

Figure 6-8. Summary of short term sensing results using single-sided MR detection. Only devices filled with MRSw functionalized to detect hCG and implanted next to a tumor showed a significant decrease in $T_{2,eff}$.

Figure 6-9 shows $T_{2,eff}$ readings for each short term *in vivo* sensing device. In each figure, the control devices (implanted in mice with no tumors) are on the left and the tumor devices (implanted in mice with tumors) are on the right. Figure 6-9a shows the data for devices filled with MRSw functionalized to detect hCG. All the tumor devices have a $T_{2,eff}$ that is significantly lower than the control devices, but the magnitude of the $T_{2,eff}$ decrease varies significantly between mice. Figure 6-9b (devices filled with non-functionalized MRSw) and Figure 6-9c (devices filled with MRSw functionalized to detect IL-2) show that there is no significant difference between the control and tumor devices for these MRSw.

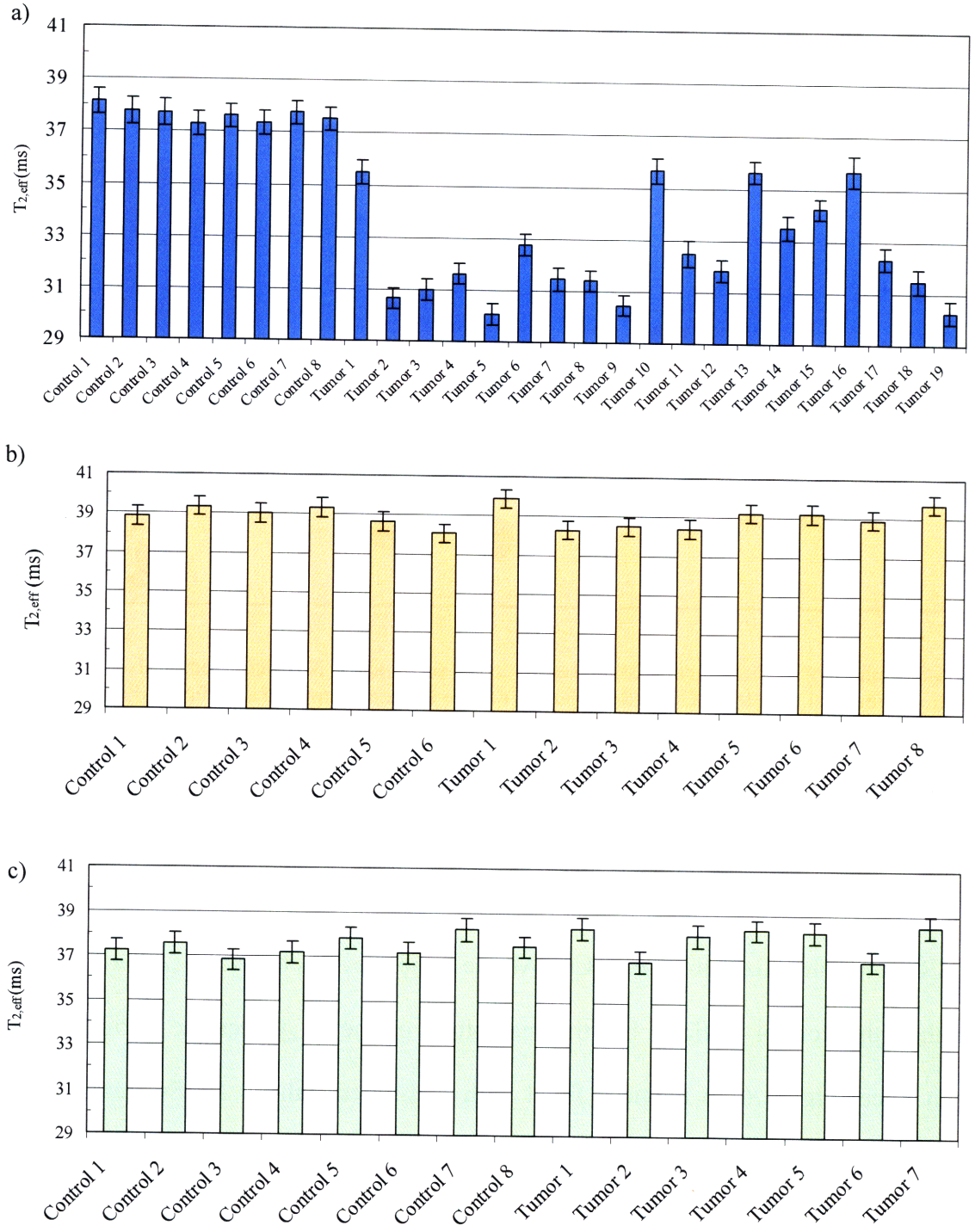

Figure 6-9. $T_{2,eff}$ readings for each short term *in vivo* sensing device. a) Devices filled with MRSw functionalized to detect hCG, b) devices filled with non-functionalized MRSw, and c) devices filled with MRSw functionalized to detect IL-2.

The variation in $T_{2,eff}$ amongst tumor devices in Figure 6-9a is most likely due to differing concentrations of hCG at the device location. Plasma samples were taken at the time of device

implant and explant, and hCG plasma concentrations were quantified with an ELISA kit. These concentrations were used to estimate the device exposure to hCG from the area under the curve (AUC) of a plasma concentration vs time plot. Figure 6-10 shows that the *in vivo* devices work very well as "switches". Every device that was exposed to hCG from the tumor demonstrated a decrease in $T_{2,eff}$ compared to control devices. The AUC of hCG calculated from plasma levels, however, did not correlate with the magnitude of decrease in $T_{2,eff}$. This is not surprising as systemic concentrations are not expected to accurately reflect the local concentration experienced by the device. The size of the mouse model was prohibitive for obtaining the local hCG concentration in the extracellular space. Even if we had an accurate measure of the hCG concentration at the device location, though, Figure 5-8 and Figure 5-11 show that during *in vitro* sensing experiments the magnitude of the decrease in $T_{2,eff}$ does not always correlate with the concentration of the analyte bath. *In vivo* devices that show a smaller decrease in $T_{2,eff}$ at day four could have gone through a minimum in $T_{2,eff}$ at an earlier time and then a gradual $T_{2,eff}$ increase due to instability of the aggregates.

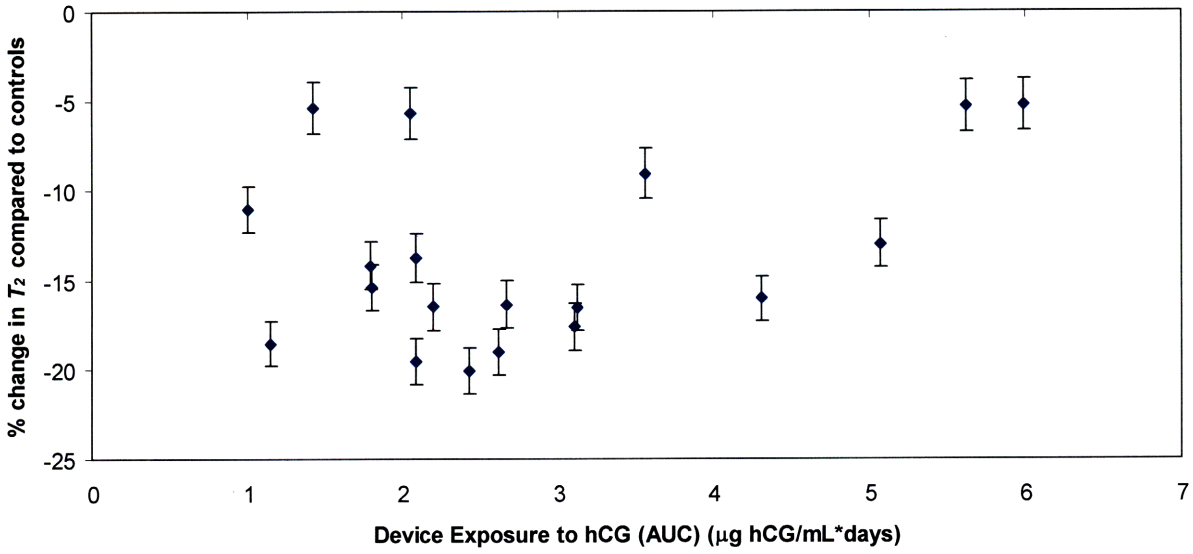

Figure 6-10. Percent change in $T_{2,eff}$ (compared to control devices) as a function of device exposure to hCG, calculated from the AUC of a plasma hCG concentration vs time plot. There is no correlation between the magnitude of the percent change in $T_{2,eff}$ and the AUC calculated from plasma hCG concentrations. This is not surprising, since plasma hCG levels are not expected to accurately reflect hCG concentrations at the tumor location.

6.5 Conclusion

This work demonstrates the feasibility of MRSw-based devices for short term applications, such as verification of successful tumor resection, and represents the first continuous monitoring device of soluble cancer biomarkers *in vivo*. The device described here could also be used for *in vivo* sensing of chemotherapeutic agents or metabolites simply by changing the MRSw contained within the device. *In vivo* performance was assessed using a commercially available human epithelial cell line (JEG-3) to produce ectopic tumors that secrete hCG in nude mice. Plasma hCG-b concentrations were quantified with an enzyme-linked immunosorbent assay (ELISA). Implantation was performed when the plasma hCG-b concentrations or tumor volume began to increase sharply. Six mice underwent live animal imaging by MRI one day and four days after device implantation to quantify T_2 of the MRSw.

All devices were measured using single-sided MR after they were explanted (two to four days after implantation). Only devices that were filled with MRSw functionalized to detect hCG and implanted next to a tumor demonstrated a decrease in $T_{2,eff}$.

Long term use of such implanted sensing devices will require demonstration of *in vivo* stability for periods exceeding one month. Future studies in a larger animal model will test the correlation between local hCG concentrations from repeated needle biopsy with each MRI measurement. Future studies will also incorporate the high porosity nano-channel membranes. These membranes with a higher P_{app} will decrease the time needed for diffusion of the analyte, allowing for real time monitoring of biomarkers and chemotherapeutic agents.

Chapter 7 Polymer Microchip for Drug Delivery

7.1 Summary

A syringe-injectable drug delivery device has been developed. This format will allow minimally invasive implantation of the device through a large-bore needle or trocar. *In vitro* release studies show that the new syringe-injectable format can achieve similar release profiles as the original dime-shaped polymer drug delivery device. A resorbable sealing method has been developed for the polymer microchip. Solvent welding at room temperature was able to achieve a leak proof seal for 14 days. This new sealing method makes the polymer microchip completely resorbable and eliminates the need to remove the device after delivery of the drug payload.

7.2 Introduction

Local delivery of multiple chemicals has been demonstrated from a resorbable polymeric microchip[16] (passive device). The microchips contain small reservoirs that are loaded with drug and separated from the outside environment by a polymer membrane on the front of the microchip and pressure sensitive adhesive on the back of the microchip. The composition, molecular weight, and thickness of the polymer membranes determine when the membrane will degrade and release the drug depot from the reservoir[16]. This polymer microchip has demonstrated *in vitro*[16,18] and *in vivo*[53,56] release of multiple compounds.

One limitation of the current polymer microchip is the device size and shape. If the current passive microchip format were used for treatment of a brain tumor, surgery would be required for tumor resection and implantation of the device. Therefore, this application is limited

to tumors that are accessible via surgery and that are large enough to leave room for placement of the microchip after tumor resection. A smaller microchip might decrease the trauma experienced by the surrounding (healthy) tissue and allow treatment of unresectable and/or small tumors that would otherwise not be treatable with the current device. The fabrication process of the passive chip is very flexible and could easily be modified to produce a device of nearly any size or shape. Of particular interest would be a thin cylindrical device, which would allow minimally invasive implantation techniques to be used, such as injection with a trocar or large-bore needle. Figure 7-1 is a schematic of the injectable format polymer microchip. Norplant® capsules (subdermal implants for long-acting contraception) are cylindrical in shape with a diameter of 2.4 mm and length of 34 mm[57]. The standard implantation protocol for these capsules is injection using a #10 trocar under local anesthesia[58]. Since the injectable polymer microchip will have a diameter that is nearly half the Norplant® diameter, a large-bore needle or trocar should also be able to implant the new device. This format change would also make the passive microchip more applicable in diverse treatments such as vaccination or hormone therapy treatment.

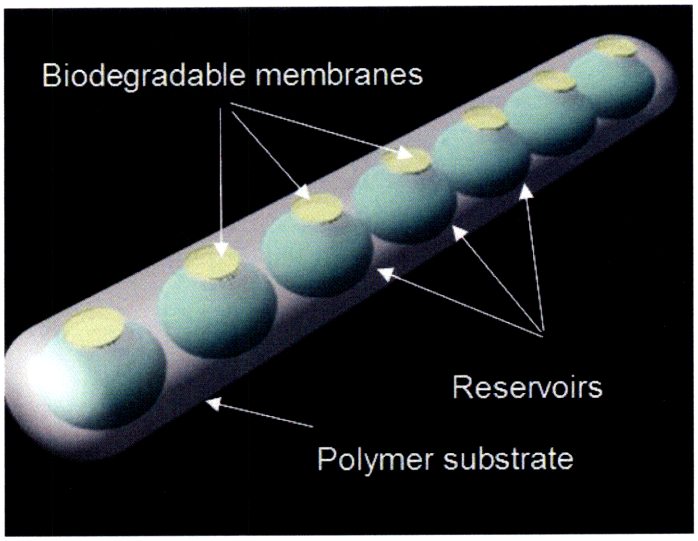

Figure 7-1. Schematic of an injectable polymer microchip for localized drug delivery. Removal of the device after it has delivered the payload is not required if the polymer substrate and membranes are resorbable.

Another limitation of the polymer microchip is that it is not fully biodegradable. The current sealing method (a non-resorbable polymeric pressure sensitive adhesive) creates an effective, leak-proof seal[18] but requires surgical removal once the device has released its payload. The new sealing layer must be biodegradable, biocompatible, prevent leakage of the drug depot, and retain the activity of the loaded drug.

7.3 Materials and Methods

7.3.1 Syringe-Injectable Format

Polymer microchip devices were fabricated as previously described[16]. Injectable format devices (a 1x6 array of reservoirs) were cut from the regular polymer microchip devices using a hot razor blade. The razor blade was heated by placing it on a hot press (370°F) for 30 seconds and then it was immediately used to cut the PLA substrate by pressing down on the blade. The dimensions of the injectable microchip are approximately 1.5 x 0.5 x 12 mm. PLGA 2A membranes (inherent viscosity of 0.16, Lakeshore Biomaterials, Birmingham, AL) were added to

the reservoirs as previously described[16]. A solution of radiolabeled dextran (^{14}C-dextran, 40 kDa, Sigma-Aldrich, St. Louis, MO) was microinjected into the reservoirs and the back of the devices was sealed with a pressure sensitive adhesive.

Some of the injectable format devices underwent a mock implantation step. A 12 gauge needle was inserted into an agarose hydrogel, the plunger was removed, and the injectable format device was loaded into the barrel of the needle. The plunger was used to advance the device to the tip of the needle, then the plunger was held stationary while the needle was withdrawn, leaving the device behind in the hydrogel. The device was carefully removed from the hydrogel and placed in one mL of PBS at 37°C. Injectable format control devices were immediately placed in one mL of PBS at 37°C, without undergoing a mock implantation step. Regular format polymer microchips were also used as control devices and were placed directly in one mL of PBS at 37°C after fabrication, loading, and sealing. The PBS was removed periodically and combined with five mL of scintillation fluid (ScintiSafe Plus 50%, Fischer Chemicals, Fairlawn, NJ) in a scintillation vial. A counting protocol for 14C was used on a Packard Tri-Carb liquid scintillation counter (Perkin Elmer, Waltham, MA). Raw data (disintegrations per minute, DPM) was converted to nanocuries (nCi) using the conversion factor 2,200 dpm = 1 nCi.

7.3.2 Resorbable Sealing Mechanism

Polymer microchip devices were fabricated as previously described[16]. A PLA (100L PLA, 200 kDa, Lakeshore Biomaterials, Birmingham, AL) backing layer was prepared using the same fabrication process as for the polymer microchip, except the aluminum die used in the hot press step did not contain any conical protrusions. The PLA backing layer was approximately 500 μm thick after polishing. The microchip devices were covered with pressure sensitive adhesive (Ideal 9144, American Biltrite, Lowell, MA) on the front and the reservoirs filled with

radiolabeled dextran (^{14}C-dextran, 40 kDa, Sigma-Aldrich, St. Louis, MO). Approximately 70 μL of either PLA or PCL dissolved in chloroform (12%, v/v) was microinjected around the reservoirs on the back side of the polymer microchip. The PLA backing layer was placed on top of the microchip, held in place with a small weight (approximately 10 g) and allowed to dry at room temperature overnight. The devices were then placed in five mL of PBS at 37°C. Control devices with pressure sensitive adhesive on both side of the microchip were also placed in five mL of PBS at 37°C. The five mL of PBS was periodically transferred to a scintillation vial with 15 mL of scintillation fluid (ScintiSafe Plus 50%, Fischer Chemicals, Fairlawn, NJ) and five mL of fresh PBS was added back to the container holding the microchip device. Time points were taken for two weeks. A counting protocol for ^{14}C was used on a Packard Tri-Carb liquid scintillation counter (Perkin Elmer, Waltham, MA).

7.4 Results

7.4.1 Syringe-injectable format

Injectable format control devices (no mock implantation step) were first tested in release experiments. The cutting process during fabrication of the injectable format device could create micro-cracks in the reservoir wall, resulting in immediate release of the loaded drug through the side of the reservoir. The injectable format also has less surface area on the back for sealing with the pressure sensitive adhesive which could lead to less reliable device performance. Figure 7-2 shows that the release profile from the injectable format control devices (1x6 arrays of reservoirs) (blue diamonds) is comparable to the release profile from the regular format polymer devices (pink squares). These results show that the injectable format device is capable of the same controlled release profiles as the regular polymer microchip.

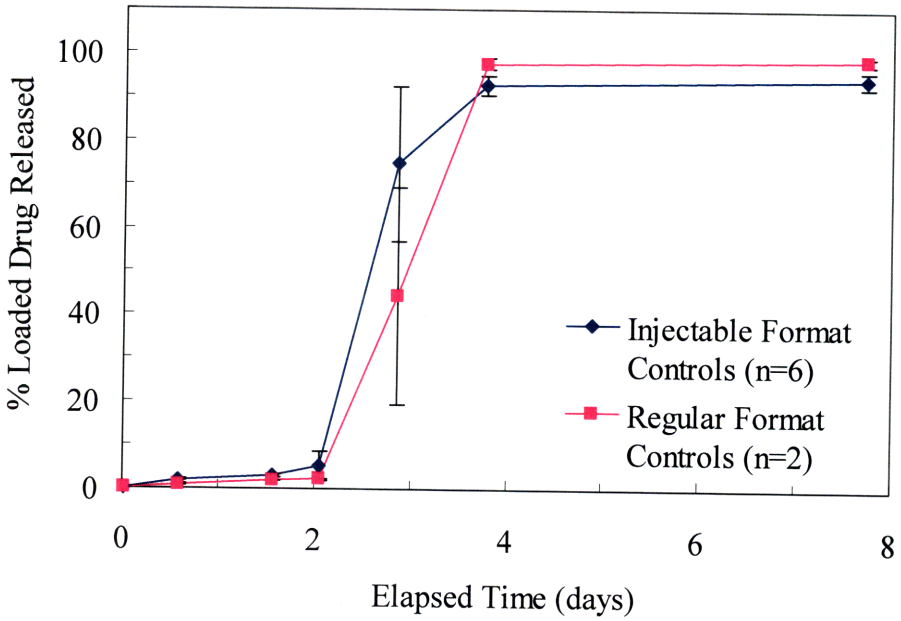

Figure 7-2. Release profiles from injectable format control devices (n = 6, no mock implantation step) and regular format microchip devices (n = 2). Both device types contain PLGA 2A membranes.

The injectable format devices were also used in release experiments after undergoing a mock implantation step. Mechanical stresses during the implantation process could damage the polymer membranes, causing immediate release of the drug payload instead of a delayed release after degradation of the polymer membranes. Figure 7-3 shows the release profile for three injectable format devices that went through a mock implantation step and the average release profile for injectable formal control devices (n = 3, no mock implantation step). The drug payload of all devices was expected to be released between two to four days. Figure 7-3 shows that there was significant variability in the behavior of the injectable format devices that underwent a mock implantation step. These devices did not, however, show immediate release of the payload as would be expected if the implantation procedure damaged the membranes. Variability of this type is relatively common with the passive polymer microchip. The variability

in the release behavior of the devices could be caused by small differences in the device substrate (reservoir diameter, air bubbles in the device substrate) or membrane (thickness of reservoir membrane).

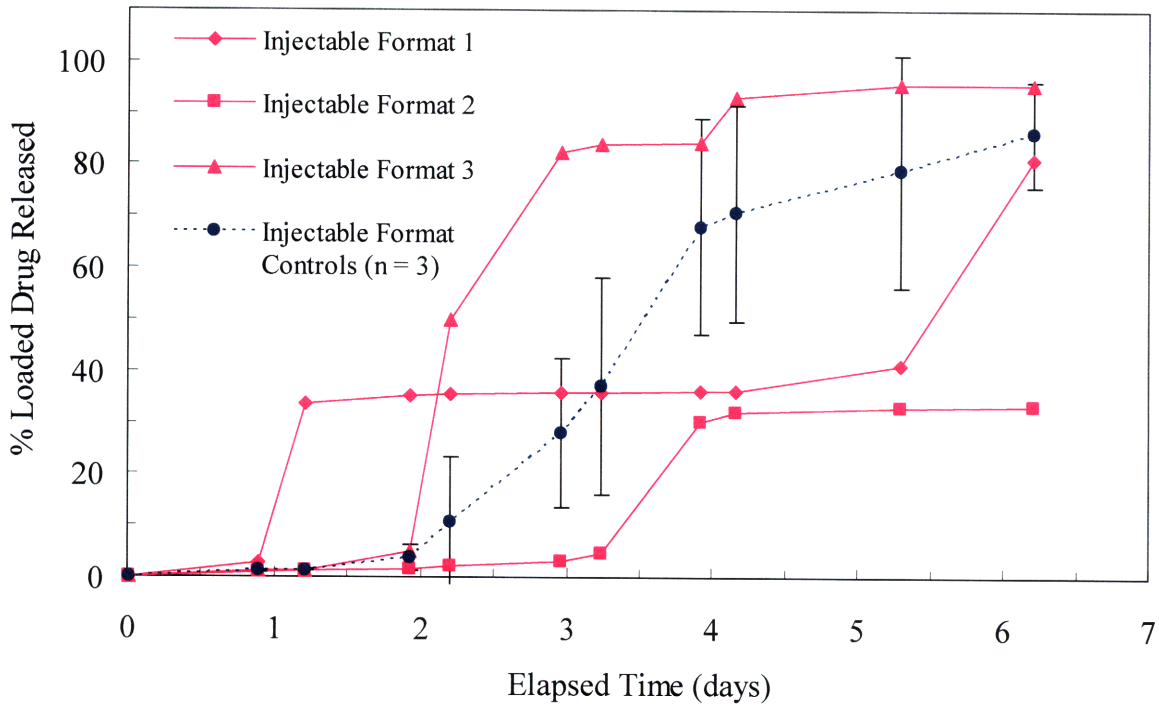

Figure 7-3. Release profile for injectable format devices that have undergone a mock implantation step.

7.4.2 Biodegradable sealing method

Room temperature solvent welding has been used to create a resorbable seal between the polymer microchip and a PLA backing layer. Figure 7-4 shows that while the seal from PCL solvent welding failed after approximately five days, the seal from PLA solvent welding was still intact after 14 days (less than 5% of the loaded drug had leaked). Less than 2% of the loaded drug had leaked from the control devices (pressure sensitive adhesive on both sides of the device) after 14 days. A resorbable seal lasting 14 days would be appropriate for some local drug delivery applications.

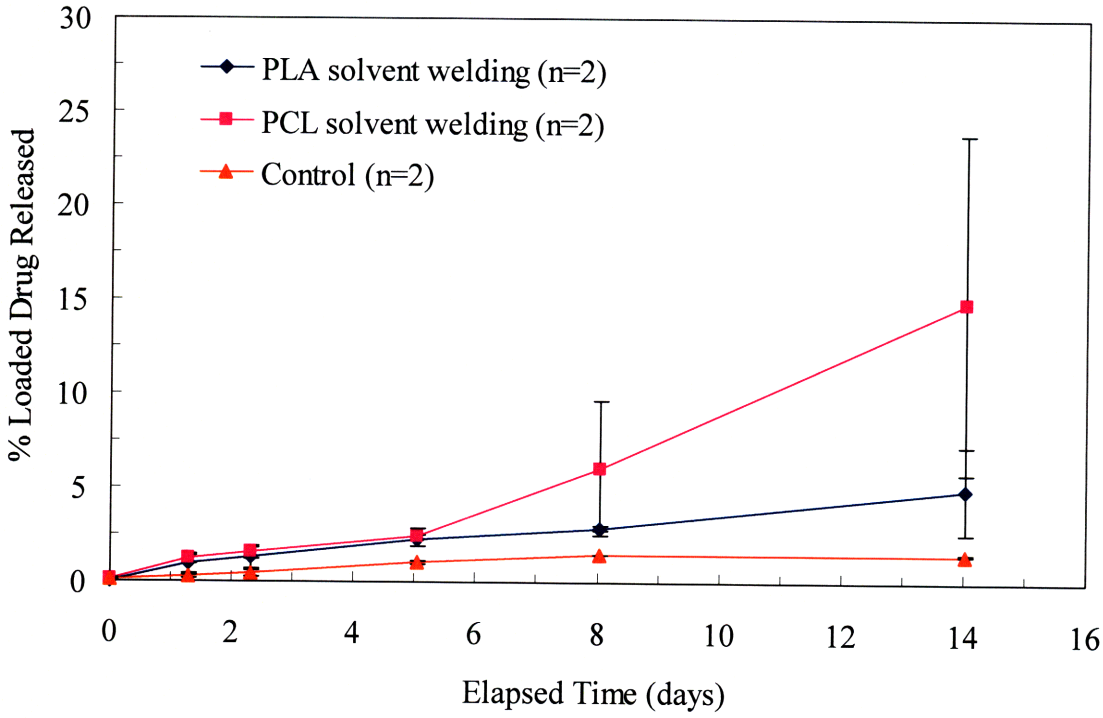

Figure 7-4. Leak test for resorbable sealing mechanism using solvent welding technique. Error bars represent st. dev. (n = 2 for each group).

7.5 Summary

Preliminary studies were performed in the development of a syringe-injectable drug delivery device. The injectable format was shown to be able to achieve delayed release of a loaded drug payload, even after going through a mock implantation step. Preliminary work was also done towards developing a completely resorbable polymer microchip. Solvent welding with PLA in chloroform was able to adhere a PLA backing layer to the substrate for 14 days. Less than 5% of the loaded drug leaked out during this time frame, compared to less than 2% leaking out of control devices (pressure sensitive adhesive on both sides of the reservoir). A 14 day seal is an appropriate time frame for some local drug delivery applications, but future studies will

need to be done to develop a resorbable sealing method that would be appropriate for long term localized drug delivery applications.

Chapter 8 Conclusions and Future Directions

8.1 Conclusions

This thesis includes several important first steps in the development of an implantable cancer sensor. This sensor device combines the polymer microchip drug delivery platform with magnetic relaxation switch (MRSw) nanoparticle sensors. MRSw are magnetic nanoparticles (iron oxide core, crosslinked dextran shell) that can detect a variety of analytes. MRSw are kept in the device by a molecular weight cut-off (MWCO) membrane which allows analytes free access to the nanoparticle sensors. The MRSw aggregate in the presence of the analyte they were designed to detect and this aggregation causes a decrease in the transverse relaxation time (T_2), which can be detected with magnetic resonance imaging (MRI) or nuclear magnetic resonance (NMR) relaxometry. *In vitro* sensing experiments were used to optimize the device design and characterize its performance. *In vivo* device-based sensing of hCG, a soluble biomarker that is elevated in testicular and ovarian cancer, has been demonstrated. The polymer microchip drug delivery device was also modified to a syringe-injectable format which will allow minimally invasive implantation through a large-bore needle or trocar. *In vitro* release studies show that the new syringe-injectable format can achieve similar release profiles as the original dime-shaped polymer drug delivery device. A resorbable sealing method has been developed for the polymer microchip. Solvent welding at room temperature was able to achieve a leak proof seal for 14 days. This new sealing method makes the polymer microchip completely resorbable and eliminates the need to remove the device after delivery of the drug payload.

8.1.1 Sensor Device Fabrication

Several different device designs were made and tested. The most reliable design is a cup-shaped device made from HDPE, with a 5 mm diameter and 2.5 mm deep reservoir. Double-sided pressure-sensitive adhesive is used to adhere a polycarbonate membrane to the device substrate. MRSw are added to the reservoir through a filling port on the back of the device which is then sealed with pressure sensitive adhesive. This device design has proven to be very reliable for the *in vitro* and *in vivo* studies carried out to date.

8.1.2 Characterization of MWCO Membranes

Several commercially available membranes were identified that are able to both retain MRSw and allow analyte diffusion. Analyte diffusion times, around 24 hours to reach equilibrium, are reasonable for an *in vivo* cancer sensor device. The effect of biomolecule adsorption on polycarbonate membranes was tested in an animal model. The diffusion of dextran (40 kDa) does not change significantly after the membranes have been implanted for up to one month. High porosity nano-channel membranes, made in the Cima group, were also tested. These membranes were able to retain MRSw functionalized to detect hCG. The apparent permeability of hCG through the nano-channel membranes is about two orders of magnitude higher than for commercially available polycarbonate membranes (10 nm pores).

8.1.3 Characterization of MRSw Aggregation

The batch of MRSw referred to as Cmix-3000 was found to retain activity after being stored at 4°C for seven months. Much of the activity of Cmix-3000 was lost, however, after incubation at 37°C for one month. The MRSw were still able to aggregate, but the operating range of hCG concentrations was significantly smaller and the decrease in $T_{2,eff}$ was less

pronounced. Stability of aggregates was found to be a function of both MRSw valency and hCG concentration, as expected. Cmix-3000 was found to form stable aggregates for a range of hCG concentrations relevant to *in vivo* experiments and this batch of MRSw was used for many device-based sensing experiments.

8.1.4 In Vitro Device-Based Sensing

Multiple *in vitro* sensing experiments have demonstrated the ability to detect the presence of hCG using MRSw that are contained within a reservoir by a semi-permeable membrane. Aggregation of the MRSw within the device was detected using both MRI and single-sided MR. Device-based sensing was successful in hCG solutions from 0.1 to 5 μg hCG/mL. Devices made with 10 nm pore membranes need approximately four days to reach the maximum decrease in $T_{2,eff}$, for the analyte and MRSw concentrations used in these experiments. Devices with 30 nm pore membranes demonstrate a faster decrease in $T_{2,eff}$, but the aggregates are less stable.

8.1.5 In Vivo Device-Based Sensing

This work demonstrates the feasibility of MRSw-based devices for short term applications, such as verification of successful tumor resection, and represents the first continuous monitoring device of soluble cancer biomarkers *in vivo*. *In vivo* performance was assessed using a commercially available human epithelial cell line (JEG-3) to produce ectopic tumors that secrete hCG in nude mice. Plasma hCG-b concentrations were quantified with an enzyme-linked immunosorbent assay (ELISA). Implantation was performed when the plasma hCG-b concentrations or tumor volume began to increase sharply. Six mice underwent live animal imaging by MRI one day and four days after device implantation to quantify T_2 of the MRSw. All devices were measured using single-sided MR after they were explanted (two to

four days after implantation). Only devices that were filled with MRSw functionalized to detect hCG and implanted next to a tumor demonstrated a decrease in $T_{2,eff}$.

8.1.6 Polymer Microchip for Drug Delivery

Preliminary studies were performed in the development of a syringe-injectable drug delivery device. The injectable format was shown to be able to achieve delayed release of a loaded drug payload, even after going through a mock implantation step. Preliminary work was also done towards developing a completely resorbable polymer microchip. Solvent welding with PLA in chloroform was able to adhere a PLA backing layer to the substrate for 14 days. Less than 5% of the loaded drug leaked out during this time frame, compared to less than 2% leaking out of control devices (pressure sensitive adhesive on both sides of the reservoir). A 14 day seal is an appropriate time frame for some local drug delivery applications.

8.2 Future Directions

8.2.1 Sensor Device Fabrication

Long term device reliability will need to be demonstrated for many clinical applications, such as detection of cancer recurrence. One likely source of device failure in longer term sensing experiments is the seal between the device substrate and the MWCO membrane. A mechanical means of attaching the MWCO membrane to the device substrate, such as two plastic pieces that are machined to fit snugly together while holding the membrane in place between them, may improve the long term reliability of the device. Future device designs should also use the high porosity nano-channel membranes. These membranes with a higher P_{app} will decrease the time needed for diffusion of the analyte, allowing for real time monitoring of biomarkers and chemotherapeutic agents.

8.2.2 MWCO Membranes

Future studies should examine the effects of longer implantation times and fibrous capsule formation on membrane biofouling and analyte transport. Recent work with a silicon device gives promising evidence that a fibrous capsule may not significantly hinder protein transport up to 6 months in beagle dogs[52]. Previous research has shown that permeability of polycarbonate membranes *in vivo* can be enhanced by plasma surface treatment[45]. We will explore this technique if *in vivo* transport kinetics vary significantly from *in vitro* results after longer implantation times.

8.2.3 MRSw Aggregation

The ability to perform long term *in vitro* and *in vivo* sensing experiments depends on MRSw that retain activity when stored at 37°C and produce stable aggregates. Previous work has demonstrated that stabilization of MRSw aggregates can be achieved by trapping them in a matrix that prevents the aggregates from precipitating out of solution[53]. Stability of the MRSw at 37°C may be able to be improved by adding PEG as a linker when attaching the antibodies to the surface of the MRSw[54] or by adding hydrophobic mutations or disulfide bonds to the antibody[55]. Reversible MRSw aggregation is another important direction for future work, since this would allow quantitative measurements of the current state of a solid tumor, instead of only cumulative measurements of past device exposure. Yibo Ling, a current graduate student in the Cima group, is working on developing reversible MRSw.

8.2.4 In Vitro Device-Based Sensing

Future studies should be performed to determine the cause of the gradual increase in T_2 observed in the devices placed in hCG solutions. Particle size data could be used to determine if

the increase in T_2 is caused by aggregates growing so large that they precipitate out of solution. This would require the volume of the reservoirs to be doubled, since the current devices do not hold enough MRSw solution for particle sizing. *In vitro* sensing experiments with matrix stabilization of the MRSw should be performed if aggregate precipitation is found to be a problem. The gradual increase in T_2 is most likely caused by thermal degradation of either the antibody or the link between the antibody and the nanoparticle, and the techniques described above (Section 8.2.3) may sufficiently address this problem.

8.2.5 In Vivo Device-Based Sensing

Long term use of implanted sensing devices will require demonstration of *in vivo* stability for periods exceeding one month. Future studies in a larger animal model will test the correlation between local hCG concentrations from repeated needle biopsy with each MRI measurement. *In vivo* device-based sensing of chemotherapeutic agents or tumor metabolites should also be performed, to demonstrate use of the sensing device in a wide range of clinical applications. Future studies that demonstrate *in vivo* sensing of multiple analytes with a single device would also increase potential clinical applications for the device.

8.2.6 Polymer Microchip for Drug Delivery

The preliminary *in vitro* studies in this thesis should be followed up with *in vivo* release studies to demonstrate reliable performance of the injectable format after implantation through a large bore needle. *In vivo* leak tests with fully resorbable devices should also be performed. A fully resorbable, syringe-injectable device will be useful in delivering chemotherapeutic agents to inoperable tumors.

References

1. Elias, J. et al. Pancreatic cancer: Correlation of MR findings, clinical features, and tumor grade. *Journal of Magnetic Resonance Imaging* **26**, 1556-1563 (2007).
2. Kettritz, U. Modern concepts of ductal carcinoma in situ (DCIS) and its diagnosis through percutaneous biopsy. *European Radiology* **18**, 343-350 (2008).
3. Koh, M. S., Tee, A., Wong, P., Antippa, P. & Irving, L. B. Advances in lung cancer diagnosis and staging: endobronchial ultrasound. *Internal Medicine Journal* **38**, 85-89 (2008).
4. Pepe, P. & Aragona, F. Saturation prostate needle biopsy and prostate cancer detection at initial and repeat evaluation. *Urology* **70**, 1131-1135 (2007).
5. Takeuchi, H., Kitajima, M. & Kitagawa, Y. Sentinel lymph node as a target of molecular diagnosis of lymphatic micrometastasis and local immunoresponse to malignant cells. *Cancer Science* **99**, 441-450 (2008).
6. Chen, Z. G. Exploration of metastasis-related proteins as biomarkers and therapeutic targets in the treatment of head and neck cancer. *Current Cancer Drug Targets* **7**, 613-622 (2007).
7. Agarwal, P. K., Black, P. C. & Kamat, A. M. Considerations on the use of diagnostic markers in management of patients with bladder cancer. *World Journal of Urology* **26**, 39-44 (2008).
8. Carney, W. P. Circulating oncoproteins HER2/neu, EGFR and CAIX (MN) as novel cancer biomarkers. *Expert Review of Molecular Diagnostics* **7**, 309-319 (2007).
9. Guerin, C., Olivi, A., Weingart, J. D., Lawson, H. C. & Brem, H. Recent Advances in Brain Tumor Therapy: Local Intracerebral Drug Delivery by Polymers. *Investigational New Drugs* **22**, 27 - 37 (2004).
10. Brem, H., Walter, K. A. & Langer, R. Polymers as Controlled Drug Delivery Devices for the Treatment of Malignant Brain Tumors. *European Journal of Pharmaceutics and Biopharmaceutics* **39**, 2-7 (1993).
11. Hanes, J. et al. Controlled Local Delivery of Interleukin-2 by Biodegradable Polymers Protects Animals from Experimental Brain Tumors and Liver Tumors. *Pharmaceutical Research* **18**, 899 - 906 (2001).
12. Sipos, E. P., Tyler, B. M., Piantadosi, S., Burger, P. C. & Brem, H. Optimizing Interstitial Delivery of BCNU from Controlled Release Polymers for the Treatment of Brain Tumors. *Cancer Chemotherapy and Pharmacology* **39**, 383-389 (1997).
13. Sampath, P. et al. Paracrine Immunotherapy with Interleukin-2 and Local Chemotherapy is Synergistic in the Treatment of Experimental Brain Tumors. *Cancer Research* **59**, 2107-2114 (1999).
14. Rhines, L. D. et al. Local Immunotherapy with Interleukin-2 Delivered from Biodegradable Polymer Microspheres Combined with Interstitial Chemotherapy: A Novel Treatment for Experimental Malignant Glioma. *Neurosurgery* **52**, 872 - 879 (2003).
15. Santini, J. T., Cima, M. J. & Langer, R. A controlled-release microchip. *Nature* **397**, 335-338 (1999).

16. Grayson, A. C. R. et al. Multi-pulse drug delivery from a resorbable polymeric microchip device. *Nature Materials* **2**, 767-772 (2003).
17. Santini, J. T., Richards, A. C., Scheidt, R., Cima, M. J. & Langer, R. Microchips as controlled drug-delivery devices. *Angewandte Chemie-International Edition* **39**, 2397-2407 (2000).
18. Grayson, A. C. R. A resorbable polymeric microreservoir device for controlled release drug delivery. *Massachusetts Institute of Technology, Doctoral Thesis* (2003).
19. Li, Y. et al. *In vivo* Release from a Drug Delivery MEMS Device. *Journal of Controlled Release* **100**, 211-219 (2004).
20. Sosnovik, D. E., Nahrendorf, M. & Weissleder, R. Magnetic nanoparticles for MR imaging: agents, techniques and cardiovascular applications. *Basic Research in Cardiology* **103**, 122-130 (2008).
21. Josephson, L., Perez, J. & Weissleder, R. Magnetic nanosensors for the detection of oligonucleotide sequences. *Angewandte Chemie Int. Ed.* **40**, 3204-3206 (2001).
22. Josephson, L., Tung, C. H., Moore, A. & Weissleder, R. High-efficiency intracellular magnetic labeling with novel superparamagnetic-tat peptide conjugates. *Bioconjugate Chemistry* **10**, 186-191 (1999).
23. Lewin, M. et al. Tat peptide-derivatized magnetic nanoparticles allow in vivo tracking and recovery of progenitor cells. *Nature Biotechnology* **18**, 410-414 (2000).
24. Perez, J. M., Josephson, L., O'Loughlin, T., Hogemann, D. & Weissleder, R. Magnetic relaxation switches capable of sensing molecular interactions. *Nature Biotechnology* **20**, 816-820 (2002).
25. Sun, E. Y., Weissleder, R. & Josephson, L. Continuous analyte sensing with magnetic nanoswitches. *Small* **2**, 1144-1147 (2006).
26. Kim, G. Y., Josephson, L., Langer, R. & Cima, M. J. Magnetic relaxation switch detection of human chorionic gonadotrophin. *Bioconjugate Chemistry* **18**, 2024-2028 (2007).
27. Schellenberger, E. A., Reynolds, F., Weissleder, R. & Josephson, L. Surface-functionalized nanoparticle library yields probes for apoptotic cells. *Chembiochem* **5**, 275-279 (2004).
28. Taktak, S., Sosnovik, D., Cima, M. J., Weissfeder, R. & Josephson, L. Multiparameter magnetic relaxation switch assays. *Analytical Chemistry* **79**, 8863-8869 (2007).
29. Badgwell, D. et al. Urinary mesothelin provides greater sensitivity for early stage ovarian cancer than serum mesothelin, urinary hCG free beta subunit and urinary hCG beta core fragment. *Gynecologic Oncology* **106**, 490-497 (2007).
30. Duffy, M. J. Clinical uses of tumor markers: A critical review. *Critical Reviews in Clinical Laboratory Sciences* **38**, 225-262 (2001).
31. Grossmann, M. et al. Measurement of Human Chorionic Gonadotropin-Related Immunoreactivity in Serum, Ascites and Tumor Cysts of Patients with Gynecological Malignancies. *European Journal of Clinical Investigation* **25**, 867-873 (1995).
32. Hoermann, R., Gerbes, A. L., Spoettl, G., Jungst, D. & Mann, K. Immunoreactive Human Chorionic-Gonadotropin and Its Free Beta-Subunit in Serum and Ascites of Patients with Malignant-Tumors. *Cancer Research* **52**, 1520-1524 (1992).
33. van Trommel, N. E. et al. Early identification of resistance to first-line single-agent methotrexate in patients with persistent trophoblastic disease. *Journal of Clinical Oncology* **24**, 52-58 (2006).

34. Costanzo, P. J., Patten, T. E. & Seery, T. A. P. Protein-ligand mediated aggregation of nanoparticles: A study of synthesis and assembly mechanism. *Chemistry of Materials* **16**, 1775-1785 (2004).
35. Yoon, J.-Y., Kim, K.-H., Choi, S.-W., Kim, J.-H. & Kim, W.-S. Effects of surface characteristics on non-specific agglutination in latex immunoagglutination antibody assay. *Colloids and Surfaces B: Biointerfaces* **27**, 3-9 (2003).
36. Ermens, A. A. M., Bayens, A. J. M., Crooymans, A., Broekman-van Hout, A. A. M. & van Duijnhoven, H. L. P. Dilution protocols for detection of hook effects/prozone phenomenon. *Clinical Chemistry* **46**, 1719-1720 (2000).
37. Goff, B. A. et al. Development of an ovarian cancer symptom index - Possibilities for earlier detection. *Cancer* **109**, 221-227 (2007).
38. Runowicz, C. D. Office laparoscopy as a screening tool for early detection of ovarian cancer. *Journal of Cellular Biochemistry*, 238-242 (1995).
39. Salama, O. et al. Chemiluminescent optical fiber immunosensor for detection of autoantibodies to ovarian and breast cancer-associated antigens. *Biosensors & Bioelectronics* **22**, 1508-1516 (2007).
40. Mok, S. C. et al. in *Advances in Cancer Research, Vol 96* 1-22 (2007).
41. Baron, A. T. et al. Soluble epidermal growth factor receptor (SEG-FR) and cancer antigen 125 (CA125) as screening and diagnostic tests for epithelial ovarian cancer. *Cancer Epidemiology Biomarkers & Prevention* **14**, 306-318 (2005).
42. Sedlaczek, P. et al. Comparative analysis of CA125, tissue polypeptide specific antigen, and soluble interleukin-2 receptor alpha levels in sera, cyst, and ascitic fluids from patients with ovarian carcinoma. *Cancer* **95**, 1886-1893 (2002).
43. Hogemann, D., Ntziachristos, V., Josephson, L. & Weissleder, R. High throughput magnetic resonance imaging for evaluating targeted nanoparticle probes. *Bioconjugate Chemistry* **13**, 116-121 (2002).
44. Daniel, K. D. et al. Multi-reservoir device for detecting a soluble cancer biomarker. *Lab on a Chip* **7**, 1288-1293 (2007).
45. Kessler, L. et al. Surface treatment of polycarbonate films aimed at biomedical application. *Journal of Biomaterials Science-Polymer Edition* **14**, 1135-1153 (2003).
46. Viville, P. et al. Excimer laser-induced surface modifications of biocompatible polymer blends. *Applied Surface Science* **96-8**, 558-562 (1996).
47. Wisniewski, N., Moussy, F. & Reichert, W. M. Characterization of implantable biosensor membrane biofouling. *Fresenius Journal of Analytical Chemistry* **366**, 611-621 (2000).
48. Van der Bruggen, B. et al. Assessment of a semi-quantitative method for estimation of the rejection of organic compounds in aqueous solution in nanofiltration. *Journal of Chemical Technology and Biotechnology* **81**, 1166-1176 (2006).
49. Chittchang, M., Mitra, A. K. & Johnston, T. P. Interplay of secondary structure and charge on the diffusion of a polypeptide through negatively charged aqueous pores. *Pharmaceutical Research* **24**, 502-511 (2007).
50. Deen, W. M., Bohrer, M. P. & Epstein, N. B. Effects of Molecular-Size and Configuration on Diffusion in Microporous Membranes. *Aiche Journal* **27**, 952-959 (1981).
51. Armstrong, J. K., Wenby, R. B., Meiselman, H. J. & Fisher, T. C. The hydrodynamic radii of macromolecules and their effect on red blood cell aggregation. *Biophysical Journal* **87**, 4259-4270 (2004).

52. Prescott, J. H. et al. Chronic, programmed polypeptide delivery from an implanted, multireservoir microchip device. *Nature Biotechnology* **24**, 437-438 (2006).
53. Kim, G. Y. in *Department of Materials Science and Engineering and Division of Health Sciences and Technology* 151 (Massachusetts Institute of Technology, Cambridge, 2008).
54. Yuan, X. F., Iijima, M., Ishi, M. & Nagasaki, Y. Structure and activity assay of nanozymes prepared by the coimmobilization of practically useful enzymes and hydrophilic block copolymers on gold nanoparticles. *Langmuir* **24**, 6903-6909 (2008).
55. Frokjaer, S. & Otzen, D. E. Protein drug stability: A formulation challenge. *Nature Reviews Drug Discovery* **4**, 298-306 (2005).
56. Kim, G. Y. et al. Resorbable polymer microchips releasing BCNU inhibit tumor growth in the rat 9L flank model. *Journal of Controlled Release* **123**, 172-178 (2007).
57. Wyeth-Ayerst. (Wyeth-Ayerst Company, Philadelphia, PA, 2003).
58. Wan, L. S., Stiber, A. & Lam, L. The Levonorgestrel Two-Rod Implant for Long-Acting Contraception: 10 Years of Clinical Experience. *Obstetrics & Gynecology* **102**, 24-26 (2003).